4-30-2011

Oxidative stress induces DNA strand breaks may lead to genomic instability in ovarian tumorigenesis

Harold-Humberto Moreno-Ortiz

Oxidative stress induces DNA strand breaks may lead to genomic instability in ovarian tumorigenesis

Comments

BRCA1||ROS||MMR||genomic instability||Ovarian cancer||SOD1

OXIDATIVE STRESS INDUCES DNA STRAND BREAKS MAY LEAD TO GENOMIC INSTABILITY IN OVARIAN TUMORIGENESIS

By

Harold-Humberto Moreno-Ortiz

A Dissertation
Submitted to the Faculty of
Mississippi State University
in Partial Fulfillment of the Requirements
for the Degree of Doctor of Philosophy
in Biology
in the Department of Biological Sciences

Mississippi State, Mississippi

April 2011

OXIDATIVE STRESS INDUCES DNA STRAND BREAKS MAY LEAD TO

GENOMIC INSTABILITY IN OVARIAN TUMORIGENESIS

By

Harold-Humberto Moreno-Ortiz

Approved:

Dwayne Wise Professor of Biological Sciences (Major Professor)	Nancy Reichert Head of the Department of Biological Sciences (Co-Major Professor)
Karen S. Coats Professor of Biological Sciences (Committee Member)	Janet R. Donaldson Assistant Professor of Biological Sciences (Committee Member)
Peter L. Ryan Professor and Interim Associate of the Provost Office (Committee Member)	Gary N. Ervin Associate Professor of Biological Sciences (Graduate Coordinator)

Gary L. Myers
Professor and Dean the College
of Arts & Sciences

Name: Harold-Humberto Moreno-Ortiz

Date of Degree: April 30, 2011

Institution: Mississippi State University

Major Field: Biology

Major Professor: Dwayne Wise

Title of Study: OXIDATIVE STRESS INDUCES DNA STRAND BREAKS MAY LEAD TO GENOMIC INSTABILITY IN OVARIAN TUMORIGENESIS

Pages in Study: 181

Candidate for Degree of Doctor of Philosophy

Oxidative stress (OS) occurs when DNA repair mechanisms are overcome by the amount of single and double strand DNA breaks caused by an accumulation of reactive oxygen species (ROS). Genomic instability (GI) by microsatellite instability (MSI) accumulation is characterized by changes in DNA single tandem repeats (STR) as a direct result of ROS. Deregulation of DNA repair and tumor suppressor pathways have been described as causes of tumor progression and metastasis. Studies in mammals have focused on GI and the implications of increased mutation frequency due to accumulation of MSI leading to development of diseases, including infertility and cancer. Ovarian cancer is a deadly disease displaying the highest mortality rate among gynecological cancers. Hereditary ovarian cancer displays GI that can be established early in primordial germinal cells (PCGs) development and migration across the genital ridge, where PGCs are exposed to ROS damage. The hypothesis of this study was ROS-induced GI is marked by the accumulation of MSI on repetitive sequences of DNA that override DNA repair, tumor suppressor and redox homeostasis pathways. In this study, we induced

ROS in human ovarian cell lines by hydrogen peroxide (H_2O_2) exposure, as well as evaluated mouse PGCs to determine whether MSI occurs in specific regions of human and mouse genomes. Our results show that MSI was present in specific markers after ROS-induced damage in human ovarian cells and in mouse *Sod1* knockout PGCs during cell migration, both of which accumulate specific mutations caused by free radical damage. Ovarian tumor cells and mouse PGCs showed an increase of MSI in 12 human and 5 mouse repetitive markers that are located near important genes related to DNA repair, tumor suppression, cell proliferation, apoptosis and differentiation. This could be a signal that leads to tumor initiation, formation and progression in adult ovarian cells due to improper DNA repair and tumor suppression mechanisms or in disruption of PGC migration that determines germinal cell pool selection during early embryonic development due to absence of cell antioxidant mechanisms. Therefore, these specific unstable STRs are novel biomarkers that could be useful in early diagnostics, prognosis, and successful therapy of ovarian tumorigenesis.

DEDICATION

Este trabajo de investigación está dedicado especialmente a mi pequeña y hermosa hija María-Lucia, a mi amada esposa Clara-Inés, a mis queridos padres María-Odilia y José-Humberto, a mis dos hermanos Javier y Carlos, a mis suegros Carlos-Julio y Arcelia, a toda mi familia y a amigos colombianos quienes han sido testigos y me han apoyado durante este gran reto. Sus oraciones han dado su fruto. Tambien quiero dedicar especialment este trabajo al tío Hernando Esteban (†) quien me dió invaluables consejos para creer en la invaluable riqueza de la educación impulsándonos a recorrer este camino para obtener nuestro doctorado. Finalmente todo este sacrificio no hubiese sido posible sin la invocación de Dios todopoderoso de quien recibí la luz de la inteligencia, la fortaleza en el alma y la esperanza en el corazón para poder ver en el día a día un nuevo y hermoso amanecer.

ACKNOWLEDGEMENTS

My sincere appreciation goes first to Dr Nancy Reichert and Dr Dwayne Wise for their support that gave me as major professors during my formation as a new researcher. My gratitude is extended to every member of my committee Dr Janet Donaldson, Dr Karen Coats and Dr Peter Ryan for their guidance and opportune observations. I would like to thank Dr Jane DuBien for her invaluable help in my statistical analysis, Dr Louis R. D'Abramo who made timely and important decisions through this process in order to reach my degree, and my colleague Kortney Wilkinson-Busha who sacrified her own time to made important editing corrections to this document. Words are not enough to appreciate my wife Clara-Ines for her constant encouragement, teachings and love that both of us put to this beautiful work. Finally, I want to acknowledge my pretty daughter Maria-Lucia who is the source of my eternal inspiration.

TABLE OF CONTENTS

Page

APPENDIX

LIST OF TABLES

LIST OF FIGURES

LIST OF ABBREVIATIONS

ACS	American Cancer Society
ANOVA	Analysis of Variance
APC	Adenomatous Polyposis Coli human gene
ASD	Autism Spectrum Disorder
ASB9	Ankyrin repeat and SOCS box-containing 9
BER	Base Excision Repair
BRCA1	Breast Cancer gene type 1
BSA	Bovine Serum Albumin
CI	Chromosomal Instability
CpG	"C phosphate G" region on the genome
dNTPs	Deoxyribonucleotide triphosphate
DMEM	Dulbecco's Modified Eagle Medium
DMSO	Dimethyl Sulfoxide
DNA	Deoxyribonucleic acid
ER	Endoplasmic Reticulum
FAM	Fluorescent Dye (6-carboxyfluorescein)
FRAXA	Fragile-X human gene
GI	Genomic Instability
GSH	Glutathione Peroxide Dismutase

HEX	Fluorescent Dye (Hexachlorofluorescein)
H_2O_2	Hydrogen Peroxide
HBOC	Hereditary Breast Ovarian Cancer Syndrome
HO	Hydroxyl Radical
HOC	Hereditary Ovarian Cacner
HNPCC	Hereditary non-polyposis colorectal cancer
HR	Homologous Recombination
LOH	Loss of Heterozygocity
LDL	Low Density Lipids
mitoETC	Mitochondrial Electro Transport Chain
MLH1	MutL homolog 1human gene
MMR	Mismatch repair
MSH2	MutS homolog 2 human gene
MSH6	MutS homolog 6 human gene
MSH3	MutS homolog 3 human gene
NO	Nitric Oxide
NED	Fluorescent Dye
NER	Nucleotide Excision Repair
NHEJ	Non Homologous End Joining
NOV	Normal Ovarian Cell Line
NOX	NAD(P)H oxidase
OS	Oxidative Stress
PBS	Phosphate Buffered Saline solution

PMS1	Postmeiotic segregation increased 1 human gene
PMS2	Postmeiotic segregation increased 2 human gene
PCR	Polymerase Chain Reaction
PGC	Primordial Germinal Cell
PTEN	Phosphatase and Tensin Homolog gene
RAD52	DNA repair protein
RLU	Relative Light Unit
ROS	Reactive Oxygen Species
SAS	Statistical Analysis Software
SKOV-3	Human ovarian cancer cell line
SOCS	Suppressor of cytokine signaling
SOD1	Superoxide dismutase 1
UTR	Untranslated Region

CHAPTER I

INTRODUCTION

On the basis of epidemiologic studies, ovarian cancer ranks fifth in cancer mortality among women in the United States (American Cancer Society, 2009). This disease has the highest mortality rate among gynecological cancers: greater than 66% of patients are diagnosed in the late stage of the disease, and the 5-year survival rate is only 20% to 30%. However, if diagnosed at early stages, the long-term survival rate increases to 90% (American Cancer Society, 2009). It has been estimated that 5-12% of invasive ovarian cancers result from hereditary susceptibility. Hereditary breast-ovarian cancer syndrome, due to *BRCA1* and *BRCA2* gene mutations, accounts for 65% to 85% of all cases of hereditary ovarian cancer (American Cancer Society, 2009). Lynch Syndrome or hereditary nonpolyposis colorectal cancer (HNPCC) is the third major cause of hereditary ovarian cancer and perhaps accounts for an additional 10% to 15% of all inherited cases. Defective DNA mismatch repair (MMR) is one of the most common and best defined molecular pathways involved in both acquired (sporadic) or inherited ovarian cancer disease (American Cancer Society, 2009).

The MMR process reverses replication errors that escape proofreading by replicative DNA polymerases (Blasi *et al.*, 2006). MMR-defective cells are incapable of correcting both base-to-base mismatches and insertion/deletion loops, which are precursors of missense and frameshift mutations (Blasi *et al.*, 2006). These mutations are specifically marked in particular sequences across the cell genome, giving rise to

genomic instability (GI), which is a hallmark of all forms of tumorigenesis. GI has been demonstrated in short, homogeneous, non-coding tandem repeats of DNA sequences (e.g. microsatellites or short tandem repeats-STR) found across human and mouse genomes (Weber and Wong, 1993). GI can be found in somatic tissues (Dubrova *et al.*, 2006) and in male germinal tissue exposed to reactive oxygen species (ROS) that are induced by genotoxic agents (Megid *et al.*, 2007; Dubrova, 2005). Studies in mice and humans have shown increases in single and double strand DNA breaks, chromatin fragility, and tandem repeat mutation frequency in the germline following exposure to doses of radiation (Bacher *et al.*, 2005; Dubrova, 2005; Li *et al.*, 2001), tobacco smoke (Yauk *et al.*, 2007), chemicals (Vilariño-Güell *et al.*, 2003), and environmental mutagens (Sommers *et al.*, 2004). Cells exposed to ROS are at risk for single strand DNA breaks, and when the level of ROS overrides normal DNA repair mechanisms, double strand DNA breaks also occur. Usually, if the cell is unable to repair this type of DNA damage, there are two pathways available. The first pathway is spontaneous cell death (apoptosis), and the wild type lineage is normally protected from nicked DNA or mutations in this way (Reed *et al.*, 2003; Reynolds *et al.*, 1994). In contrast, the second pathway occurs from chronic exposure to elevated ROS that can override DNA repair mechanisms, and the cells live on with mutated DNA instead of following the normal apoptotic pathway. This second pathway leads to GI, which can be measured through quantitative analysis of gains or losses of repetitive base pairs using PCR experiments. Studies in mammals have focused on GI and the implications of increased mutation frequency at repetitive loci in the development of diseases, including infertility and tumorigenesis (Yauk *et al.*, 2007).

The central dogma in tumorigenesis states that high levels of ROS can cause direct damage to the genome, encouraging progression of disease, while lower levels of

ROS might induce GI through specific pathways such as microsatellite instability (MSI) (Weinberg and Navdeep, 2009). Errors in replication, recombination, or DNA repair originate from the contraction or expansion of repeat units. This deleterious effect could be attributable to the inactivation of mismatch repair mechanisms through the accumulation of oxidative stress. According to this hypothesis, human cancers exhibit GI and increased mutation rate due to underlying defects in DNA repair genes, such as MLH1 and *BRCA1*, during cancer progression. This mechanism of induced mutability is poorly understood, and defining the role of MMR gene mutations in colorectal cancer predisposition is not always easy (Blasi *et al.*, 2006). A significant proportion, 17%, of cases of ovarian clear cell carcinomas hiding MSI and/or MMR protein mutations, escape detection with current screening strategies (Jensen *et al.*, 2008). Thus, new assays are required to evaluate, to define the functional significance of, and to determine the contribution of MSI related to MMR mutation. Therefore, it is important to fully understand the mechanisms responsible for spontaneous or induced mutations and the implications of GI as a prognostic of genetic disease development. Using single to double genome equivalent amplification, ROS has already been shown to directly induce GI in human testis, fibroblasts, and ROS sensitive mouse models (Megid *et al.*, 2007).

Important genes that play key roles in mammal ovarian differentiation and development have been identified. Studies in Rhesus monkeys and mice have identified the genes of MMR (*Mlh1, Pms2, Msh4 and Msh5*) which play a critical role in gametogenesis, such as chromosome recombination, pairing, and promotion of crossing over during meisosis (Jaroudi and SenGupta, 2007). Therefore, MMR is an important pathway in both mitotic proliferation and meiotic gonad formation. In human preimplantation embryos, various studies have reported expression patterns of different

genes (*BRCA1, BRCA2, ATM, TP53, RB1, MAD2, BUB1, APC, and beta-Actin*). Alteration of their expression has been associated with abnormal embryo morphologies. For example, in human embryos, upregulation of *RB1, ATM* and *beta-Actin* gene expression and repression of *BRCA1* gene expression were associated with embryo fragmentation, which is a substantial cause of spontaneous abortions and infertility (Jaroudi and SenGupta, 2007). STRs, located in promoter regions, untranslated regions (UTRs), and introns, can be important regulators of gene expression (Eckert and Hile, 2009). Due to microsatellite sequences that are highly polymorphic and contribute to gene regulations, changes in these sequences may provide a greater variety of phenotypic hereditable alterations (Eckert and Hile, 2009). Hence, we determined the relative stability of these microsatellites in the associated genes. STR mutations, which arise by gain or loss of base pairs, were measured following an exposure to H_2O_2 in normal human ovarian cell lines, human ovarian tumor cell lines, and in mouse germinal cells according to methods developed in our lab. From our preliminary experiments, ROS-sensitive repeat motifs from across the human and mouse genomes, including the X-chromosome, have been identified. Stability of these microsatellites was determined using single to double molecular genome equivalents from normal human ovarian cells, human ovarian cancer cells, and mouse germinal cells.

Our central hypothesis is that H_2O_2-induced oxidative stress (OS) causes single and double strand DNA breaks through ROS accumulation that overrides DNA repair mechanisms, thereby inducing GI that is marked by microsatellite instability. To test this hypothesis, our objectives were: (1) to establish baseline genomic stability in control normal human ovarian cell lines by measuring microsatellite instability using a panel of 33 markers found in both autosomes and X-chromosome; (2) to determine the response

of a normal human ovarian cell line to free radical damage in terms of relative alterations in GI as measured by single to double molecular genome equivalent amplifications of our marker panel both before and after exposure of cells to H_2O_2 in culture; (3) to compare the response of a mismatch repair deficient ovarian cancer cell line (*MLH1-/-*) in terms of baseline and induced genomic instability of our marker panel both before and after exposure of cells to H_2O_2 in culture; (4) to compare the response of human ovarian cancer cell line, *BRCA1*$^{-/-}$ to human ovarian cancer cell line *BRCA1*-positive in terms of baseline and induced genomic instability of our marker panel both before and after exposure of cells to H_2O_2 in culture; (5) to measure microsatellite instability in mouse in specific ROS sensitive and MMR sensitive panels for cultured female (*Sod1*$^{+/+}$, *Sod1*$^{+/-}$, and *SOD1*$^{-/-}$) and male (*Sod1*$^{+/+}$, *Sod1*$^{+/-}$, and *SOD1*$^{-/-}$) mouse primordial germinal cells (PGCs) isolated from 10.5 and 18 days post-coitum embryos; (6) to compare the rates of GI in cultured PGCs from knockout *Sod1* mice (*Sod1*$^{-/-}$), carrier (*Sod1*$^{+/-}$) and wild type controls (*Sod1*$^{+/+}$).

1.1 References

American Cancer Society. (2009) Cancer Facts and Figures. American Cancer Society, Inc.; Atlanta, GA. Available at: http://www.cancer.org/docroot/CRI/content/. Accessed February 02, 2010.

Bacher JW, Abdel Megid WM, Kent-First MG, and Halberg RB. (2005) Use of mononucleotide repeat markers for detection of microsatellite instability in mouse tumors. Mol Carcinog 44:285-292.

Blasi MF, Ventura I, Aquilina G, Degan P, Bertario L, Bassi C, Radice P, Bignami M. (2006) A human cell-based assay to evaluate the effects of alterations in the MLH1 mismatch repair gene. Cancer Res 66:9036-9044.

Dubrova YE. (2005) Radiation-induced mutation at tandem repeat DNA loci in the mouse germline: spectra and doubling doses. Radiat Res 163:200-207.

Dubrova YE, Ploshchanskaya OG, Kozionova OS, Akleyev AV. (2006) Minisatellite germline mutation rate in the Techa River population. Mutat Res 602:74-82.

Eckert KA, Hile SE. (2009) Every microsatellite is different: Intrinsic DNA features dictate mutagenesis of common microsatellites present in the human genome. Mol Carcinog 48:379-388.

Jaroudi S, SenGupta S. (2007) DNA repair in mammalian embryos. Mutat Res 635:53-77.

Jensen KC, Mariappan MR, Putcha GV, Husain A, Chun N, Ford JM, Schijver I, Longacre TA. (2008) Microsatellite instability and mismatch repair protein defects in ovarian epithelial neoplasms in patients 50 years of age and younger. Am J Surg Pathol 32:1029-1037.

Li CY, Little JB, Hu K, Zhang W, Zhang L, Dewhirst MW, Huang Q. (2001) Persistent genetic instability in cancer cells induced by non-DNA-damaging stress exposures. Cancer Res 61:428-432.

Megid WA, Ensenberger MG, Halberg RB, Stanhope SA, Kent-First MG, Prolla TA, Bacher JW. (2007) A novel method for biodosimetry. Radiat Environ Biophys 46:147-154.

Reed JC, Doctor K, Rojas A. (2003) Comparative analysis of apoptosis and inflammation genes of mice and human. Genome Res 13:1376-1388.

Reynolds JE, Yang T, Qian L. (1994) Mcl-1, a member of the Bcl-2 family, delays apoptosis induced by c-Myc overexpression in Chinese hamster ovary cells. Cancer Res 54:6348-6352.

Sommers CM, Mc Carry BE, Malek F, Quinn JS. (2004) Reduction of particulae air pollution lowers the risk of heritable mutations in mice. Science 304:1008-1010.

Vilariño-Güell C, Smith AG, Dubrova YE. (2003) Germline mutation induction at mouse repeat DNA loci by chemical mutagens. Mutat Res 526:63-73.

Weber JL, Wong C. (1993) Mutation of human short tandem repeats. Hum Mol Genet 2:1123-1128.

Weinberg F, Navdeep SC. (2009) Reactive oxygen species-dependent signaling regulates cancer. Cell Mol Life Sci 66:3663-3673.

Yauk CL, Berndt ML, Williams A, Rowan-Carroll A, Douglas GR, Stämpfli MR. (2007) Mainstream tobacco smoke causes paternal germ-line DNA mutation. Cancer Res 67:5103-5106.

CHAPTER II

REVIEW OF PERTINENT LITERATURE

2.1 Ovarian development

2.1.1 Human ovarian development

The sexual genotype is responsible for directing gonadal development in both sexes. In humans, as in most mammals, the presence of the SRY (Sex-determining region of the Y chromosome) gene results in the development of a male embryo, while the absence of SRY results in the development of a female embryo (Bogart and Ort, 2007). The cascade of events that leads to female development is controlled not only by sex chromosomes, but also by hormones and other molecular factors, most of which are encoded in the autosomes. The human ovaries develop from the intermediate mesoderm behind the peritoneum (Bogart and Ort, 2007). At 3 weeks of gestation, large primordial germinal cells (PGCs) originate from the primitive streak. In the primitive streak, PGCs begin to migrate and settle in the endoderm of the yolk sac. Once these cells arrive at the yolk sac, they appear to mix with other types of cells. From there, PGCs migrate toward the genital ridge through the dorsal mesentery. Once there, somatic support cells surround clusters of PGCs, and these germinal cells then differentiate into oogonia, first proliferating and then entering the first meiotic division in order to form primary oocytes. Four weeks after fertilization, indifferent gonads appear at the genital ridge, and at this stage, a thickening of coelomic epithelium occurs due to rapid cell proliferation. This thickening occurs medial and parallel to the urogenital ridge (Schoenwolf *et al.*, 2009).

Prior to the 5th week, indifferent gonads consist of surface germinal epithelium, which originates from the primitive mesoderm that is coated by coelomic epithelium, surrounding the internal blastema. The blastema is a primordial mesenchymal cellular mass that eventually becomes the ovarian medulla. The medullary region of the ovary is devoted to vessels, nerves, and connective tissue. After the 5th week, the germinal epithelium covers the blastema, and projections from the germinal epithelium are extended into the blastema, forming the primary sex cords (Schoenwolf *et al.*, 2009). At the 6th week of gestation, the XX somatic support cells, derived from coelomic epithelium, differentiate as follicle cells instead of Sertoli cells. In males, Sertoli cells produce Antimullerian hormone, which inhibits the formation of the mullerian ducts, which are precursors to the Fallopian tubes, uterus, and cranial portion of the vagina. The somatic support cells have a flattened appearance and can differentiate into two kinds of cells: 1) granullosa cells (surface/coelomic epithelial origin) and 2) theca cells (mesenchymal origin). These flattened cells play a critical role: they protect the PGCs to prevent their degeneration (Schoenwolf *et al.*, 2009). Starting at the 7th week of gestation, the male and female systems begin to diverge on separate developmental pathways according to their genotypic sex. At this time, the ovaries begin to display a round shape, reducing the area of contact with mesonephros. As the ovaries continue to develop, granullosa cells, thecal cells, and primary oocytes, all of which are now called primordial follicles, congregate in the cortical region of the future ovary. The ovarian cortex, or tunica albuginea, develops by the 8th or 9th week of gestation and gives support to the ovarian cells. The definitive human ovary does not appear until some time between the 12th and 16th week of gestation. At 20 weeks after fertilization, ovarian follicles become evident (Schoenwolf *et al.*, 2009).

2.1.2 Prenatal development of the mouse ovary and germ cells

Early in mouse embryonic development, the cells that give rise to the primordial germ cells (PGCs) can first be identified as a cluster of cells in the proximal margin of the 6.5 days post coitum (dpc) epiblast, in close proximity to the extraembryonic ectoderm (Lawson and Hage, 1994). By 7.5 dpc, PGCs have migrated to the extraembryonic mesoderm at the posterior end of the primitive streak near the base of the allantois. They can be identified by staining for endogenous alkaline phosphatase (AP) (Ginsburg *et al.*, 1990). The PGCs then become associated with the hindgut endoderm and migrate through the gut mesentery, arriving at the genital ridges by 10.5 dpc. During the process of moving from the posterior primitive streak to the genital ridges, PGCs increase in number from about 150 cells at 8.5 dpc, to approximately 25,000 cells at 13.5 dpc (Tam and Snow, 1981). By 13.5 dpc, PGCs within the genital ridge stop dividing in both male and female embryos. In the female embryo, at 13.5 dpc, PGCs enter meiosis, while those in the male embryo undergo mitotic arrest (Labosky *et al.*, 1994). Unlike the testis, in which spermatogonia constantly divide and produce gametes, the ovary has a finite supply of oocytes. The size and rate of depletion of the oocyte pool determine the female reproductive lifespan. The molecular mechanisms controlling gonadogenesis require interaction among diverse regulators, including growth factors, receptors, and transcription factors (Elvin and Matzuk, 1998). However, the role that the endogenous and exogenous cellular environment plays in ovarian development and function is not entirely clear.

2.1.3 Post natal development of the ovary

Sex determination and gonadal development in both male and female must occur in a tightly regulated cascade of genetic events if normal gender determination and

fertility is to occur (Wallis *et al.*, 2008; DiNapoli and Capel, 2007). Events, such as regulated allocation and maturation of oocytes and the proliferation and differentiation of the surrounding somatic cells that occur during folliculogenesis, play an important role in ensuring female fertility. In contrast to the continuous proliferation of male germ cells, proliferation of female oogonia occurs only prenatally in mice and other mammals. At birth, the female has a finite oocyte population, and in prepubescence, some oocytes begin to grow in response to intragonadal factors, while others remain quiescent until the onset of puberty, prolonging the female reproductive lifespan (Labosky *et al.*, 1994). Folliculogenesis is controlled at two stages: 1) intragonadal factors initiate follicular growth and coordinate the development of the oocyte, granulosa cells and thecal cells (components of the follicle) at least at early stages of folliculogenesis; and 2) extragonadal factors synchronize the function of granulosa cells and thecal cells for later in folliculogenesis, and these factors integrate the reproductive system with the physiology of the rest of the organism (Adashi, 1994). The assembly of the primordial follicles occurs at two times: early in ovarian development and later, in the subsequent development and transition of the primordial follicle to the primary follicle. The pool of primordial follicles is then continually depleted with each menstrual cycle, giving rise to a successful ovulation or atresia until menopause occurs. In menopause, there are two important mechanisms that play an important role in this transitional period: gradual loss of estrogens/progestagens and loss of antioxidant effects on low density lipoproteins (LDL). As a consequence of these two mechanisms, permanent cessation of ovarian function occurs as a natural human event.

Abnormalities in primordial follicle development lead to female infertility and tumorigenesis (Skinner, 2005). The age-related decline in female fertility and

tumorigenesis has been attributed to a variety of causes, including progressive oocyte depletion, stress response impairments, DNA repair mechanism deficiency, meiotic irregularities, and mitochondrial dysfunction (Steuerwald, 2007). By the age of 40, the average woman's fertility potential begins to decline considerably. Aging in the female ovary may be due to a lowering of enzymatic defenses and a simultaneous increase of ROS production, possibly originated from multiple cells within the gonad (Wiener-Megnazi *et al.*, 2004). Expression of superoxide dismutase (SOD) and glutathione peroxidase (GSH), two antioxidant defense pathways, have been shown to decrease from the premenopausal to menopausal ovary. This down-regulation of antioxidant genes leads to the accumulation of ROS, primarily resulting in mitochondrial DNA damage (Okatani *et al.*, 1997).

2.2 Ovarian cancer

2.2.1 Epidemiology, risk factors, and familial predisposition

Ovarian cancer is a deadly disease. In the United States, the National Cancer Institute reported 21,880 new cases and 13,850 deaths in 2009 (Jemal *et al.*, 2010). Most of these cases (90%) are epithelial ovarian cancers, which supports Fathalla's theory that incessant ovulation, throughout the fertile life of women, promotes the growth of transformed epithelial ovarian cells during tissue wound repair of the surface epithelium damaged by ovulation (Fathalla, 1971). These changes increase the risk of acquiring genetic abnormalities, giving rise to dysplastic changes in epithelial cells as an early transformation in ovarian cancer (Farley *et al.*, 2008). While the majority of ovarian cancers are sporadic, clinical studies have identified several risk factors that increase the possibility of acquiring ovarian cancer. Examples of risk factors are nulliparity, age at

first parity, age at first menarche, and the use of hormone replacement therapy for postmenopausal women (Marsden and Sturdee, 2009). It has also been noted that hereditary and genetic factors play equally crucial roles as causes of ovarian cancer and it is estimated that between 5-12% of invasive ovarian cancers are caused by hereditary susceptibility. Overall, the lifetime risk for developing ovarian cancer in the general population is 1.6%, increasing to approximately 5% risk if a woman has one first-degree relative with the disease, and 7% risk if a woman has two first-degree relatives with ovarian cancer. Therefore, there is a strong risk factor indicated in families with a history of ovarian cancer (Pharoah and Ponder, 2002; Werness and Eltabbakh, 2001). Familial predisposition to ovarian cancer has also been linked with other types of cancer, such as breast and colon (American Cancer Society, 2009; Brown *et al.*, 2001). In fact, two major ovarian cancer syndromes have been identified. Ninety percent of the hereditary ovarian cases are identified as hereditary breast-ovarian cancer (HBOC) syndrome, also called hereditary ovarian cancer (HOC) syndrome, and is associated with germ-line mutations of *BRCA1* and *BRCA2* genes. Most of the remaining 10% of hereditary ovarian cases are identified as Lynch syndrome, also called hereditary non-polyposis colon cancer (HPNCC), and are associated with germ-line mutations in the DNA mismatch repair (MMR) genes, such as *hMLH1* and *hMSH2* (Boyd, 2003; Risch *et al.*, 2001; Lynch *et al.*, 1997).

2.2.2 Histopathology

Histopathologically, ovarian cancer is classified into two main groups: 1) cases of surface epithelial-stromal origin (90%), and 2) cases of non-epithelial origin (10%). The least common type of ovarian cancer, non-epithelial origin, includes sex cord-stromal

tumors (6%), germ cell tumors (3%), including teratomas and disgerminomas, and indeterminate tumors (1%) (Kosary, 2007). The most common group (surface epithelial-stromal origin), can be further divided into two sub-groups: 1)10-20% are low malignant potential tumors (non-stromal invasion), characterized by a high rate of cellular proliferation without compromising ovarian stroma, and 2) 80-90% are invasive epithelial tumors. Of the invasive epithelial ovarian cancers, 75-80% are papillary serous (cystadenocarcinoma), 10% are mucinous, 9% are endometroid and less than 1% include types as clear cell, Brenner, small cell, and undifferentiated carcinoma (Figure 2.1).

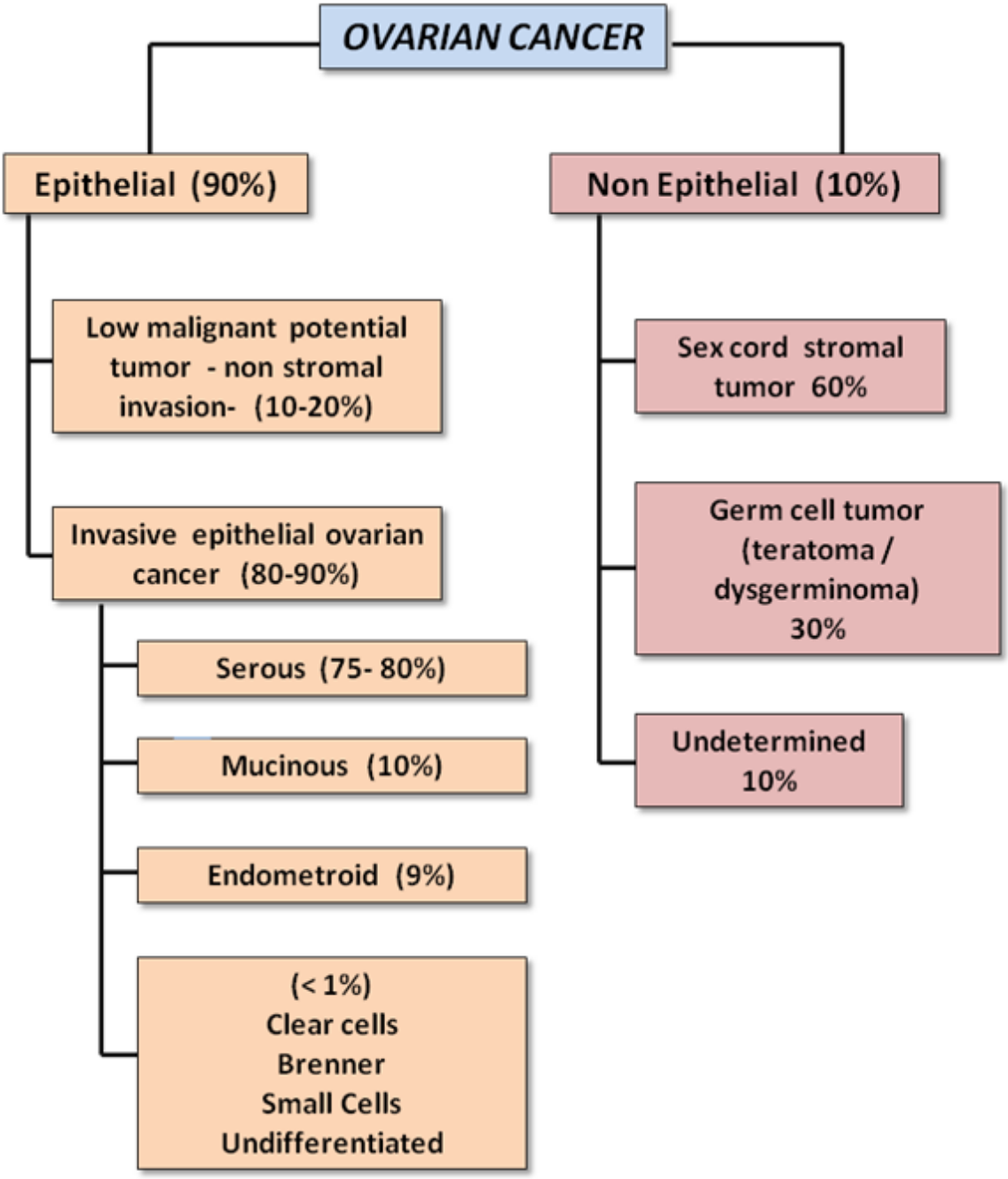

Figure 2.1 Histological classification of ovarian cancer. Adapted from Kosary, 2007

2.2.3 Origin of ovarian cancer

Many adverse factors have been found to be involved as part of the origin of ovarian cancer. Genetic (hereditary), environmental, and endocrinological factors are directly or indirectly related to tumorigenesis. However, the precise origin of the epithelial ovarian cancer remains unknown (Farley *et al.*, 2008). Many theories propose that long periods of ovulations and/or uninterrupted ovulations (incessant ovulation hypothesis: Fathalla's theory) induce repeated trauma along with subsequent repair of the ovulation scar in the single-cell layer of epithelial cells that covers the ovarian surface (Fathalla, 1971). This repetitive process of trauma and repair produces chronic inflammation, generating a stromal microenvironment that is characterized by activated fibroblast formation, microvessel proliferation, immune cell infiltration, and basement membrane degradation. It has been demonstrated that epithelial ovarian cells exposed to adverse factors can cause dysplastic changes, genetic abnormalities, and malignant transformation (Dauplat *et al.*, 2009; Farley, 2008). Another hypothesis reasons that after each ovulation, epithelial ovarian cells die and form inclusion cysts in the ovarian stroma (Mullerian ovarian inclusion cysts). These cysts are then exposed to different growth factors and signaling molecules, and can produce local cell transformation (Dauplat *et al.*, 2009). In 2009, Chene G. *et al*, have concluded that hormonal ovarian stimulation, in terms of time and dose, used in infertile patients also has a potential role in ovarian carcinogenesis, indicating a possible relationship between ovulation-inducing drugs and ovarian surface epithelial dysplasia (Chene *et al.*, 2009).

2.2.4 Diagnosing ovarian cancer

One of the greatest challenges in ovarian cancer diagnostics is that most tumors are asymptomatic until they are in the advanced stage, resulting in poor prognosis,

decreased life expectance, and low quality of life. Less than 30% of the women diagnosed with advanced-stage ovarian cancer survive over the long term (more than 5 years). Conversely, more than 90% of women diagnosed in early stages of the disease survive without any signs of recurrence after initial treatment with the current protocols that are available (Bast, 2004). The difficulty of diagnosis in the early stages has motivated the scientific community to develop screening programs for ovarian cancer. However, the value of screening for epithelial ovarian cancer with routine annual pelvic examinations, tumor markers, and ultrasound has been met with limited success. To have a significant impact on ovarian cancer, all examinations should seek an early detection of the disease in order to establish early and more efficient treatment and lead to complete remission of the disease (Badgwell and Bast, 2007). Routine pelvic examinations used alone as screening for ovarian malignancies cannot be justified for early detection because small masses (less than 1 or 2 cm in diameter) located in ovaries may go unnoticed due to low sensitivity and specificity of the examination (Stewart and Thistlethwaite, 2006). Transvaginal sonography (TVS) has permitted more precise imaging of each ovary and has displayed increasing sensitivity for the detection of early ovarian cancer, but the specificity of TVS continues to be limited (Bast, 2004). CA125 measurements, a serum marker for detection of ovarian cancer, have been used to detect primary disease in early stages, monitor the disease response after conventional treatment, and predict both residual and clinically undetected ovarian cancer post-treatment (Bast, 2004). Monitoring CA125 over time or the combination of these two methods has demonstrated greater specificity in ovarian tumor detection, allowing for the early implementation of more efficient anti-cancer treatments. Both TVS and CA125 have so far proven to be cost effective diagnostic methods that are available for the early

detection of ovarian cancer, significantly improving median survival of patients (5 year survival rate > 75%) (Badgwell and Bast D, 2007; Stewart and Thistlethwaite, 2006).

2.3 Reactive oxygen species (ROS)

Reactive oxygen species (ROS) are small molecules that are derivatives of oxygen and include oxygen ions, peroxides, and free radicals. Free radical species are unstable and highly reactive. They are generated both as normal by products of cellular metabolism, as well as through abnormal exogenous means. While the acquisition of electrons from nucleic acids, lipids, proteins, carbohydrates, or any nearby molecule ultimately leads to a stable state for the free radical, it also initiates a cascade of chain reactions that can result in DNA mutation, cellular damage, and tumorigenesis (Halliwell *et al.*, 1992). The three major types of ROS are: 1) superoxide (O_2^-), formed when electrons leak from the electron transport chain; 2) hydrogen peroxide (H_2O_2), resulting from the dismutation of superoxide or directly from the action of oxidase enzymes; and 3) hydroxyl (OH^-), a highly reactive species that can modify both purines and pyrimidines and can cause single and double strand breaks that result in DNA damage (Mello-Filho *et al.*, 1984). Many environmental pollutants (benzene, formaldehyde, polycyclic aromatic hydrocarbons, etc) which damage DNA via one of the ROS pathways have been implicated in tumorigenesis, and have both physiological and pathological roles in all body systems, most importantly in the development and maintenance of the female reproductive tract (Tovalin *et al.*, 2006).

Reproductive cells and tissues remain stable when free radical production and scavenging antioxidants are in equilibrium. Oxidative stress (OS) occurs when the balance between ROS production and the cell's ability to eliminate reactive intermediates

or repair the resulting damage is disrupted (Agarwal *et al.*, 2005). The sequential mechanism of O_2^- and H_2O_2 generation can impair the natural mechanisms of DNA repair and tumor suppression. This cascade of events can cause mitochondrial damage, induce abnormal apoptosis, affect ovarian development, and induce tumorigenesis (Suzuki *et al.*, 1999). Under physiological conditions, ROS are maintained at proper levels by a balance between their generation and elimination. The ovary, however, is sensitive to OS, especially as it develops during embryogenesis. Abnormal exposure may be marked by genomic instability, modification of transcription factors (modification of DNA methylation), and gene expression. Figure 2.2 shows the delicate balance of the stable state of ROS and how it could readily change if any step in ROS production or scavenging is disturbed. An increase in ROS generation, a decrease in antioxidant capacity, or a combination of both can lead to oxidative stress (Lu *et al.*, 2007).

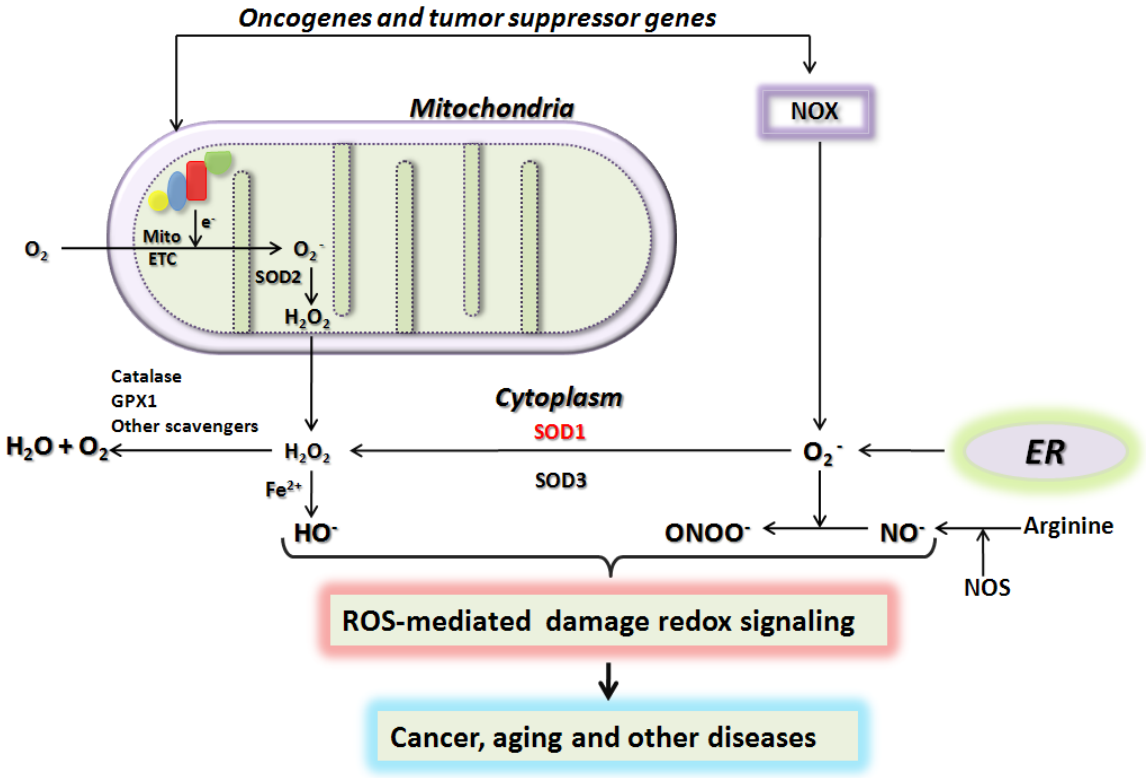

Figure 2.2 Cellular reactive oxygen species (ROS) metabolism

Notes: Different cell sites are source of ROS production: The mitochondrial electron transport chain (Mito-ETC), the endoplasmic reticulum (ER) system, and the NAD(P)H oxidase (NOX) cell membrane complex. Superoxide (O_2^-) is the initial main free radical oxygen species. Inside of the mitochondria, superoxide is generated by the capture of electrons escaping from the mito-ETC by way of molecular oxygen, and it can be rapidly converted into H_2O_2 by SOD2 or in water through scavengers such as catalase, GPX1, and others. The mito-ETC is composed of four enzymes localized in the inner mitochondrial membrane: complex I (NADH dehydrogenase), complex II (succinate dehydrogenase), complex III (Cytochrome bc1 complex), and complex IV (cytochrome C oxidase). In the presence of cytoplasmic metals such as Iron (Fe^{2+}), H_2O_2 can be converted to hydroxyl radical (HO^-) which is highly reactive and toxic to proteins, lipids, and DNA. Nitric oxide (NO^-) is produced from arginine by nitric oxide synthase (NOS). NO^- has a short half-life and can react with superoxide and produce peroxy nitrite $ONOO^-$ which can modify the structure and function of proteins. Through unclear mechanisms, oncogenic molecules such as Ras, Bcr-Abl, c-Myc increase ROS production. However, the tumor suppressor gene p53 decreases ROS production, influencing the mito ETC and NOX complex. Balance between production and elimination of ROS is sustained by the cell in order to prevent harmful effects. GPX1, glutathione peroxidase 1; HO^-, hydroxyl radical; NO, nitric oxide; $ONOO^-$, peroxy nitrite, SOD, superoxide dismutase. Adapted from Lu *et al.*, 2007.

One of the most common examples of tumorigenesis in women is ovarian epithelial cancer, which is also the most common type of ovarian cancer. Inflammation of the ovarian surface epithelium has been suggested as an etiological factor in ovarian epithelial cancer (Behrman *et al.*, 2001). According to Ness and Cottreau, (1999), follicular rupture results in the exposure of the ovarian surface epithelial cells to ROS, by inflammation and cytokines secreted during repeated ovulatory cycles over the reproductive life of the female. In fact, the risk of ovarian epithelial cancer is directly correlated with the number of ovulatory cycles that occurs during the fertile life of the woman. However, according to a collaborative study of the World Health Organization, factors that inhibit ovulation, such as hormonal contraceptives and pregnancy, have helped to reduce the risk of ovarian cancer (World Health Organization, 1989).

2.4 Antioxidative redox system

Antioxidants are substances that significantly delay or inhibit the oxidation of a substrate. These scavengers oppose the action of ROS and serve a protective role. An imbalance in the equilibrium of antioxidants and pro-oxidants can result in oxidative stress (OS), a phenomenon that is becoming recognized as a key element in the pathogenesis of several diseases such as cancer and male factor infertility (Bacher *et al.*, 2005; Quere *et al.*, 2001). Antioxidative defenses are divided into: 1) enzymatic or natural antioxidants including superoxide dismutase (*SOD*), catalase, glutathione (*GSH*) peroxidase, and GSH reductase; and 2) non enzymatic antioxidants which are represented by ascorbic acid (vitamin C), α-tocopherol (vitamin E), gluthatione (GSH), carotenoids, flavonoids, and other antioxidants. The activities and intracellular levels of these

antioxidants have to be balanced to assuring cell viability (Valko *et al.*, 2007). As an aim of this research, it will be focused on enzymatic or natural antioxidants.

2.4.1 Superoxide dismutase (*SOD*)

The superoxide anion is produced when the charge of an oxygen molecule is reduced by the loss of one electron, thus initiating a radical chain reaction. *Sod1* is largely cytosolic and encodes Cu-Zn-SOD, which contains Cu and Zn as metal cofactors. *Sod1* mutant mice display a pleiotropic phenotype that includes neurodegeneration, immunodeficiency, cancer predisposition, and hypersensitivity to ionizing radiation (Peled-Kamar *et al.*, 1995). Although *Sod1* knockout mice are born and develop normally, *SOD1* deficient female mice are subfertile and display a marked increase in postimplantation embryonic lethality (Ho *et al.*, 1998). *Sod1* is involved in the elimination of superoxide anions that are generated during steroideogenesis in the ovary and are present in growing follicles in the granulosa of Graafian follicles, ovulated follicles and in ovarian blood vessels (Jozwik *et al.*, 1999). Female *Sod1*$^{-/-}$ mice exhibit normal ovarian histology, including number, size, morphology of antral follicles, and morphology of corpus luteum. These results suggest that infertility in *Sod1*$^{-/-}$ female mice could possibly result from a defect in embryonic implantation or from premature death of the fetuses (Ho *et al.*, 1998). *Sod1* plays a critical role during endometrial receptivity, protecting embryo and uterus from oxygen radical cytotoxicity. High concentrations of *Sod1* have been demonstrated during the midsecretory phase of the menstrual cycle, coinciding with the period of embryo implantation (Makker *et al.*, 2006). Later in life, *Sod1*$^{-/-}$ mice develop tumors, such as hepatocarcinoma, and the rate of spontaneous mutation increases in these knockout mice (Elchuri *et al.*, 2005). *Sod1* is

known primarily as a scavenger of superoxide and is thought to interact with estrogen receptor alpha as both an enhancer for the survival of breast cancer cells and tumor progression by the regulation of estrogen responsive gene expression (Rao *et al.*, 2008; Schultz-Norton *et al.*, 2006).

In humans, it has been suggested that *Sod1* plays a role in both ovarian and breast cancer, although the mechanism is unclear. Statistically, it has been shown that the frequency of ovarian and breast cancer increases with advancing age of the patients, and accumulated oxidative damage of DNA has been implicated in the initiation of these tumors by alterations in the activity of proteins involved in the regulation of transcription. The ability of estrogen receptor α to bind to DNA is compromised in 1/3 of all estrogen receptor-positive tumors that are observed in women over 50 years of age (Merajver *et al.*, 1995). This study will explore the role of oxidative stress in female and male primordial germs cells isolated from *SOD1* knockout mice.

2.4.2 Catalase

Normally localized in the peroxisome, catalase is an enzyme that eliminates H_2O_2, and therefore, it serves to protect the cell from the potentially toxic effects of hydrogen peroxide by catalyzing its decomposition into molecular oxygen and water without the production of free radicals (Zámocký and Koller, 1999). Senthil K, *et al*., (2004), observed low levels of catalase, as an antioxidant defense mechanism, in patients diagnosed with ovarian cancer. There are two possible explanations for low catalase concentration that is seen in ovarian cancer: 1) increased peroxidation gives rise to high concentration of lipid peroxides that need to be removed by catalase and 2) catalase

sequestration by tumor cells. These observations are related to, and consistent with, high concentrations of circulating lipid peroxides measured from the same patients.

2.4.3 Glutathione peroxidase (*GPX1*)

GPX1 is an abundant and ubiquitously expressed selenoprotein and functions as a major intracellular peroxide-scavenging enzyme. It utilizes glutathione as a substrate to catalyze the reduction of H_2O_2 and lipid peroxides. The *GPX1* knockout mouse shows an increased susceptibility to oxidative injuries, such as those induced by paraquat, whereas *Gpx* overexpressing transgenic mice have been shown to be more resistant to ROS stress that *Gpx* knockout mice (Badran W, unpublished data). Transgenic mice that overexpress *Gpx* and *Sod1* have an increased incidence of tumorigenesis in 12-O-tetradecanoylphorbol-13-acetate (TPA) induced skin carcinogenesis, indicating the importance of precise redox homeostasis (Lu *et al.*, 2007).

2.5 Genomic instability

Genomic instability (GI) is defined as the increased rate of acquisition of alterations in the somatic and/or germinal genome (Barber *et al.*, 2004). GI is one of the hallmarks of cancer, and it is caused by the increasing instability of mitotic and meiotic pathways. GI, associated with the development of a tumor phenotype, is also usually associated with the loss of function of one or more genes involved in mismatch repair (MMR). Most of the genes required for MMR are expressed in the soma. However, two of these genes, *PMS2* (male) and *MLH1* (female), are expressed in both the germline and soma, and they have relevance to germ cell function (Prolla *et al.*, 1998; Baker *et al.*, 1996).

GI is used to track tumor progression in somatic cell tumors, particularly in tumors associated with human non polyposis colorectal cancer (HNPCC) (Fearnhead, *et al.*, 2002). Indeed, tumor-specific GI is usually marked by either microsatellite instability (MSI) or chromosomal instability (CI) (Umar *et al.*, 2004). MSI is characterized by expansion or contraction of the repeat motifs and can induce mutations within microsatellites (Umar *et al.*, 2004), whereas CI refers to an elevated rate of gain or loss of whole or parts of chromosomes in each cycle of cell division (Lengauer *et al.*, 1997). However, while these two indicators usually do not occur in the same tumor or at the same time, these two events are not 100% mutually exclusive (Loeb, 2001).

More recently, a similar "mutator phenotype" has been linked to germ cell tumors in the male. Notably, germline-specific GI has been shown to be ROS induced, and although MMR may be either disrupted or insufficient in the presence of ROS, MMR gene mutation is not the direct inducer of germline-specific GI (Megid *et al.*, 2007; Bacher *et al.*, 2005). Indeed, specific microsatellite repeats have been shown to be ROS sensitive, however most of these markers are stable in somatic cell MMR deficient tumors, indicating that although MMR may be compromised, ROS has the ability to directly induce genomic instability.

ROS has been shown to directly induce GI in the testis, in ROS-sensitive mouse models, and in fibroblasts subjected to free radical challenge (Megid *et al.*, 2007). CI and loss of heterozygocity, measured as germline aneuploidy, occur as both parallel and independent pathways to germline specific GI. This has also been demonstrated in human subfertile testis and in developed seminomas (Bacher *et al.*, 2004). Furthermore, ROS induces mutation patterns that are similar to those described in MMR deficient

tumors. However, the extent and expression of this germline specific GI has not been fully defined and is part of the aim of this dissertation.

Generally, CI is associated with the suppressor pathways for aneuploid cancers, while MSI underlies the mutator pathways for diploid cancers (Imai and Yamamoto, 2007). The CI phenotype is found in 85% of sporadic cancers and is characterized by aneuploidy, multiple chromosomal rearrangements, and accumulation of somatic mutations in oncogenes, such as *k-ras*, and tumor suppressor genes, such as *APC* and *p53* (Liu and Bodmer, 2006; Lamlum *et al.*, 2000). MSI occurs in more than 90% of hereditary colon cancers as well as in about 15% of sporadic cancers that develop in the bladder, lung, stomach, and endometrium. MSI is associated with small insertions and deletions of the repetitive sequences found in microsatellites (Imai and Yamamoto, 2007). Interestingly, the occurrence of the entire latter group of tumors is associated with smoking or exposure to environmental mutagens that are ROS-mediated (Yauk *et al.*, 2007; Sommers *et al.*, 2004). MSI is an important element of the phenotype of cells that are deficient in MMR, and consequently, it is a marker of risk for familial predisposition or secondary malignancies in a range of hereditary cancers including colon, endometrial, intestinal, gastric, renal and ovarian cancers (Soliman and Lu, 2007).

When GI is diagnosed in a somatic cell MMR deficient tumor, the relative frequency of individual cells that exhibit new mutant alleles, MSI, or loss of heterozygosity is high when compared with the wildtype cells. MSI can be accurately measured by small pool PCR amplification of a panel of markers that has been shown to be the first to exhibit instability in MMR deficient tumors (Megid *et al.*, 2007; Bacher *et al.*, 2005). Microsatellites are regions of DNA in which there are stretches of repeat motifs, ranging from mononucleotide $(T)_{30}$ to hexanucleotide $(CCAAGT)_9$ repeats.

When the microsatellite repeat length in a tumor differs from those found in normal tissue, this is indicative of an abnormally functioning DNA MMR mechanism. The National Institutes of Health has identified a standard panel of microsatellites (*BAT25, BAT26, D5S346, D2S123*, and *D17S250*) that are clinically diagnostic of MSI in MMR deficient tumors (Umar, 2004). In addition, five supplemental markers are commercially available for use for clinical diagnosis and monitoring the progression of MMR deficient tumors (NR21, NR24, BAT40, TGF-B receptor, and D18S58) (Promega MSI Multiplex System). By convention, allelic mutations in none, 1 or >2 of the five microsatellites is indicative of a MSI-stable (MSI-S), MSI-low (MSI-L) or MSI-high (MSI-H) tumor, respectively.

2.6 DNA repair mechanisms

DNA and cell cycle integrity are challenged by the damaging effect of numerous chemical and physical agents (endogenous-spontaneous and exogenous-environmental) that usually produce single and/or double DNA strand breaks. Eukaryotic cells have multiple responses to counteract the deleterious effects of DNA damage (Friedberg *et al.*, 2004). Once DNA damage has been detected, different DNA repair mechanisms are initiated to prevent genomic instability or DNA mutations. In addition, cell cycle checkpoints are activated to arrest cell cycle progression giving enough time for repair before mutations are passed to new cell generations, and the induction of transcriptional processes enhances DNA repair pathways. Indeed, it has been proposed that much of the DNA repair machinery has evolved to contend with DNA damage generated by the byproducts of normal cellular metabolism such as ROS, endogenous alkylating agents, and DNA single- and double-strand breaks resulting from collapsed DNA replication

forks or from oxidative destruction of deoxyribose residues (Peterson and Cote, 2004). Failure to repair such lesions leads to a deleterious mutation rate, genomic instability, initiation and/or progression of neoplasia, or apoptosis (Peterson and Cote, 2004) (Figure 2.3). All of these processes are carefully coordinated so that genetic material is faithfully maintained, duplicated, and segregated within the cell (Lindahl, 1999).

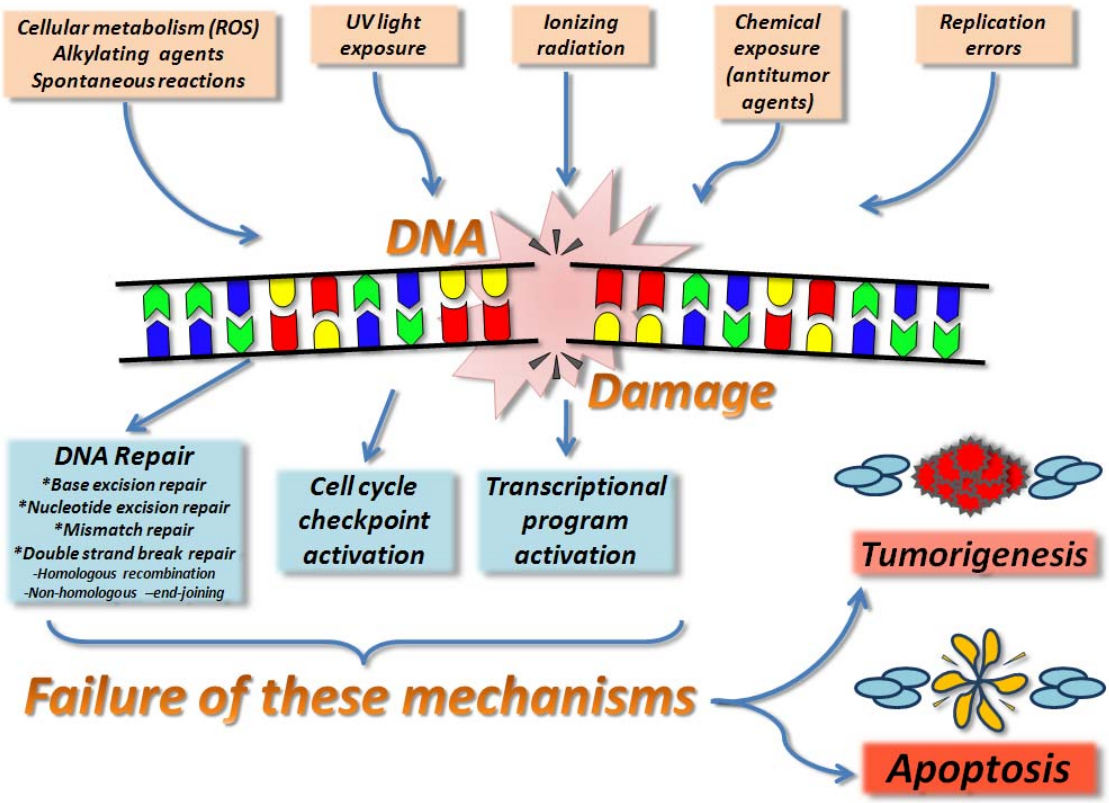

Figure 2.3 Various sources of DNA damage and alternative response pathways

Notes: Endogenous (cellular) and exogenous (environmental) sources can cause DNA damage. The cellular answer for these noxious effects may involve the use of various DNA repair mechanisms, cell cycle checkpoint proteins, use of transcriptional programs, and if the damage is severe and the cell is unable to repair its genomic content, tumorigenesis or initiation of apoptosis occurs. Adapted from Peterson and Cote, 2007.

2.6.1 Homologous recombination (HR) and non-homologous end joining (NHEJ)

Double strand breaks (DSBs) are the most serious form of DNA damage. As a consequence of this, cells can face problems in transcription, DNA replication, and chromosomal duplication, leading to impaired gene expression and tumorigenesis (Hoeijmakers, 2001). To neutralize the detrimental effects of these potent lesions, cells have two different pathways of DSB repair: Homologous recombination (HR) and non-homologous end joining (NHEJ). The cellular decision as to which pathway to use is influenced by the current cell cycle stage at the time of damage acquisition (Takata *et al.*, 1998). HR takes place before the cell enters mitosis (S, and G2 cell cycle phases) during and immediately after DNA replication. In contrast, NHEJ is predominately of the G1 phase, when the cell is growing and it is not ready to divide. HR-directed repair is a major pathway used by all eukaryotic cells to repair DSBs due to environmental insults such as ionizing radiation or chemical exposure, endogenously generated ROS, replication of single-stranded DNA breaks, and mechanical stress on the chromosomes. This pathway uses a mechanism that retrieves genetic information from homologous, undamaged DNA molecules. The majority of HR-based repair takes place in late S- and G2- phases of the cell cycle once an undamaged sister chromatid is available as a template. This mechanism requires members of the *RAD 52* epistasis group of genes, which are highly conserved among all eukaryotes (Peterson and Cote, 2004). This gene group includes *RAD50, RAD51, RAD52, RAD52D, RAD54*, *RAD57* and *MRE11*. The *RAD52* protein itself is thought to be the initial sensor of the DNA rupture. After detection of the DSBs, the 5' strands are resected, producing long 3' single stranded DNA tails that then serve as a substrate for assembly of a *RAD51* nucleoprotein filament (Peterson and Cote, 2004). This presynaptic complex also contains *BRCA1, BRCA2,*

NBS1, RPA, RAD50, *RAD52, RAD54,* and several additional *RAD51*-related proteins as accessory factors in filament assembly (Jackson, 2002). The *RAD51* nucleoprotein filament complex then searches the genome for DNA sequence homology for subsequent strand invasion (referred to as DNA strand exchange) and serves as a homologous repair template. Once a joint molecule is formed, the incoming DNA strand is extended by DNA branch migration and subsequent ligation by DNA ligase I yields a heteroduplexed DNA structure. This recombination intermediate is then resolved and ultimately leads to the restoration of genetic information spanning the break, resulting in an error-free correction of the DSB (For review see Peterson and Cote, 2004; Jackson, 2002).

Cells in G1 phase, however, have only the homologous chromosome for recombination repair, making it difficult to find within the entire genome. NHEJ, as an alternative pathway, does not require a homologous template for repairing DSB. Essential to NHEJ, the heterodimer *Ku70/Ku80* protein complex simply links, protects, aligns, approximates the ends, and recruits other NHEJ factors such as DNA protein kinase, *XRCC4*, and DNA ligase IV to the site of DNA damage. Phosphorylation of *p53*, *Ku*, and the DNA ligase IV cofactor *XRCC4* by DNA protein kinase facilitates the repair process. Also, the *MR11/RAD50/NBS1* complex, *FEN-1*, and Artemis proteins have nuclease activity that leads to a relatively uncomplicated and direct repair of the DNA damage. The final step in NHEJ repair is the ligation of the DNA ends by ligase IV, *XRCC4*, and the *Ku* complex (Jackson, 2002).

2.6.2 DNA base excision repair (BER)

Base excision repair (BER) is a process that corrects non-bulky damage to bases resulting from oxidation, methylation, deamination, or spontaneous loss of the DNA base

itself (Memisoglu and Samson, 2000). The BER process is responsible for the repair of oxidized and alkylated DNA bases, as well as abasic sites generated by spontaneous depurination (Lindahl, 2000). In general, DNA lesions that are appropriate for BER include those that do not distort the DNA backbone sufficiently to stall DNA replication forks. BER has two pathways: 1) a short patch repair pathway that replaces the lesion with a single nucleotide (represents 80 – 90% of all BER), and 2) a long patch repair pathway that replaces the lesion with approximately 2 to 10 nucleotides (represents 10-20% of all BER). Perhaps the most prevalent and highly mutagenic of the DNA lesions that must be corrected by BER is the oxidized base, 8-oxoguanine (also known as 8-oxoG or 8-oxo-7,8-dihydroguanine), which can base pair efficiently with either cytosine or adenine. If left undetected, 8-oxoG results in G:C → T:A transformations, which are the second most common mutation found in human cancers (Bruner *et al.*, 2000). Consequently, inactivation of the BER pathways can be highly mutagenic, cause genomic instability, and is a significant threat to genome fidelity.

2.6.3 DNA nucleotide Excision Repair (NER)

Nucleotide excision repair (NER) is a versatile mechanism for DNA damage removal that repairs a multitude of DNA lesions, including major types of damage induced by environmental sources (de Laat, 1999). This mechanism removes DNA lesions (pyrimidine dimers), especially caused by exposure of DNA bases to ultraviolet (UV) radiation. The NER mechanism removes genome lesions characterized by helical distortions of the DNA duplex and those that cause a modification of the DNA chemistry. NER uses one of two pathways to repair DNA damage: 1) global surveillance and repair of the genome, and 2) blocking of elongation of transcription complexes (Peterson and

Cote, 2004; de Laat, 1999). NER is also a repair mechanism that is generally used to repair expansion sequences in microsatellites due to effects of ROS damage (Volker *et al.*, 2001). Two clinical conditions have brought considerable insight into understanding the NER human process. These disorders, caused by a recessive allele, are known as xeroderma pigmentosum (XP) and cockayne syndrome (CS), and they are genetically heterogeneous. Individuals affected with either of these diseases show severe UV hypersensitivity. Mutations in one of seven genes (XPA to XPG) can cause XP syndrome, and mutations in one of two genes (CSA or CSB) can cause CS syndrome. Gene products of XP syndrome perform different functions during DNA damage recognition and DNA incision, whereas gene products of CS are required for NER-based repair of transcriptionally active genes (Lindahl, 2000; Hess *et al.*, 1997).

2.6.4 DNA mismatch repair (MMR)

A critical pathway, known as DNA mismatch repair (MMR), is another way to prevent deleterious effects and ensure the integrity of the genome. This pathway corrects DNA mismatches generated during DNA replication, thereby preventing mutations from becoming permanent in dividing cells. Errors such as base to base mismatches and insertion/deletion loops (IDLs), that could originate as a consequence of DNA polymerase misincorporation of base pairs or from template slippage can be repaired by the MMR mechanism. Defects in MMR increase the spontaneous mutation rate that is associated with hereditary and sporadic human cancers (Li, 2008). Equally, inactivation of MMR leads to the occurrence of unrepaired deletions in mono-and dinucleotide repeats, resulting in variable lengths of these repeats. This is called microsatellite instability (MSI), which can, therefore, be used as a marker for MMR deficiency. MSI

can be caused by genetic or epigenetic inactivation of several genes involved in MMR. Generally, MMR gene knockout mice exhibit a mutator phenotype, are MSI-positive, and are cancer prone (Wei *et al.*, 2002; Buermeyer *et al.*, 1999; Prolla *et al.*, 1998).

The MMR mechanism has critical steps in that the DNA damage (mismatched nucleotide or IDL) is recognized, a base pair sequence containing the lesion is excised, and the strand is fixed by DNA repair synthesis and re-ligation (Marti *et al.*, 2002). The MMR pathway is initiated by DNA damage (mismatch or IDL) recognition by *MSH2-MSH5* and *MSH2-MSH3* heterodimers, known as MutS alpha and MutS beta, respectively. MutS alpha identifies the predominant base to base mismatch and the single-base IDL, whereas MutS beta identifies larger IDLs. Following the lesion identification, MutS alpha or beta binds to ATP which changes its conformational structure and translocating along the DNA away from the site of the damage until new additional proteins are encountered such as *MLH1-PMS2* and *MLH1–PMS1* (Hsieh and Yamane, 2008). Higher order protein complexes are then originated, including those containing the heterodimeric proteins of *MLH1-PMS2* and *MLH1–PMS1* (MutL alpha beta, respectively), *MLH1* and *MLH3*, and replication factors. Interaction between MutL alpha and the replication accessory factor, *PCNA*, have an effect on strand discrimination. This interaction provides a physical link between DNA lesion recognition and identification of the newly synthesized DNA strand at the replication fork. Excision and synthesis of the corrected strand (including the mismatched nucleotide or IDL) is performed by different factors (eg. *PCNA, RPA, RFC*, exonuclease I, DNA polymerases delta and epsilon, endonuclease *FEN1*, and others).

In this study, we will explore the relationship of ROS and the MMR pathway (*MLH1* null ovarian cell line) in female ovarian development and tumorigenesis. MMR

genes with dual somatic and germ cell expression patterns are of particular interest, specially the gene *MLH1*. Abnormal methylation patterns in the *MLH1* promoter have been associated with inactivation of this MMR gene in 10 to 15% of sporadic colorectal cancers that exhibit MSI-High (Herman *et al.*, 1998). *MLH1* deficient mice display genomic instability and are susceptible to tumors such as lymphoma, skin, and ovarian tumors (Baker *et al.*, 1996). *MLH1* knockout mice exhibit MSI and sensitivity to tumor formation associated with an infertile germline phenotype (Prolla *et al.*, 1998; Baker *et al.*, 1996).

2.6.4.1 MLH1

Germline hemi-allelic methylation of *MLH1* is referred to as an epimutation and has been reported to be a cause of tumorigenesis (Herman *et al.*, 1998). Endometrial cancers have been associated with hypermethylation of the promoter region of *MLH1* (Veigl *et al.*, 1998). This type of methylation pattern is analogous to the "methylator phenotype" that is associated with somatic cell tumors and was first described by Markowitz and Vogelstein (1994). Tissues that exhibit a methylator phenotype are genomically unstable. However, the instability is measured by the occurrence of aberrant methylation patterns of genes required in normal cell cycles. These changes in methylation may result in complete gene silencing (hypermethylation) at a time when the gene should normally be turned on, or a failure to silence the gene (hypomethylation) at a time when the gene should normally be turned off.

2.6.4.2 BRCA1 gene (breast cancer 1)

The *BRCA1* gene appears to be a signal sensor and it participates in different mechanisms of response to several types of DNA damage. *BRCA1* is important for the

repair of DNA double strand breaks by the homologous recombination repair mechanism. Cells that lack this protein repair these lesions by alternative mechanisms which are prone to errors (Evers and Jonkers, 2006). *BRCA1* has not been found to be mutated in sporadic ovarian or breast cancer (Merajver *et al.*, 1995). In this study, we will analyze the relationship between *BRCA1* as a factor that participates in DNA repair response in MSI on ovarian tumor cell lines and its role in ROS damage as an inducer of tumorigenesis. To this end, we will use one ovarian tumor cell line, *BRCA 1* negative, and its wild type pair.

2.7 References

Adashi EY. (1994) Endocrinology of the ovary. Hum Reprod 9:815-827.

Agarwal A, Gupta S, and Sharma RK. (2005) Role of oxidative stress in female reproduction. Reprod Biol Endocrinol 3:28-49.

American Cancer Society. (2009) Cancer Facts and Figures. American Cancer Society, Inc.; Atlanta, GA. Available at: http://www.cancer.org/docroot/CRI/content/. Accessed February 02, 2010.

Bacher JW, Abdel Megid WM, Kent-First MG, and Halberg RB. (2005) Use of mononucleotide repeat markers for detection of microsatellite instability in mouse tumors. Mol Carcinog 44:285-292.

Bacher JW, Flanagan LA, Smalley RL, Nassif NA, Burgart LJ, Halberg RB, Megid WM, and Thibodeau SN. (2004) Development of a fluorescent multiplex assay for detection of MSI-high tumors. Dis Markers 20:237-250.

Badgwell D, and Bast RC Jr. (2007) Early detection of ovarian cancer. Dis Markers 23:397-410.

Baker SM, Plug AW, and Prolla TA. (1996) Involvement of mouse Mlh1 in DNA mismatch repair and meiotic crossing over. Nat Genet 85:1125-1134.

Barber RC, Miccoli L, van Buul PP, Burr KL, van Duyn-Goedhart A, Angulo JF, and Dubrova YE. (2004) Germline mutation rates at tandem repeat loci in DNA-repair deficient mice. Mutant Res 554:287-295.

Bast RC Jr. (2004) Early detection of ovarian cancer: new technologies in pursuit of a disease that is neither common nor rare. Trans Am Clin Climatol Assoc 115:233-247.

Behrman HR, Kodaman PH, Preston SL, and Gao S. (2001) Oxidative stress and the ovary. J Soc Gynecol Investig 8:S40-S42.

Bogart BI, and Ort VH. (2007) Integrated Anatomy and Embryology. 1st Ed. Elsevier Inc., Philadelphia, PA.

Boyd J. (2003) Specific Keynote: hereditary ovarian cancer: what we know. Gynecol Oncol 88:S8-S10.

Brown GJ, St John DJ, Macrae FA, and Aittomäki K. (2001) Cancer risk in young women at risk of hereditary nonpolyposis colorectal cancer: implications for gynecologic surveillance. Gynecol Oncol 80:346-349.

Bruner, SD, Norman, DP, and Verdine, GL. (2000) Structural basis for recognition and repair of the endogenous mutagen 8-oxoguanine in DNA. Nature 403:859–866.

Buermeyer AB, Deschenes SM, Baker SM, and Liskay RM. (1999) Mammalian DNA mismatch repair. Annu Rev Genet 33:533-564.

Chene G, Penault-Llorca F, Le Bouëdec G, Mishellany F, Dauplat MM, Jaffeux P, Aublet-Cuvelier B, Pouly JL, Dechelotte P, and Dauplat J (2009) Ovarian epithelial dysplasia after ovulation induction: time and dose effects. Hum Reprod 24: 132-138.

Dauplat J, Chene G, Pomel C, Dauplat MM, Le Bouëdec G, Mishellany F, Lagarde N, Bignon YJ, Jaffeux P, Aublet-Cuvelier B, Dechelotte P, Pouly JL, and Penault-Llorca F. (2009) Comparison of dysplasia profiles in stimulated ovaries and in those with a genetic risk for ovarian cancer. Eur J Cancer 45:2977-2983.

de Laat WL, Jaspers NG, and Hoeijmakers JH.. (1999) Molecular mechanism of nucleotide excision repair. *Genes & Dev* 13:768-785.

DiNapoli L, and Capel B. (2007) SRY and the standoff in sex determination. Mol Endocrinol 22(1):1-9.

Dubrova YE, Ploshchanskaya OG, Kozionova OS, and Akleyev AV. (2006) Minisatellite germline mutation rate in the Techa River population. Mutat Res 602:74-82.

Dubrova YE. (2005) Radiation-induced mutation at tandem repeat DNA loci in the mouse germline: spectra and doubling doses. Radiat Res 163:200-207.

Elchuri S, Oberley TD, Qi W, Eisenstein RS, Jackson Roberts L, Van Remmen H, Epstein CJ, and Huang TT. (2005) Cu-Zn SOD deficiency leads to persistent and widespread oxidative damage and hepatocarcinoma later in life. Oncogene 24:367-380.

Elvin J, and Matzuk M. (1998) Mouse models of ovarian failure. Rev Reprod. 3:183-195.

Evers B, and Jonkers J. (2006) Mouse models of BRCA and BRCA2 deficiency: past lessons, current understanding and future prospects. Oncogene 25:5885-5897.

Farley J, Ozbun LL, and Birrer MJ. (2008) Genomic analysis of epithelial ovarian cancer. Cell Res 18:538-548.

Fearnhead NS, Wilding JL, and Bodmer WF. (2002) Genetics of colorectal cancer: hereditary aspects and overview of colorectal tumorigenesis. Br Med Bull 64:27-43.

Fathalla MF. (1971) Incessant ovulation--a factor in ovarian neoplasia? Lancet 2:163.

Friedberg EC, McDaniel LD, and Schultz RA (2004) The role of endogenous and exogenous DNA damage and mutagenesis. Curr Opin Genet Dev14:5-10.

Ginsburg M, Snow MH, and McLaren, A. (1990) Primordial germ cells in the mouse embryo during gastrulation. Development 110:521-528.

Halliwell B, Gutteridge JM, and Cross CE. (1992) Free radicals, antioxidants, and human disease. J Lab Clin Med 19:598-620.

Herman JG, Umar A, Polyak K, Graff JR, Ahuja N, Issa JP, Markowitz S, Willson JK, Hamilton SR, Kinzler KW, Kane MF, Kolodner RD, Vogelstein B, Kunkel TA, and Baylin SB. (1998) Incidence and functional consequences of MLH1 promoter hypermethylation in colorectal cancer carcinoma. Proc Natl Act Sci USA 95:6870-6875.

Hess MT, Schwitter U, Petretta M, Giese B, and Naegeli H. (1997) Bipartite substrate discrimination by human nucleotide excision repair. Proc Natl Acad Sci USA 94:6664-6669.

Ho YZ, Magnenat JL, Gargano M, and Cao J. (1998) The nature of antioxidant defense mechanisms: a lesson from transgenic studies. Environ Health Perspect 106 (suppl 5): 1219-1228.

Hoeijmakers JH (2001) Genome maintenance mechanisms for preventing cancer. Nature 411:366-374.

Hsieh P, Yamane K. (2008) DNA mismatch repair: molecular mechanism, cancer, and ageing. Mech Ageing Dev 129:391-407.

Imai K, and Yamamoto H. (2007) Carcinogenesis and microsatellite instability: the interrelationship between genetics and epigenetics. Carcinogenesis 29:673-680.

Jackson SP (2002) Sensing and repairing DNA double-strand breaks. Carcinogenesis 23: 687-696.

Jemal A, Siegel R, Xu J, and Ward E. (2010) Cancer statistics 2010. CA Cancer J Clin [Epub ahead of print]

Jozwik M, Wolczynski S, and Szamatowicz M. (1999) Oxidative stress markers in preovulatory follicular fluid in humans. Mol Hum Reprod 5:409-413.

Labosky PA, Barlow DP, and Hogan BL. (1994) Mouse embryonic germ (EG) cell lines: transmission through the germline and differences in the methylation imprint of insulin-like growth factor 2 receptor (Igf2r) gene compared with embryonic stem (ES) cell lines. Development 120:3197-3204.

Lamlum H, Al Tassan N, and Jaeger, E. (2000) Germline APC variants in patients with multiple colorectal adenomas, with evidence for the particular importance of E1317Q. Hum Mol Genet 9:2215-2221.

Lawson KA, and Hage WJ. (1994) Clonal analysis of the origin of primordial germ cells in the mouse. Ciba Found Symp182:68-84.

Lengauer C, Kinzler KW, and Vogelstein B. (1997) Genetic instability in colorectal cancers. Nature 386:623-627.

Li GM. (2008) Mechanisms and functions of DNA mismatch repair. Cell Research 18:85-98.

Lindahl T, and Wood RD. (1999) Quality control by DNA repair. Science 286:1897-1905.

Lindahl T. (2000) Suppression of spontaneous mutagenesis in human cells by BER. Mutat Res 462:129-135.

Liu Y, and Bodmer WF. (2006) Analysis of P53 mutations and their expression in 56 colorectal cancer cell lines. Proc Natl Acad Sci USA 103:976-981.

Loeb L. (2001) A Mutator phenotype in cancer. Cancer Res 61:3230-39.

Lu W, Ogasawara MA, Huang P. (2007) Models of reactive oxygen species in cancer. Drug Discov Today Dis Models 4:67-73.

Lynch HT, Smyrk T, and Lynch J. (1997) An update of HNPCC (Lynch Syndrome) Cancer Genet Cytogenet 93:84-99.

Makker A, Bansode FW, Srivastava VM, and Singh MM. (2006) Antioxidant defense system during endometrial receptivity in the guinea pig: effect of ormeloxifene, a selective estrogen receptor modulator. J Endocrinol 188:121-134.

Markowitz S, Wang J, Myeroff L, Parsons R, Sun L, Lutterbaugh J, Fan RS, Zborowska E, Kinzler KW, and Vogelstein B. (1994) Inactivation of the type II TGF-beta receptor in colon cancer cells with microsatellite instability. Science 268:1336-1338.

Marsden J, and Sturdee D. (2009) Cancer issues. Best Pract Res Clin Obstet Gynecol 23:87-107.

Marti TM, Kunz C, and Fleck O. (2002) DNA mismatch repair and mutation avoidance pathways. J Cell Physiol 191:28-41.

Megid WA, Ensenberger MG, Halberg RB, Stanhope SA, Kent-First MG, Prolla TA, and Bacher JW. (2007) A novel method for biodosimetry. Radiat Environ Biophys 46:147-154.

Mello-Filho AC, Hoffman ME, and Meneghini R. (1984) Cell killing and DNA damage by hydrogen peroxide are mediated by intracellular iron. Biochem J 218:273-275.

Memisoglu A, and Samson L (2000) Base excision repair in yeast and mammals. Mutat Res 451(1-2):39-51.

Merajver SD, Pham TM, Caduff RF, Chen M, Poy EL, Cooney KA, Weber BL, Collins FS, Johnston C, and Fran TS (1995) Somatic mutations in the BRCA 1 gene in sporadic ovarian tumors. Nat Genet 9:439-443.

Ness RB, and Cottreau C. (1999) Possible role of ovarian epithelial inflammation in ovarian cancer. J Natl Cancer Inst 91:1459-1467.

Okatani Y, Morioka N, Wakatsuki A, Nakano Y, Sagara Y. (1997) Role of the free radical-scavenger system in aromatase activity of the human ovary. Horm Res 39:22-27.

Peled-Kamar M, Lotem J, Okon E, Sachs L, and Groner Y. (1995) Thymic abnormalities and enhanced apoptosis of thymocites and bone marrow cells in transgenic mice overexpresing Cu-Zn SOD: implication in Down Syndrome. EMBO 14:4985-4993.

Peterson C, and Cote J. (2004) Cellular machineries for chromosomal DNA repair. *Genes & Dev* 18:602-616.

Pharoah PD, and Ponder BAJ. (2002) The genetics of ovarian cancer. Best Pract Res Clin Obstet Gynecol 16:449-68.

Prolla TA, Baker SM, Harris AC, Tsao JL, Yao X, Bronner CE, Zheng B, Gordon M, Reneker J, Arnheim N, Shibata D, Bradley A, and Liskay RM. (1998) Tumour susceptibility and spontaneous mutation in mice deficient in Mlh1, Pms1 and Pms2 DNA mismatch repair. Nat Genet 18:276-279.

Quere I, Mercier E, Bellet H, Janbon C, Mares P, and Gris JC. (2001) Vitamin supplementation and pregnancy outcome in women with recurrent early pregnancy loss and hyperhomocysteinemia. Fertil Steril 75:823-825.

Rao AK, Ziegler YS, McLeod IX, Yates JR, and Nardulli AM. (2008) Effects of Cu/Zn superoxide dismutase on estrogen responsiveness and oxidative stress in human breast cancer cells. Mol Endocrinol 22:1113-1124.

Risch HA, McLaughlin JR, Cole DE, Rosen B, Bradley L, Kwan E, Jack E, Vesprini DJ, Kuperstein G, Abrahamson JL, Fan I, Wong B, and Narod SA. (2001) Prevalence and penetrance of germline BRCA1 and BRCA2 mutations in a population series of 649 women with ovarian cancer. Am J Hum Genet 68:700-710.

Schoenwolf GC, Bleyl SB, Brauer P, and Francis-West PH. (2009) Larsen's Human Embryology, 4th ed. Elsevier Inc., Philadelphia, PA.

Schultz-Norton JR, McDonald WH, Yates JR, and Nardulli AM. (2006) Protein disulfide isomerase serves as a molecule chaperone to maintain estrogen receptor alpha structure and function. Mol Endocrinol 20:1982-1995.

Senthil K, Aranganathan S, and Nalini N. (2004) Evidence of oxidative stress in the circulation of ovarian cancer patients. Clin Chim Acta 339(1-2):27-32.

Skinner MK. (2005) Regulation of primordial follicle assembly and development. Hum Reprod 11:461-475.

Soliman P, and Lu K. (2007) Endometrial cancer associated with defective DNA mismatch repair. Obstet Gynecol Clin N Am 34:701-715.

Sommers CM, Mc Carry BE, Malek F, and Quinn JS. (2004) Reduction of particulae air pollution lowers the risk of heritable mutations in mice. Science 304:1008-1010.

Steuerwald NM. (2007) Maternal age-related differential global expression profiles observed in human oocytes. RBMOnline 14:700-708.

Stewart RA, and Thistlethwaite J. (2006) Routine pelvic examination for asymptomatic women--exploring the evidence. Aust Fam Physician 35:873-877.

Suzuki T, Sugino N, Fukaya T, Suguyama S, Ucla T, Takaya R, Yahima A, and Sasano H. (1999) Superoxide dismutase in normal cycling human ovaries: immunohistochemical localization and characterization. Fertil Steril 72:720-726.

Takata M, Sasaki MS, Sonoda E, Morrison C, Hashimoto M, Utsumi H, Yamaguchi-Iwai Y, Shinohara A, and Takeda S. (1998) Homologous recombination and non-homologous end-joining pathways of DNA double-strand break repair have overlapping roles in the maintenance of chromosomal integrity in vertebrate cells. EMBO J 18:5497-5508.

Tam P, and Snow MH. (1981) Proliferation and migration of primordial germ cells during compensatory growth in mouse embryos. J Embryol Exp Morph 64:133-147.

Tovalin H, Valverde M, Morandi MT, Blanco S, Whitehead L, and Rojas E. (2006) DNA damage in outdoor workers occupationally exposed to environmental air pollutants. Occup Environ Med 63:230-236.

Umar A, Boland CR, Terdiman JP, Syngal S, de la Chapelle A, Rüschoff J, Fishel R, Lindor NM, Burgart LJ, Hamelin R, Hamilton SR, Hiatt RA, Jass J, Lindblom A, Lynch HT, Peltomaki P, Ramsey SD, Rodriguez-Bigas MA, Vasen HF, Hawk ET, Barrett JC, Freedman AN, and Srivastava S. (2004) Revised Bethesda Guidelines for hereditary nonpolyposis colorectal cancer (Lynch syndrome) and microsatellite instability. J Natl Cancer Inst 96:261-268.

Umar A. (2004) Lynch syndrome (HNPCC) and microsatellite instability. Dis Markers 20:179-180.

Valko M, Leibfritz D, Moncol J, Cronin MT, Mazur M, and Telser J. (2007) Free radicals and antioxidants in normal physiological functions and human disease. Int J Biochem Cell Biol 39:44-84.

Veigl ML, Katsuri L, Olechnowicz J, Ma AH, Lutterbaugh JD, Periyasamy S, Li GM, Drummond J, Modrich PL, Sedwick WD, and Markowitz SD. (1998) Biallelic inactivation of hMLH1 by epigenetic gene silencing, a novel mechanism causing human MSI cancers. Proc Natl Acad Sci USA 95:8698-8702.

Volker M, Moné MJ, Karmakar P, van Hoffen A, Schul W, Vermeulen W, Hoeijmakers JH, van Driel R, van Zeeland AA, and Mullenders LH. (2001) Sequential assembly of the nucleotide excision repair factors in vivo. Mol Cell 8:213-224.

Wallis MC, Waters PD, and Graves JA. (2008) Sex determination in mammals-before and after the evolution of SRY. Cell Mol Life Sci 65:3182-3195.

Wei K, Kucherlapati R, and Edelman W. (2002) Mouse models for human mismatch repair gene defects. Trends Mol Med 8:346-353.

Werness BA, and Eltabbakh GH. (2001) Familial ovarian cancer and early ovarian cancer: biologic, pathologic, and clinical features. Int J Gynecol Pathol 20:48-63.

World Health Organization. (1989) Epithelial ovarian cancer and combined oral contraceptives. The WHO Collaborative Study of Neoplasia and Steroid Contraceptives. *Int J Epidemiol* 18:538-545.

Wiener-Megnazi Z, Vardi L, Lissak A, Shnizer S, Reznick AZ, Ishai D, Lahav-Baratz S, Shiloh H, Koifman M, and Dimfeld M. (2004) Oxidative stress indices in follicular fluid as measured by thermochemiluminescence assay correlate with outcome parameters in *in vitro* fertilization. Fertil Steril 82 (suppl 3):1171-1176.

Yauk CL, Berndt ML, Williams A, Rowan-Carroll A, Douglas GR, and Stämpfli MR. (2007) Mainstream tobacco smoke causes paternal germ-line DNA mutation. Cancer Res 67:5103-5106.

Zámocký M, and Koller F. (1999) Understanding the structure and function of catalases: clues from molecular evolution and in vitro mutagenesis. Prog Biophys Mol Biol 72(1):19-65.

CHAPTER III

NOVEL UNSTABLE MARKERS IN OVARIAN TUMOR INITIATION AND PROGRESSION RESULTING FROM OXIDATIVE STRESS

3.1 Abstract

Oxidative stress (OS) occurs when DNA repair mechanisms are overcome by the amount of single and double strand DNA breaks caused by an accumulation of reactive oxygen species (ROS). Microsatellite instability (MSI), characterized by changes in DNA tandem repeats, is a direct result of ROS. We hypothesize that ROS-induced genomic instability is marked by the accumulation of MSI on target sequences of DNA, leading to OS and overriding DNA repair mechanisms. In this study we induced ROS in both normal and tumor human ovarian cell lines by hydrogen peroxide (H_2O_2) exposure to determine whether MSI occurs in specific regions on the genome. Detection and quantification of MSI from 33 microsatellites, including both autosomes and sex chromosomes, were determined by single cell PCR methods. There were eight markers that demonstrated significant instability. These markers showed a linear response as a function of time in a dose-dependent manner according to cell type. Interestingly, as a part of ovarian tumor progression, ovarian tumor cells showed an increase in MSI in specific novel target genes unrelated to DNA repair. In contrast, normal ovarian cells showed instability in completely different markers. These markers are in, or near, genes that function in cell differentiation and regulation of DNA transcription. Our results indicate that the accumulation of ROS-induced damage plays a critical role at the

molecular level when unrepaired genomic instability is present during ovarian tumor initiation and progression.

3.2 Introduction

Ovarian cancer is one of the most common cancers in women in the United States. Its mortality reaches 66%, a very high rate among gynecological cancers (American Cancer Society, 2009). It is estimated that 5-12% of invasive ovarian cancers are associated with hereditary susceptibility. Familial predisposition to ovarian cancer has also been linked with other types of cancer, such as breast and colon (American Cancer Society, 2009; Brown *et al.*, 2001). Breast cancer related with ovarian cancer accounts for 10% of inherited cases (Hanson and Hodgson, 2010). This disease is caused by specific mutations of the tumor suppressor *BRCA1* gene that is involved in genomic DNA repair by homologous recombination (Hanson and Hodgson, 2010; Brown *et al.*, 2001). Hereditary nonpolyposis colorectal cancer (HNPCC), a genetic autosomal dominant cancer, increases the risk of hereditary ovarian cancer in approximately 12% of all inherited cases (Huan et al, 2008; Brown *et al.*, 2001). Germline mutations in mismatch repair genes, such as *MLH1, MSH2, MSH6, MSH3, PMS1,* and *PMS2,* may explain cancer progression in HNPCC (Boland, 2008; Huan et al, 2008; Umar, 2004; Suraweera *et al.*, 2002; Prolla *et al.*, 1998).

Proficient genome maintenance involves global DNA repair, ensuring normal cell cycle and apoptosis pathways. However, genomic DNA damage by exogenous agents is considerable, and it is estimated to be as high as 10^4 events/cell/day (Lindahl, 1993). If DNA damage is established and not repaired, the cell has several responses that trigger cell cycle arrest, programmed cell death, or uncontrolled cell proliferation. Across the

human genome there are specific target sequences that are sensitive to spontaneous DNA damage (Perucho, 1996). These sequences, known as microsatellites, can be located in or near promoters or regulatory regions (Goel *et al.*, 2010; Boland, 2008). Microsatellites are short tandem repeats of DNA that contain a 1-5 base pair repeat motif sequence that can be repeated from 10 to 30 times (Brinkmann *et al.*, 1998). Mutations in microsatellites are characterized by expansion or contraction of the repeat motifs and can induce microsatellite instability (MSI). MSI frequency varies depending on the repeat motif sequence, the chromosome affected, and neighboring sequence context. Accumulation of MSI is associated with a gradual decline in the activity of tumor suppressor genes, as well as the improper activity of oncogenes (Duval and Hamelin, 2002). Therefore, MSI has been a marker for certain forms of cancer. The National Cancer Institute (NCI) has established criteria to determine MSI in cancer. A panel of five microsatellites has been used to classify instability depending on the number of compromised markers (Umar *et al.*, 2004; Suraweera *et al.*, 2002; Boland, 1998). MSI is high (MSI-H) when more than two markers are unstable. It is low (MSH-L) when one marker is unstable, and stable (MS-S) when none of the markers are unstable (Boland, 1998). For example, HNPCC shows 90% MSI, while sporadic colorectal tumors show approximately 20% MSI (Mead *et al.*, 2007; Helleman *et al.*, 2006; Murphy *et al.*, 2006; Geisler *et al.*, 2003). However, an optimal panel of markers has not been established for hereditary ovarian cancer.

The majority of cell oncogenic pathways are sporadically triggered by exogenous factors. Exogenous agents such as genotoxic compounds (Megid *et al.*, 2007; Dubrova, 2005; Li *et al.*, 2001), tobacco smoke (Yauk *et al.*, 2007), chemicals (Vilariño-Güell *et al.*, 2003), and environmental mutagens (Sommers *et al.*, 2004) are identified as

producers of oxidative stress (OS). OS is a condition that describes widespread DNA damage caused by increased and prolonged exposure to reactive oxygen species (ROS) (Ionov *et al.*, 1993; Strand *et al.*, 1993). Chronic and persistent exposure to ROS leads to an accumulation of MSI in specific DNA repair genes, tumor suppressor genes, and cell cycle genes, leading to deficient DNA repair processes (Perucho M, 1996). These collective deficiencies in repair processes are progressive and multistep events by which cell oncogenic pathways inducing tumorigenesis are deregulated (Lu *et al.*, 2007; Halliwell *et al.*, 1992). It was shown that cells deficient in mismatch repair (MMR) mechanisms tend to accumulate MSI, giving rise to erroneous intracellular signals. These signals can result in extensive alterations in cellular processes such as chromatin modification, DNA methylation, histone phosphorylation, and protein modification (Abedini *et al.*, 2010; Cai *et al.*, 2009; Izutsu *et al.*, 2008; Hung and Chaung, 1998). As a part of these alterations, ovarian cancer cell lines have shown hypermethylation of the *hMLH1* promoter, leading to the modification of gene expression, reduced response to OS and further facilitation of the accumulation of MSI through gene replication errors (Davis *et al.*, 1998; Veigl *et al.*, 1998).

We hypothesize that ROS-induced genomic instability is marked by the accumulation of MSI in specific sequences of DNA, leading to OS and overriding DNA repair mechanisms. In the present study, we applied efficient and sensitive procedures for quantifying MSI by single cell PCR methods that allowed for the identification of low frequency mutant alleles as well as wild type alleles in each pool of the DNA sample. For this purpose, we used different markers to compare and determine MSI frequencies in both normal and tumor human ovarian cell lines that were exposed to hydrogen peroxide (H_2O_2) as a source of ROS. Our results show that the accumulation of ROS, induced by

H_2O_2 exposure, shows a corresponding increase in MSI over time. From this study, we identified specific microsatellite markers that displayed increased sensitivity to MSI and permit reliable molecular analysis in the developmental stages of ovarian cancer.

3.3 Materials and Methods

3.3.1 Cell Lines

A human epithelial ovarian cancer cell line (SKOV-3) was purchased from American Type Culture Collection, (ATCC Rockville, MD). A primary culture was initiated from a biopsied ovarian cyst obtained from a regional hospital with consent of the patient IRB # 11-088. A stromal cell line was initiated and used as the control in the experiments: normal ovarian stromal cell line (NOV). All cells were maintained in T-25 culture flasks (Falcon, Becton Dickinson Labware, Franklin Lakes, NJ). The culture medium consisted of Dulbecco's Modified Eagle Medium (DMEM), Glutamax high glucose medium (GibcoBRL, Gaithersburg, MD), supplemented with 10% heat-inactivated fetal bovine serum (GibcoBRL, Gaithersburg, MD), 30 mg/ml of L-glutamine (GibcoBRL, Gaithersburg, MD), and 1% antibiotic/antimycotic solution (Invitrogen, Carlsbad, CA). Cells were maintained at 37ºC in a humidified atmosphere with 5% CO_2.

3.3.2 In vitro exposure to ROS (H_2O_2)

Initial cell cultures were plated in triplicate at a density of 1 x 10^5 cells/cm^2. When the initial culture reached 80% confluency, cells were trypsinized and treated with 0, 10, and 30 μM concentrations of H_2O_2 (Fisher Scientific, Houston, TX) in 1X PBS (GibcoBRL, Gaithersburg, MD). Titration curves for H_2O_2 were determined in previous studies, and the concentrations of H_2O_2 were designed to achieve 80% cell viability after initial exposure (data unpublished). These cells were treated with H_2O_2 or 1X PBS for 1

hour at 37ºC in a humidified atmosphere with 5% CO_2. Cells were then centrifuged at 125 *X g* for 5 min. The supernatant was discarded, and cells were washed twice with fresh 1X PBS. Both control and treated cells were resuspended in 1ml of DMEM, and an aliquot of cells was used to measure proliferation and caspase 3/7 activity. After H_2O_2 exposure, each sample group was plated in triplicate at a density of 1 x 10^5 cells/ml and cultured at 37ºC in a humidified atmosphere with 5% CO_2.

3.3.3 Cell counting and apoptosis

The tumor and normal ovarian cells were harvested, and an aliquot (10 µl) of each sample was manually counted in a hemocytometer chamber under a microscope to determine the number of cells per ml at days 0, 3, 6, and 9 post-H_2O_2 exposure. In addition, cellular apoptosis was determined by measurement of caspase using the Glo 3/7 assay kit (Promega, Madison, WI) according to the manufacturer's instructions. A 100 µl cell suspension of 1 x 10^4 cells and 100 µl of the caspase reagent were added to each well of a 96 well plate, including medium only, untreated cells, and H_2O_2 treated cells. The plate was then incubated at room temperature for 2 hours, and the luminescence of each sample was measured with a Lmax luminometer (Molecular Devices Corporation, Sunnyvale, CA). All samples were assayed in triplicate. Luminescence was expressed as relative light units (RLU) which, according to the manufacturer's protocol, is proportional to the amount of caspase activity present in the sample.

3.3.4 Single cell PCR

DNA was purified from the cultured human cells with the ChargeSwitch® Genomic DNA Purification Kit following the manufacturer's protocol (Invitrogen Corporation, Carlsbad, CA). Previously, individual standardization of each microsatellite

marker was established by PCR methods (Parsons *et al.*, 2007; Mulero *et al.*, 2006; Butler *et al.*, 2002; Berg *et al.*, 2000). DNA genotyping was done to identify the wild type alleles by large pool PCR (0.1 ng/µl DNA) in each cell line prior to single cell PCR methods (7-14 pg/µl DNA concentration). Single cell PCR was then performed for 33 labeled microsatellites with different fluorescent dyes (FAM, HEX, NED) to allow for resolution and quality control with automatic detection by fragment analysis in an AB 3130XL Genetic Analyzer (Applied Biosystems, Foster City, CA) in the presence of Gene Scan 500 LIZ Ladder (Applied Biosystems, Foster City, CA) following the manufacturer's protocol. Out of the 33 markers used, five markers are included in the National Cancer Institute guidelines, eight have been used in previous studies on ovarian cancer, twelve have been evaluated in other types of cancers such as colon, lung, melanoma, and prostate, and seven additional markers were selected by their location on the X chromosome in critical regions that have been shown to be related with autism spectrum disorder (*ASD*) and mental retardation related to the *FRAXA* gene (Table 3.1) (Weber *et al.*, 2009; Sirchia *et al.*, 2009; Ramocki *et al.*, 2009; Gong *et al.*, 2009; Barbosa *et al.*, 2009; Trimeche *et al.*, 2008; Schweppe *et al.*, 2008; Nagarajan *et al.*, 2008; Boland et al, 2008; Prat *et al.*, 2005, Umar *et al.*, 2004; Nakayama *et al.*, 2004; Friedrichsen *et al.*, 2004; Sieben *et al.*, 2003; Funato *et al.*, 2002; Goddard *et al.*, 2001; Jirtle *et al.*, 2000).

DNA concentrations were measured with a Nanodrop ® ND-1000 spectrophotometer, and then DNA serial dilutions were made at 0.1 ng/µl, 0.05 ng/µl, and 0.025 ng/µl. Using these serial DNA dilutions, Poisson analysis of the amplified alleles was performed to calculate the correct genomic equivalent value for each sample in order to obtain less than two diploid genome equivalents of DNA (sample genome equivalents

range between 25-50 pg/µl). According to Coolbaugh-Murphy *et al.* (2004, 2005), estimates between 0.5-2 diploid genome-equivalents do not require large numbers of single cell PCR replicates for accurate data analysis. We were then able to use less than a single diploid genome-equivalent of DNA to perform single cell PCR analysis with 44-60 single cell replicates for each marker. This concentration of DNA allowed sufficient sensitivity to distinguish between wild type and mutated alleles at their appropriate frequency.

PCR amplifications were performed in a total reaction volume of 10 µl containing 1 X of buffer D [800 mM Tris HCl, 200 mM $(NH_4)_2SO_4$, 0.2% w/v Tween 20] (US DNA, Fort Worth, TX), 2.5 mM $MgCl_2$ (US DNA, Fort Worth, TX), 1 X of Solution L (US DNA, Fort Worth, TX), 1.25 U Hot-MultiTaq DNA polymerase (5 U/µl; US DNA, Fort Worth, TX), 4% DMSO (Sigma Aldrich, Saint Louis, MO), 0.4 mg/µL bovine albumin serum (Thermo Scientific, Rockford, IL), 300 µM dNTPs (Applied Biosystems, Foster City, CA), and 0.5 and 1.8 µM mixed primer (forward and reverse) respectively. Solution L (1X) was used as an additive that facilitates amplification of difficult templates. PCR was performed on a PE 9600 thermocycler using a ramping cycling protocol: 1 cycle of 95 ºC for 11 minutes; 1 cycle of 96 ºC for 1 minute; 10 cycles of [94 ºC for 30 seconds, ramp 68 seconds to 58 ºC (hold for 30 seconds), ramp 50 seconds to 70 ºC (hold for 60 seconds)]; 25 cycles of [90 ºC for 30 seconds, ramp 60 seconds to 58 ºC (hold for 30 seconds), ramp 50 seconds to 70 ºC (hold for 60 seconds)]; 1 cycle of 60ºC for 30 minutes for final extension; and hold at 4ºC. Negative controls and reaction mixtures were included in each PCR to monitor for contamination.

Products amplified by single cell PCR were separated and detected by fragment analysis on an AB 3130XL Genetic Analyzer (Applied Biosystems, Foster City, CA) in

the presence of Gene Scan 500 LIZ Ladder (Applied Biosystems, Foster City, CA) following the manufacturer's protocol. Wild type and mutated alleles were quantified by GeneMapper version 4.0 software package (Applied Biosystems, Foster City, CA). Presence of wild type and/or mutant alleles was scored in each single cell (replicate). An average of 44-60 replicates per sample were amplified and scored for both control and experimental groups.

3.3.5 Genomic instability statistical analysis

We amplified less than a single diploid genome-equivalent of DNA with single cell PCR methods to estimate oxidative stress-induced mutation frequencies in specific microsatellite repeat markers. DNA concentrations were adjusted to obtain 0.5-2 genome equivalents, on average, per single cell PCR reaction. The average number of amplifiable DNA molecules (λ) in each PCR reaction was calculated using the Poisson distribution: $\lambda = -\ln(K_1/K)$, where K_1 = the total number of alleles expected minus the number of alleles observed, and K = the total number of alleles expected as it has been described (Coolbaugh-Murphy *et al.*, 2004; Zhang *et al.*, 2002).

As mentioned, we previously determined the size of the wild type allele from each microsatellite. Repeat shifts from wild type standardized alleles are considered mutant alleles (Coolbaugh-Murphy *et al.*, 2004; Coolbaugh-Murphy *et al.*, 2005). Mutant allele cutoff levels were determined by a repeat shift greater than 3 repeats or less than 3 repeats for mononucleotide markers (e.g. *BAT26, BAT60*), a shift greater than 2 repeats or less than 3 repeats for dinucleotide markers (e.g. *D2S123*), and a shift greater than 1 repeat or less than 2 repeats for trinucleotide markers (e.g. *DXS7424*), tetranucleotides (e.g. *DXS9902, DXS6801*, *DXS6800*), and pentanucleotides (e.g. *PENTA C, PENTA D*)

(Bacher *et al.*, 2005; Bacher *et al.*, 2004; Gao *et al.*, 2008; Goel *et al.*, 2010; Idury and Cardon, 1997; Daley *et al.*, 2008; Geisler *et al.*, 2003; Helleman *et al.*, 2006; Bacon *et al.*, 2000; Sood *et al.*, 2004).

Mutation frequencies for each marker by sample type, dose, and time were calculated by SP-PCR software version 2.0 (M.D. Anderson Cancer Center, Houston, TX). Maximum likelihood estimates of the mean number of mutant alleles and wild type alleles in each pool, as well as their bootstrap standard deviations were also calculated by SP-PCR software version 1.0 (M.D. Anderson Cancer Center, Houston, TX). These analysis methods have been previously described (Coolbaugh-Murphy *et al.*, 2004). Differences in the estimation of mutation frequencies were calculated with a two tailed *t*-test using raw mutation frequencies. A three way cross class ANOVA, assuming no third factor interaction, (using Procedure GLM from statistical package SAS/win 9.2, SAS Institute Inc., Cary, NC, USA) and appropriate LSD multiple comparison (*t*-test) outputs were also produced. Results were considered statistically significant with a $p<0.05$. Total mutation frequencies for informative markers of each cell type were analyzed by Chi Squared and Fisher's Exact Test.

3.4 Results

3.4.1 ROS exposure affects ovarian cell proliferation

In contrast to normal cells, tumor cells grew with different kinetics, exhibiting quick doubling times. Throughout the treatment time both cancerous and normal ovarian cells displayed rounding up and detachment from the plate after H_2O_2 (10μM and 30μM) exposure, however the unexposed cells remained attached to the plate. We observed differences in the number of viable cells between cancerous and normal cells after H_2O_2 exposure (0μM, 10μM and 30μM) at different times (3, 6 and 9 days) (Figure 3.1). Ovarian cancer cells showed increased proliferation in contrast to normal cells ($p=0.0039$, *t*-test, Figure 3.1A). In cancerous cells, proliferation occurred steadily for all H_2O_2 concentrations (0μM, 10μM and 30μM) overtime, but was increasingly hindered as H_2O_2 concentrations increased ($p<0.05$, *t*-test, Figure 3.1A). On day 3, cancerous cells increased in number after 10μM and 30μM H_2O_2 exposure (Figure 3.1A). In contrast, normal ovarian cells grew much slower and had decreased proliferation (Figure 3.1B). Normal cells showed a viability of 60% and 35% after 10μM and 30μM H_2O_2 at 3 days, respectively. During 3-6 days after both 10 and 30 μM H_2O_2 exposure, cancerous and normal cells showed no statistically significant differences in proliferation.

3.4.2 Apoptosis occurs in ovarian cells after oxidative stress exposure

Activation of the pro-apoptotic proteins caspase 3 and 7 was caused by the initial damage created by ROS exposure. At 3 days post-exposure (10 μM and 30 μM), caspase activity increased in normal ovarian cells approximately 3-6 fold when compared with exposed tumor ovarian cells ($p=0.03$, *t*-test, Figure 3.2). The mean proportion of apoptotic cells was higher in normal ovarian cells post H_2O_2 exposure (10 μM and 30

μM) than in untreated cells (PBS with 0 μM H_2O_2) at both 3 and 6 days (3 days p=0.0037 and 6 days p=0.0045, *t*-test, Figure 3.2). In contrast, throughout treatment time (0-9 days), cancerous cells showed lower levels of apoptosis and increased tolerance to cell damage.

3.4.3 ROS induces MSI in normal and tumor ovarian cells

We investigated the capacity of H_2O_2, a source of ROS, to induce MSI in tumor and normal ovarian cell lines. We analyzed MSI post-exposure to H_2O_2 using different markers localized on autosome and sex chromosomes (Table 3.1). Normal ovarian cells showed one or two peaks at the expected size for each examined microsatellite. Both cell lines treated with H_2O_2 showed changes in the original peak pattern (Figure 3.3 A, B for *BAT 26* marker and panel F for the rest of markers). Changes in the original peak pattern indicate that these are sensitive markers for mutated peak criteria (Figure 3.3 and genomic instability statistical analysis). Normal and mutant allele sizes were estimated using an internal size standard. Alleles with a different size from the wild type allele were identified as a mutation. The total number of normal and mutated alleles was counted, and mutation frequencies per marker were calculated by SPPCR software. Not all analyzed markers showed significant mutation frequencies after ROS exposure. After statistical analysis, MSI was significantly induced in 8 out of 33 studied markers (Table 3.2). Both normal and cancerous ovarian cell lines showed unstable markers with statistical significance. Higher mutation frequencies were observed in *D2S123, BAT26, DXS6801*, and *DXS9902* markers ($p<0.05$, *t*-test, Figure 3.4). Other unstable markers were *BAT60, DXS6800, DXS7424*, and *D7S3046*, but they showed less siginificance of mutation frequency than the previously mentioned markers ($p<0.1$, *t*-test, Figure 3.4).

3.4.4 Mutation frequencies increased as a function of time in normal and tumor ovarian cell lines after ROS damage

MSI is a basic pathway in tumorigenesis. Accumulation of unrepaired DNA damage over time leads to uncontrolled cell cycle responses (Coletta *et al.*, 2008). We hypothesized that ROS induces DNA damage, which is accumulated in normal ovarian cells over time. To test this hypothesis, we measure MSI at 3, 6, and 9 days post-exposure of H_2O_2 (10 and 30 μM) to allow the DNA damage tolerance or cell repair in both cell lines. We observed MSI in *D2S123* and *BAT26* markers that increased as a function of time in normal and tumor ovarian cell lines after ROS damage. These markers showed high mutation frequencies in both cancerous and normal ovarian cells but at different points of time post-exposure. Ovarian tumor cells showed increased MSI during the first 6 days and then reached a plateau status. In contrast, normal ovarian cells did not exhibit mutation during the first three days, but increased mutation frequencies occurred after 6 days post-exposure (*D2S123* $p=0.035$ and *BAT 26* $p=0.03$, ANOVA, Figure 3.5A, 3.5B). These results suggest that normal ovarian cells accumulate DNA damage after ROS exposure, and if the damage is not promptly repaired, MSI will increase.

3.4.5 Ovarian tumor cells show high MSI in repetitive regions unrelated to DNA repair genes

DXS9902, *BAT60*, and *DXS7424* markers are localized in, or close to, genes involved in transcription and cell differentiation (Table 3.3). These markers specifically showed higher mutation frequencies in ovarian tumor cells compared to normal ovarian cells that were stable after ROS exposure (Figure 3.6). The highest frequency of MSI was observed in *DXS9902* marker in a linear dose response after H_2O_2 (10 and 30 μM) exposure of tumor cells (Figure 3.6A). These results allowed us to characterize *DXS9902*

as a highly sensitive marker to ROS damage, specifically in ovarian tumor cells (p= 0.007, F-test, Figure 3.6A). *BAT60* and *DXS7424* are also sensitive to ROS damage in ovarian tumor cells but have lower frequencies of MSI values (p=0.058, and p=0.06 respectively) compared to *DXS9902* (Figure 3.4, Figure 3.6B and Figure 3.6c).

3.4.6 Ovarian normal cells showed sensitivity to ROS in linear dose response over time

MSI frequency for markers *DXS6800, DXS6801*, and *D7S3046* was observed in normal ovarian cells at higher frequencies compared to tumor cells. In these markers, an increase in MSI frequencies was observed following a linear dose response over time (Figure 3.7). In normal cells, low H_2O_2 concentration (10 μM) displayed a plateau response until 6 days post-exposure, but at 9 days, showed an increase of MSI for these specific markers. For normal cells at high H_2O_2 (30μM) concentration, responses varied between these three markers. At 9 days, MSI frequencies increased three fold for *DXS6800* (p=0.06, F-test, Figure 3.7A) and two fold for *DXS6801* (p=0.02, F-test, Figure 3.7B). For *D7S3046*, MSI frequency increased at 6 days but not at 9 days post-exposure (p=0.1, F-test, Figure 3.7C).

3.4.7 Identification of potential biomarkers in ovarian cancer

Specific and repetitive DNA sequences showed genetic variability and could possibly play a genetic role during ovarian tumorigenesis. Comparisons were made between normal and mutated alleles that displayed sensitivity to ROS in both normal and tumor cells. Our study considered mutated allele frequencies that were <0.01 to be significant. Table 3.2 summarizes the markers that met this criteria showing the mutated and normal allele frequencies for *D2S123, BAT26, DXS9902, BAT60*, and *DXS7424*

markers. In tumor cells, mutated allele frequencies from this panel of five markers was higher (f=0.0352) in comparison to normal cells (f=0.0106) (Table 3.4). This result suggests that mutated alleles from *DXS9902, BAT60*, and *DXS7424* markers are genetically associated with ovarian cancer progression. In contrast, MSI on *D2S123* and *BAT26* markers in tumor and normal ovarian cells did not show significant differences between mean frequencies (f=0.029 and f=0.026, respectively) (Table 3.4). Taken together, these data suggest that these markers are involved in two different steps involving the accumulation of MSI during ovarian tumor initiation (*D2S123* and *BAT26*) and tumor progression (*DXS9902*, *BAT60*, and *DXS7424*) (Figure 3.8).

3.5 Discussion

Tumorigenesis is characterized by deregulation of inter-and intracellular signaling pathways. This could be caused through the gain of functional mutations that accumulate in a progressive manner, modifying genetic and epigenetic cell information. As part of this cellular deregulation, MSI has been implicated as an important pathway in tumorigenesis, including therapy resistance, tumor recurrence, and poor tumor prognosis in comparison to other genetic misbalances such as amplification of chromosomal regions or aneuploidies (Kavanagh *et al.*, 1995; Zhang *et al.*, 2008). Ovarian cancer is a model that displays these negative effects, and it continues to be one of the most fatal gynecological cancers in the United States (Jemal *et al.*, 2008).

Few assays are predictable indicators of ovarian tumorigenesis (Huan *et al.*, 2008). Therefore, it is necessary to validate new biomarkers that allow early diagnosis and promote a better understanding of molecular pathways in ovarian cancer development. The data reported in this study, based on molecular pathways and their genetic effect on the repeat sequences, has provided insights to future experiments needed to increase our understanding of mechanisms involving induced mutations and generation of MSI. There is a clear need to evaluate reliable new genetic biomarkers to monitor and predict ovarian tumor progression to increase treatment efficiency, novel therapeutic approaches, and life expectancy in patients with ovarian cancer.

We identified 8 microsatellite markers that are localized in or close to sets of genes that play a role in cellular responses after DNA damage. These genes are involved in several different inter-and intra-cellular signals including cell cycle, DNA repair, apoptosis, and tumor suppression, indicating their genetic involvement in tumorigenesis. Through MSI analysis of several markers in both normal and tumor ovarian cells after

ROS exposure, we demonstrated that some markers show MSI in specific dose-time manner. During ovarian tumor development, two steps were indicated by our results (Figure 3.8). First, we have identified (hypothetized) a tumor initiation step: MSI affecting DNA repair, indicated by our observations of MSI in markers related to DNA repair mechanisms (*BAT26* and *D2S123*). *BAT26* and *D2S123* markers are located upstream of the MMR genes (*MSH2* and *MSH6*) that have been thoroughly studied in HNPCC tumors (Table 3.3). It has been noted that DNA repair deficiencies are involved with colon cancer, as well as other types of cancer such as endometrial and ovarian. MMR pathways are also involved in different cell stress responses (Davis *et al.*, 1998). Human ovarian tumor cells that are deficient in MMR after exposure to ROS induce DNA breaks that are increasingly accumulated. This increased DNA damage then affects other novel target genes that are related to various cell stress response processes. We also demonstrated that these two specific markers, *D2S123* and *BAT26*, displayed MSI in normal ovarian cells as a time-response of ROS induced DNA damage accumulation in the cell. Further indicating this first step, tumor ovarian cells showed MSI on these markers due to their established oncogenic status itself (Figure 3.5). Second, we have identified (hypothetized) a tumor progression step: MSI on novel markers related to cell differentiation and gene transcription processes. This step was seen after DNA repair mechanisms were impaired by MSI in microsatellite markers close to MMR genes. Genetic instability was observed in these new markers (*DXS9902, BAT60*, and *DXS7424*) that are localized close to genes involved in cell differentiation and transcription processes (Table 3.3). These three markers showed higher MSI frequencies in ovarian tumor cells when compared to normal ovarian cells, suggesting that these markers play specific roles in ovarian tumor progression (Figure 3.6).

Normal ovarian cells show the same two-step process for tumorigenesis: First, these cells accumulate ROS damage that overrides MMR mechanisms during the quiescence status observed during the first 6 days post H_2O_2 treatment. Second, once the MMR mechanism is saturated, the normal ovarian cell shows MSI in different markers (*DXS 6800, DXS 6801*, and *D7S3046*) in order to acquire tumor transformation. These data indicate that in normal ovarian cells, ROS damage accumulation is key to inducing MSI first in markers related to DNA repair genes, and second in markers related to cell differentiation and gene transcription. These three markers, *DXS6800, DXS6801*, and *D7S3046* showed the highest frequency of MSI instability in normal cells when compared with ovarian tumor cells (Figure 3.7). Our results also support the idea that these unstable markers, localized in specific genes, are novel candidates to evaluate ovarian cancer risk and their role in tumor initiation step.

It is known that MSI occurs more frequently in repeat regions localized in critical points of the genome. Repeats located in or close to promoters, introns, exons, CpG islands, or 5' or 3' UTR sequences can accumulate mutations in protein coding genes that control ovarian epithelial cell growth and differentiation. Specific mutations caused by MSI can lead to protein modifications due to transcription errors or epigenetic changes (Toyota and Issa, 1999; Ahuja *et al.*, 1998; Esteller *et al.*, 2001; Armour, 2006). Table 3.3 shows the location, repeat motif and repeat-gene location of the 8 most sensitive markers. The highest MSI was reported for marker *DXS9902*, which is localized in the 5' UTR region (0.02 Mb) of the *ASB9/ASB11* (Ankyrin repeat and suppressor of cytokine signaling box containing 9/11). The two genes *ASB9* and *ASB11* are involved in intracellular signaling cascades. They are part of the E3-ubiquitin ligase complexes and mediate protein degradation through their N-terminal regions. These genes have been

implicated in relation to the aging process, cardiovascular diseases, and psychiatric disorders through the accumulation of ROS (Zubenko *et al.*, 2007). Recent reports found that the Ankyrin gene is also connected to resistant chemotherapy pathways in breast and ovarian tumor cells (Bourguignon *et al.*, 2008). In conjunction with data, this indicates that MSI in 5' UTR region of *ASB9* and *ASB11* could impair the gene function playing a key role in ovarian tumor progression, including metastasis and drug resistance. However, future experiments are needed to further test this association between MSI and functional protein modification.

Our goal in this study was to analyze MSI using novel markers to increase specificity in the ability to predict tumor progression. Our data revealed new sensitive biomarkers that had not previously been identified for molecular ovarian tumor analysis, and they are promising candidates to assess gene regulation, specifically in epithelial ovarian tissue. Some markers were more informative than others in regards to cell type or stage of tumorigenesis. We showed that *DXS9902, BAT60*, and *DXS7424* displayed a higher total mean frequency of MSI in tumor ovarian cells as part of tumor progression. Markers such as *DXS6800, DXS6801*, and *D7S3046* were more unstable in normal ovarian cells after ROS exposure. The latter three markers appear to be involved in tumor initiation, but they are not necessarily related to tumor transformation and progression.

In conclusion, our results indicate that maintenance of genome integrity is impaired by MSI through the accumulation of ROS. This can be found on triggered genes involved in other cellular processes like chromatin structure, DNA methylation, histone phosphorylation, and protein ubiquitination. As a clear result of this, the epigenetic misbalance facilitates full oncogenic pathways of transformation over the

ovarian cell epithelium (Ehrlich, 2006). The role of MSI is clearly more complex and an integral part of tumorigenesis than we had initially perceived. However, the data we generated support our hypothesis that the accumulation of MSI is the main causative factor of genomic instability that leads to OS and override in DNA repair mechanisms during tumor initiation and progression. We anticipate that the 8 novel biomarkers can be used to complement the current predictive tools for tumor progression, therapeutic efficiency, and clinical prognosis in ovarian cancer treatment.

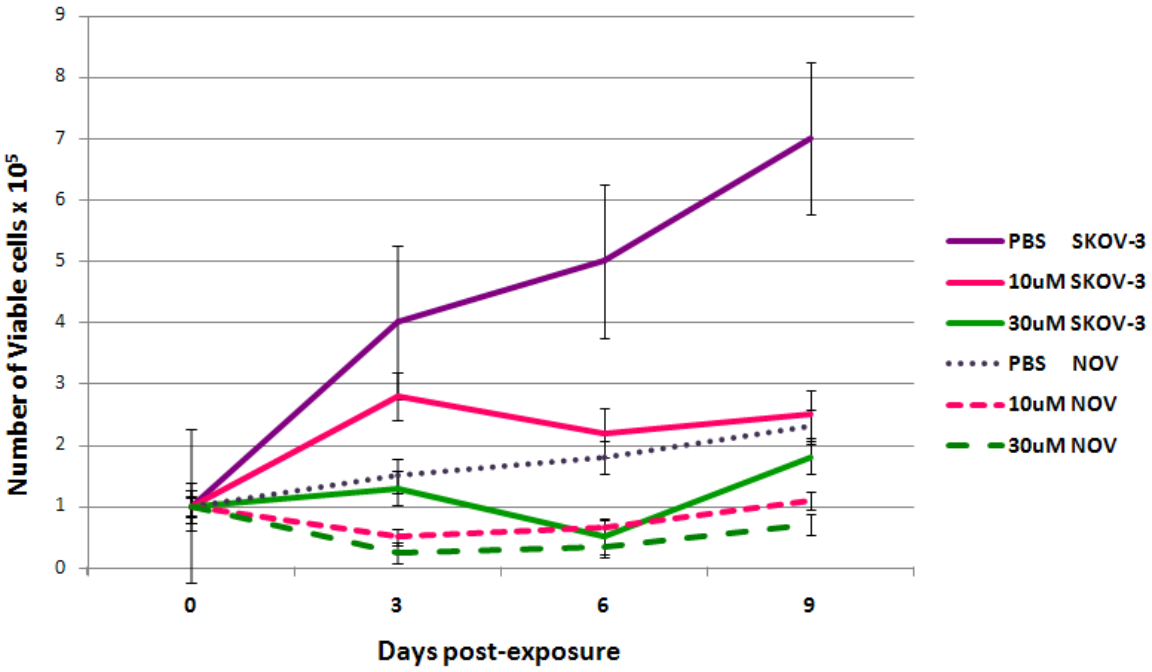

Figure 3.1 Different kinetics of ovarian normal and tumor cell proliferation

Notes: Ovarian tumor cell proliferation was significantly different compared to ovarian normal cells (p=0.0039 by t-test). Cell growth curve of ovarian tumor cells were significantly different after H_2O_2 exposure in comparison to the untreated cells (p=0.05 by t-test). Ovarian normal cell line growth differences related to the untreated cells was observed, but not found to be statistically significant. Cell cultures were treated with three different concentrations of H_2O_2 (0 µM-PBS, 10 µM, and 30 µM) and measured at 3, 6, and 9 days. Cells were harvested and manually counted in a hemocytometer chamber under a light microscope. Total cell counts reflect the total number of cells per ml at 0, 3, 6, and 9 days after H_2O_2 exposure. The values expressed in this figure represent the mean and standard error from triplicate determinations.

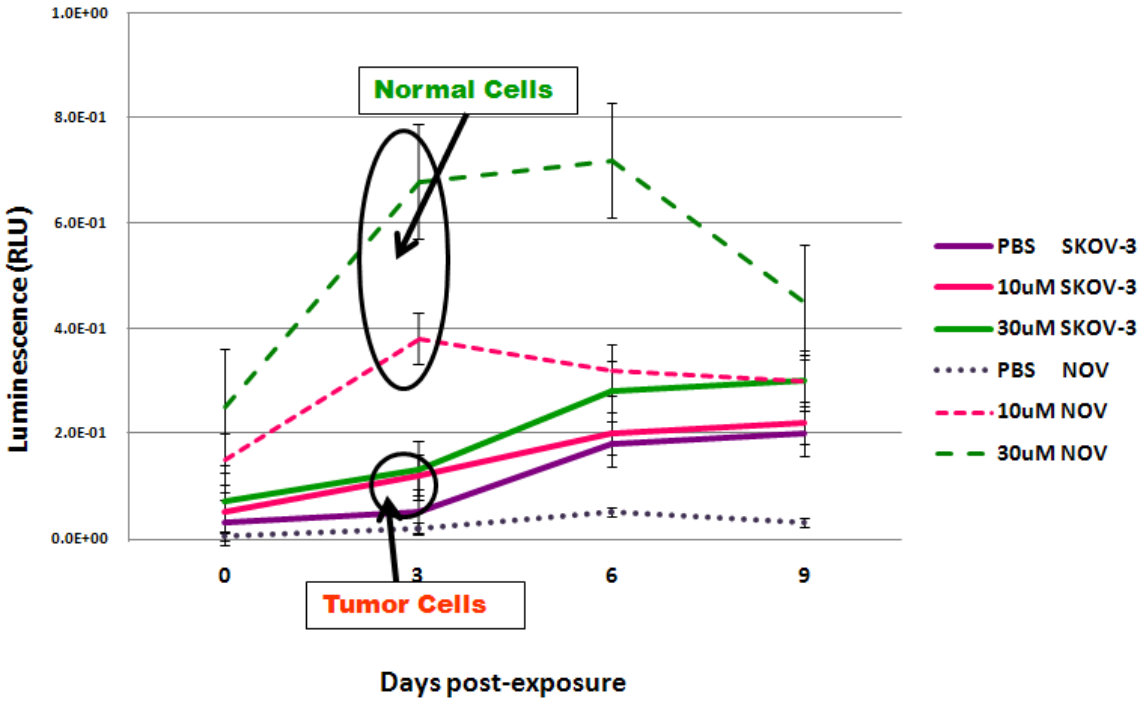

Figure 3.2 Activation of apoptotic pathways as a response of ROS damage

Notes: Caspase 3 and 7 activity was measured at 3, 6, and 9 days from ovarian tumor and ovarian normal cell line cultures treated with three different concentrations of H_2O_2 (0 µM-PBS, 10 µM, and 30 µM). Significant differences were observed between ovarian tumor and ovarian normal cells at 3 days ($p=0.03$ by t-test). Luminescence was expressed as relative light units (RLU) that were proportional to the amount of caspase activity present in the sample. The values expressed in figure represent the mean and standard error from triplicate determinations.

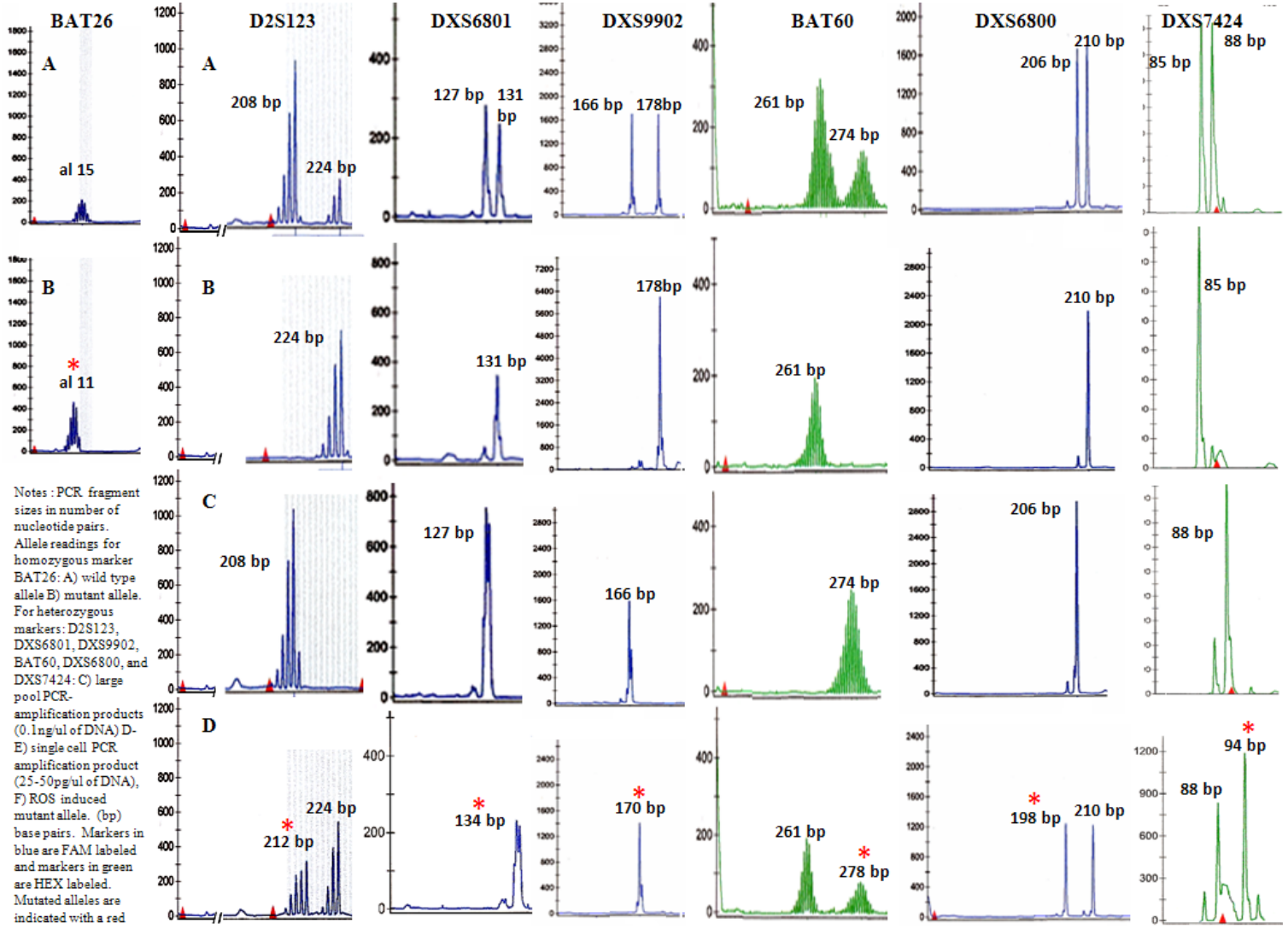

Notes : PCR fragment sizes in number of nucleotide pairs. Allele readings for homozygous marker BAT26: A) wild type allele B) mutant allele. For heterozygous markers: D2S123, DXS6801, DXS9902, BAT60, DXS6800, and DXS7424: C) large pool PCR-amplification products (0.1ng/ul of DNA) D-E) single cell PCR amplification product (25-50pg/ul of DNA), F) ROS induced mutant allele. (bp) base pairs. Markers in blue are FAM labeled and markers in green are HEX labeled. Mutated alleles are indicated with a red

Figure 3.3 Representative microsatellite electropherograms

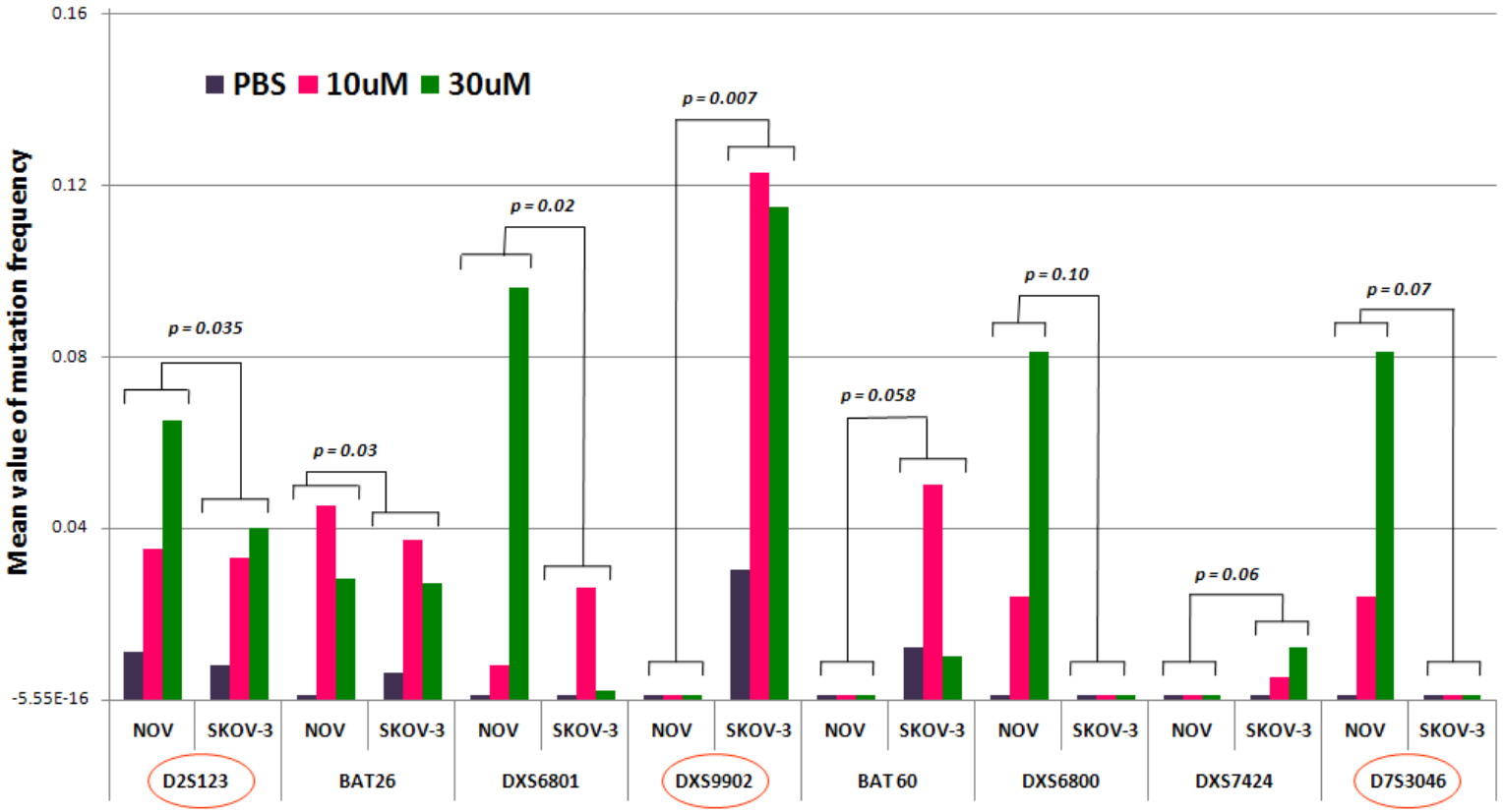

Figure 3.4 Comparison of the mutation frequency in the H_2O_2-treated versus untreated control NOV and SKOV-3 cell lines of 8 informative markers

Notes: (p-values are shown at the top of each bar). Values expressed in the figure represent the mean value of 48-60 replicates. $p<0.05$ are in bold, $p<0.10$are in italic. Mean value of mutation frequency calculated by small pool-PCR (SP-PCR) software version 1.0 (M.D. Anderson Cancer Center. Houston, TX). † D2S123 marker shows instability in untreated cells (NOV f = 0.011, SKOV f = 0.008) but it was not significative in comparison with its reported spontaneous mutation frequency (f = 0.024) (Bacon et al., 2000).

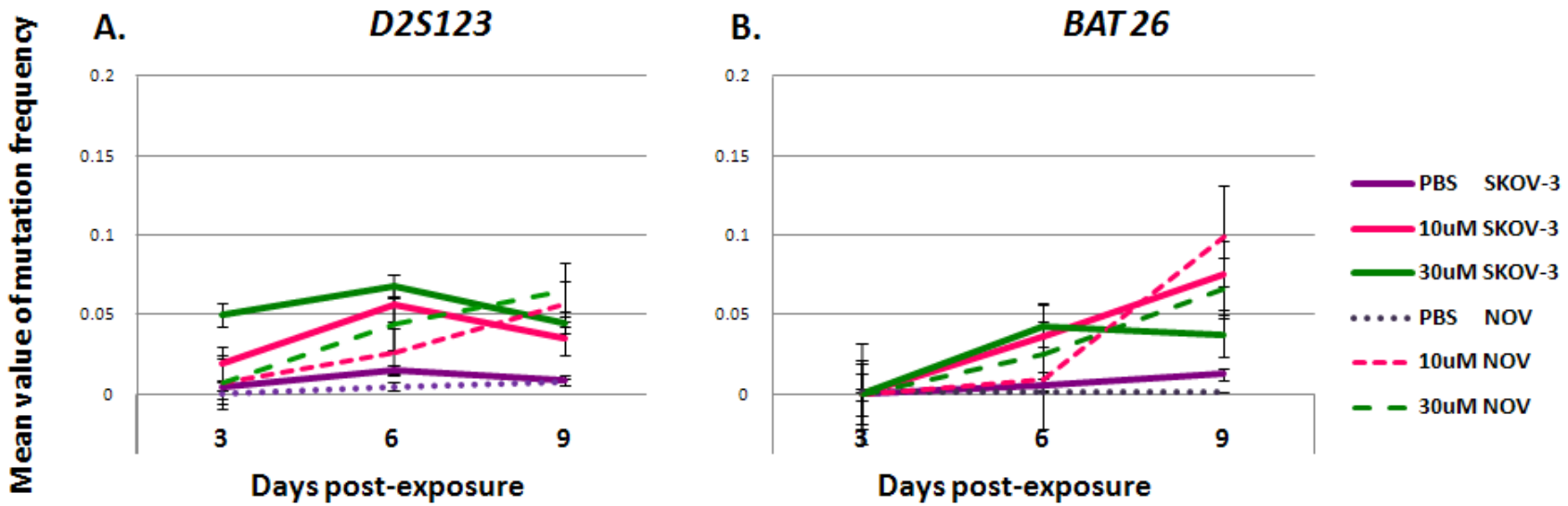

Figure 3.5 Variation of mutation frequency over time

Notes: Comparison of mutation frequency in the H_2O_2 treated versus untreated ovarian normal NOV and ovarian tumor SKOV-3 cell lines at 3, 6, and 9 days. Human normal ovarian cell line accumulates ROS damage at 3 to 6 days and shows increase of MSI after 6 days post-exposure in comparison with human tumor ovarian cell line. A) D2S123 marker significantly increased MSI over time ($p=0.035$). B) BAT26 marker significantly increased MSI over time ($p=0.03$) (p-values were calculated by *t*-test.) Mean value of mutation frequency was calculated by SP-PCR software version 1.0 (M.D. Anderson Cancer Center. Houston, TX).

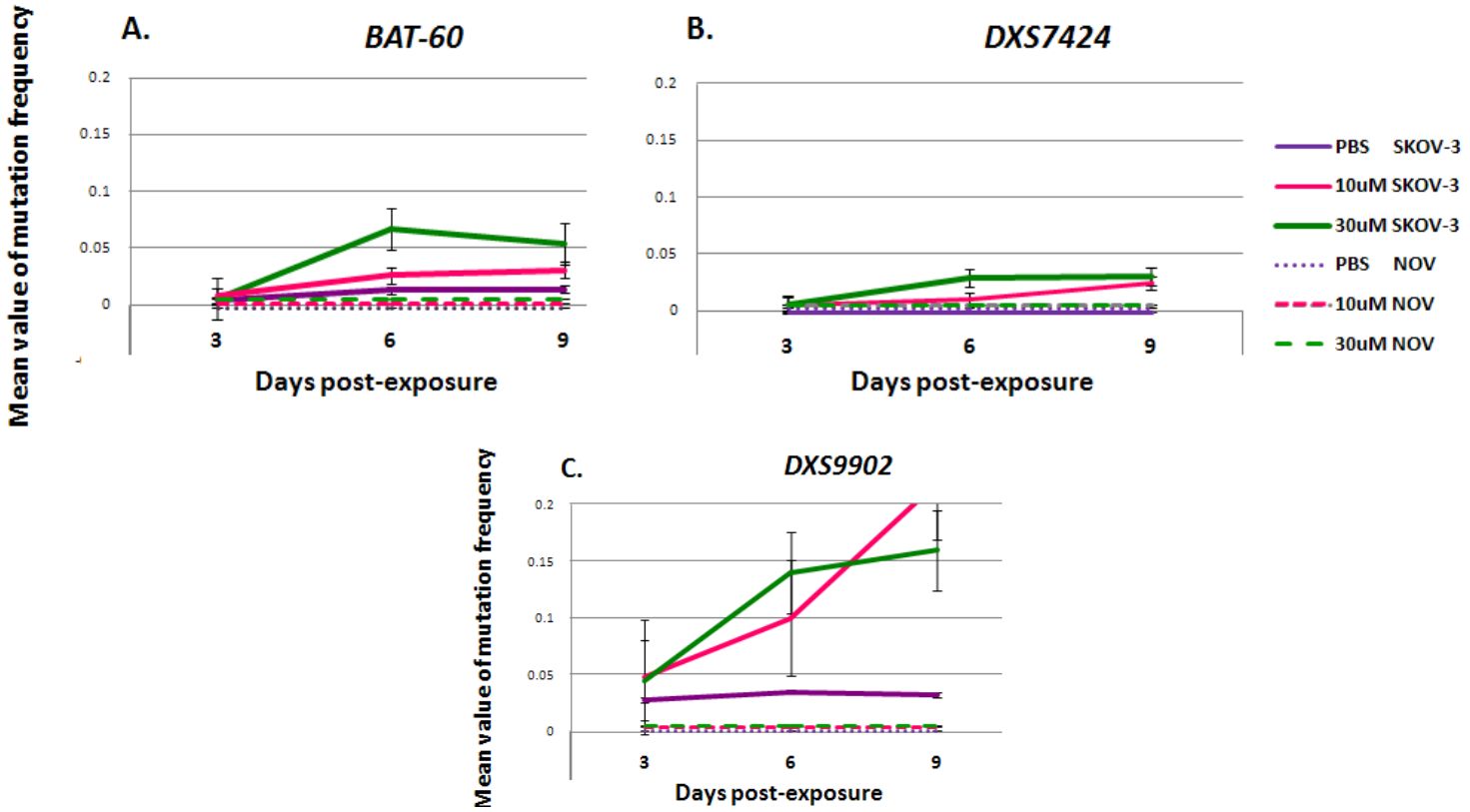

Figure 3.6 Mutation frequencies of novel markers relative to transcription and cell differentiation genes

Notes: Comparison of mutation frequency in the H_2O_2-treated versus untreated ovarian normal NOV and ovarian tumor SKOV-3 cell lines at 3, 6, and 9 days. These markers show higher mutation frequencies in human cancer ovarian cell line than human normal ovarian cell line after ROS damage. A) BAT60 marker significantly increased MSI over time and dose (p=0.058). B) DXS7424 marker significantly increased MSI over time and dose (p=0.06). C) DXS9902 marker significantly increased MSI over time and dose (p=0.007). (p-values were calculated by *t*-test.) Mean values of mutation frequency were calculated by SP-PCR software version 1.0 (M.D. Anderson Cancer Center. Houston, TX).

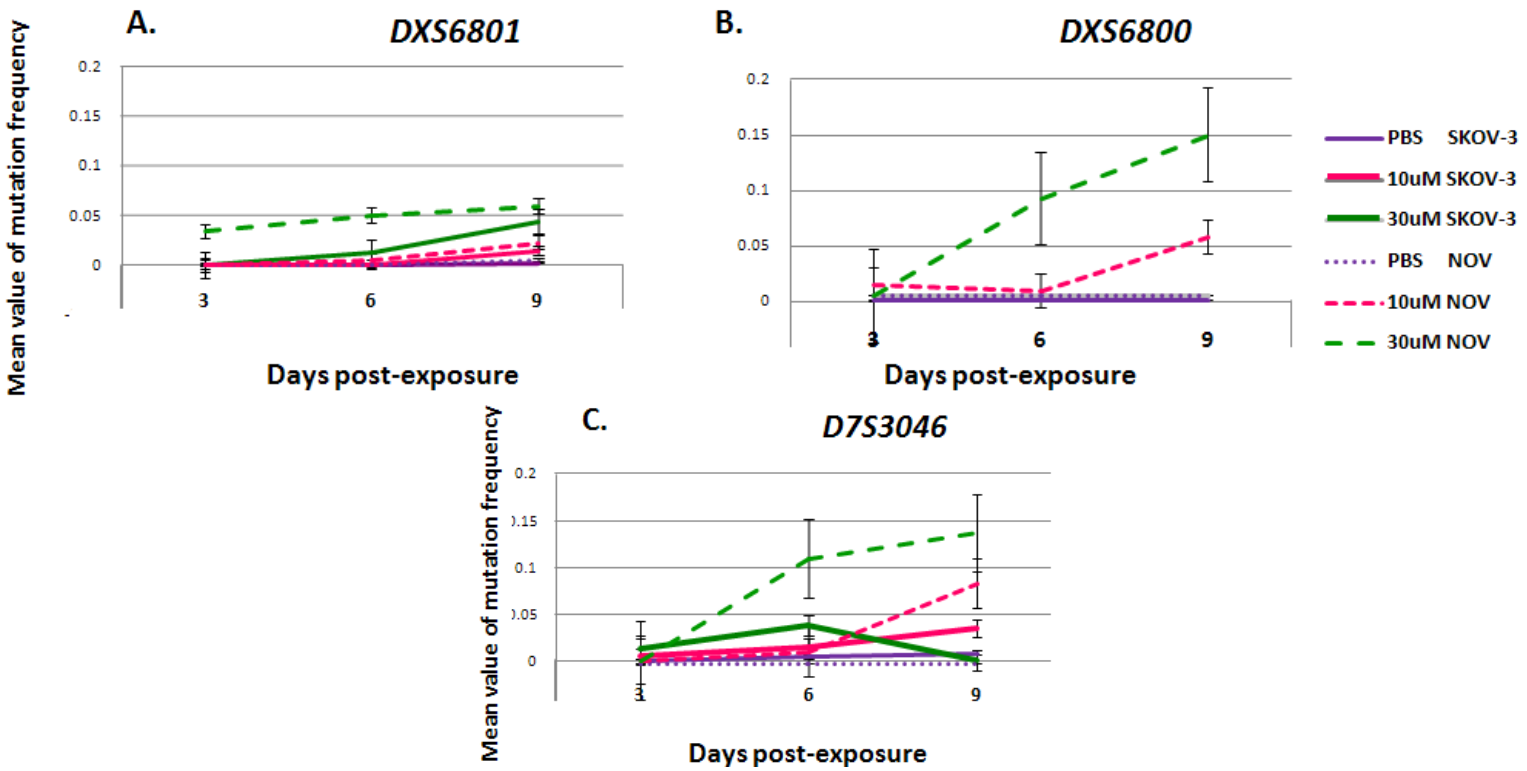

Figure 3.7 Dose time mutation frequency responses

Notes: Comparison of the mutation frequency in the H_2O_2-treated versus untreated normal NOV and tumor SKOV-3 cell lines at 3, 6, and 9 days. A) DXS6801 marker significantly increased MSI over time and dose (p=0.02). B) DXS6800 marker significantly increased MSI over time and dose (p=0.06). C) D7S3046 marker significantly increased MSI over time and dose (p=0.1). Human normal ovarian cell line shows higher number of mutation frequencies than human cancer ovarian cell line. (p-values were calculated by *t*-test.) Mean values of mutation frequency were calculated by small pool-PCR (SP-PCR) software version 1.0 (M.D. Anderson Cancer Center. Houston, TX).

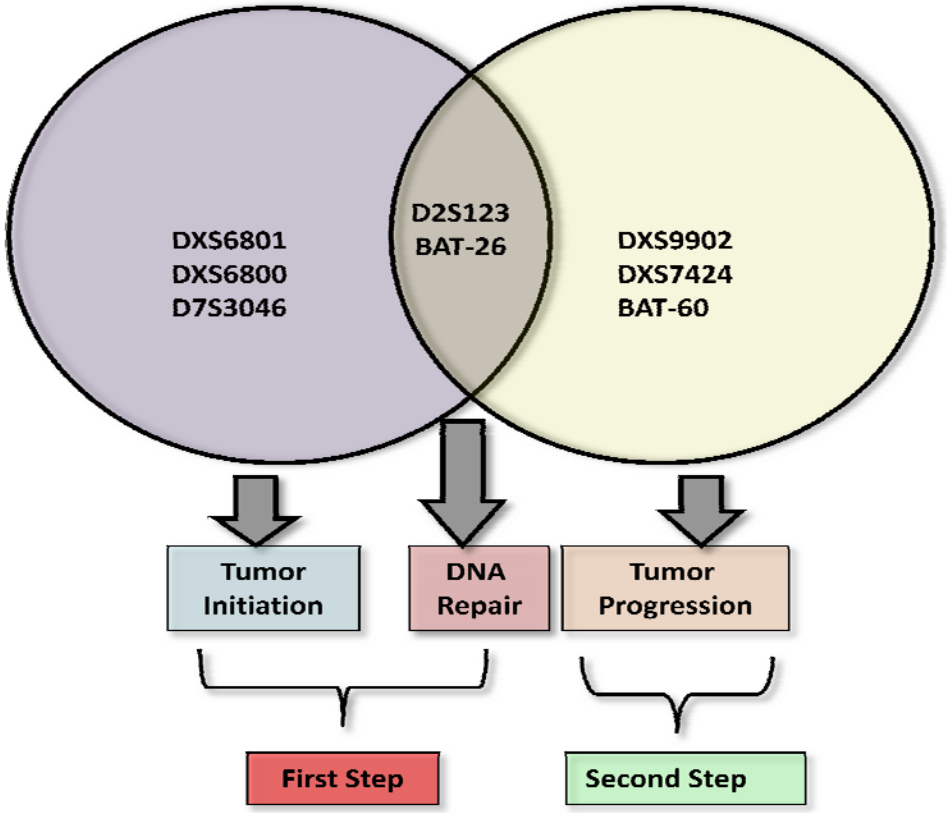

Figure 3.8 Venn diagram illustrating DNA markers involved in the two MSI steps during ovarian tumor initiation and ovarian tumor progression.

Notes: Two markers (intercept) were unstable in both ovarian normal and ovarian tumor cell lines after H_2O_2 exposure. Three markers (left diagram) were unstable in ovarian normal cell line only (named as novel markers involved in first step: tumor initiation). Three markers (right diagram) were unstable in ovarian tumor cells only (named as novel markers involved in second step: tumor progression).

Table 3.1 Microsatellite markers for detection of MSI in human ovarian normal and human ovarian cancer cell lines.

n.	MARKER	CHROMOSOMAL LOCATION	SIZE RANGE (bp)	REPEAT MOTIF	GENBANK NUMBER	PRIMER SEQUENCES	FLUORESCENT LABELS
1	BAT 26	2p22-p21	100 - 138	(A)26	AC079775	TGACTACTTTTGACTTCAGCCAGT AACCATTCAACATTTTTAACCCTT	FAM (*)
2	D2S123	2p16.3	200 - 232	(CA)21	Z16551	AAACAGGATGCCTGCCTTTA GGACTTTCCACCTATGGGAC	FAM (*)
3	MONO27	2p22.3	142 - 164	(T)27	AC007684	TGTGAACCACCTATGAATTGCAGA ATTGCTTGCAGTGAGCAGAGATCGTT	HEX (*)
4	NR24	2q11.2	124 - 136	(A)24	HSZNF2	CCATTGCTGAATTTTACCTC ATTGTGCCATTGCATTCCAA	HEX (*)
5	D3S1067	3p14.2	80- 96	(CA)21	GDB:188716	TCATCTATCTCCCAACTGTTGAG GAGCACTACCTGTTTAAGATAGG	FAM (**)
6	BAT 25	4q11-q12	114 - 124	(A)25	L04143	TCGCCTCCAAGAATGTAAGT ATTTCTGCATTTTAACTATGGCTC	HEX (*)
7	D7S3046	7q21.1	200 - 260	(GATA)12	G10353	GAGGAGACAGCCAGGGATATA ATTTCTCTATAACCTCTCTCCCTATCT	FAM (**)
8	D7S3070	7q36.1	100 - 152	(GATA)16	G27340	CATTTCTTCTGCCCCCATGA ATTTGACAGCTGAAAAGGTGCAGATG	FAM (**)
9	D7S1808	7p15.2-p15.1	200 - 220	(GGAA)18	G08643	GGAGGAAAAGTCTTAAACGTGAAT ATTGGCCTTGATGTGTTTGTTACT	FAM (**)
10	BAT 60	8q21.1	255 - 280	(A)60	NT_008183	TCTCATTTGAGTGGTGGAAGTGACTGGT TATTCTTTCGGGATGTAATCTCT	HEX (**)
11	PENTA C	9p13.3-p12	143 - 194	(GTTTT)12	AL138752	CATGGCATTGGGGACATGAACACA CACTGAGCGCTTCTAGGGACTTCT	NED (**)
12	D10S1426	10p11,2	152-180	(GATA)14	G08812	GCCGATCCTGAAGCAATAGC ATTCCCCTTGGTGGTGTCATCCT	FAM (**)
13	NR21	14q11.2	96 - 100	(A)21	XM_033393	CGGAGTCGCTGGCACAGTTCTATT TCGCGTTTACAAACAAGAAAAGTGT	HEX (**)
14	PENTA E	15q26.2	379 - 474	(GAAAA)5	_	ATTACCAACATGAAAGGGTACCAATA TGGGTTATTAATTGAGAAAACTCCTTACAATTT	FAM (**)
15	TP53	17p13.1	103-120	(AC)12	7157	ACTGCCACTCCTTGCCCATTC AGGGATACTATTCAGCCCGAGGTG	FAM (**)
16	D18S51	18q21.3	280 - 340	(AGAA)23	HUMUT574	CATGCCACTGCACTTCACTC CCGACTACCAGCAACAACAC	FAM (**)
17	PENTA D	21q	376 - 449	(GAAAA)13	AP001752	CAGCCTAGGTGACAGAGCAAGACA ATTTGCCTAACCTATGGTCATAAC	FAM (**)
18	DXS101	Xq22.1	150-219	(TTC)18	158931	GTTTTATCCCCGCTACAGGA CTGCATATTCTGCGCATGT	FAM (***)
19	DXS981	Xq11.2	182 - 220	(ATCT)12	57760	TCAGAGGAAAAGAAGTAGACATACT TTCTCTCCACTTTTCAGAGTCA	FAM (***)
20	DXS6797	Xq22.3	250 - 270	(ATCT)12	G08100	TTCCCTCTCTCCCTCTGTCT ACACACACCCAAAACCAGAT	HEX (***)
21	DXS6807	Xp22.3	250-273	(ATCT)8	G09662	TCCATCTTTCTCTGAACCTTCC TGCTTTAGGCTGATGTGAGG	FAM (***)
22	DXS6789	Xq23q26	118-150	(ATGT)9	G08105	GTTGGTACTTAATAAACCCTCTTT AAGAAGTTATTTGATGTCCTATTGT	HEX (***)
23	DXS6801	Xq21.32	126-134	(ATCT)10	G09742	CATTTCCTCTAACAAGTCTCC CAGAGAGTCAGAATCAGTAG	FAM (***)
24	DXS8377	Xq28	203-241	(AAG)29	100294364	CACTTCATGGCTTACCACAG GACCTTTGGAAAGCTAGTGT	FAM (***)
25	DXS9902	Xp22.31	170-186	(AGAT)10	G27261	TGGAGTCTCTGGGTGAAGAG CAGGAGTATGGGATCACCAG	FAM (***)
26	DXS6800	Xq23-q26	197-221	(AGAT)14	G09609	GTGGGACCTTGTGATTGTGTGAG CTGGCTGACACTTAGGGAAA	FAM (***)
27	DXS7130	Xq24	131-191	(ATCT)14	G10303	TCCCCTCTCATCTATCTGACTG CACTCCTGGTGCCAAACTCT	HEX (****)
28	DXS6799	Xq21.33	241-261	(ATCT)15	G08099	ATGAATTCAGAATTATCCTCATACC GAACCAACCTGCTTTTCTGA	FAM (****)
29	DXS6795	Xp22.11	279-291	(ATA)28	G09877	TGTCTGCTAATGAATGATTTGG CCATCCCCTAAACCTCTCAT	HEX (****)
30	DXS7133	Xq22.3	126-127	(ATAG)12	G08113	AGCTTCCTTAGATGGCATTCA GTTTTTAACGGTGTTCATGCTT	FAM (****)
31	DXS6804	Xq23-q24	172-196	(ATCT)13	G08108	CCCAGATATTTTGACCACCA GGCATGTGGTTGCTATAACC	FAM (****)
32	DXS7424	Xq21.33-q22	82-150	(AAT)17	695	AAAACAGGAAGACCCCATC GGCTAAGAAGAATCCCGCACA	HEX (****)
33	DXS7423	Xq28	161-187	(CCAT)11	sWXD2772	GTCTTCCTGTCATCTCCCAAC TAGCTTAGCGCCTGGCACATA	HEX (****)

Table 3.1 continued

Notes: It shows chromosome location, size, repeat motifs, Genbank access number, primer sequences from NCBI, NLM, NIH databases or by reference papers, and dye labels for each marker. (*) Markers included in the National Cancer Institute guidelines. (**) Markers have been evaluated in other type of cancers such as colon, lung, melanoma, and prostate. (***) Markers have been used in previous studies of ovarian cancer. (****) Markers selected by their location on the X chromosome in critical regions that have been shown to be related with autism spectrum disorder (ASD) and mental retardation.

Table 3.2 Frequencies of MSI at eight informative microsatellite loci in ovarian normal (NOV) and ovarian tumor (SKOV-3) cell lines.

Cell line and Days post-exposure	H_2O_2 Concentration	*LOCI* *																								
		D2S123			*BAT26*			*DXS9902*			*BAT 60*			*DXS7424*			*DXS6800*			*DXS6801*			*D7S3046*		
		n	*m*	*f*	*n*	*m*	*f*	*n*	*m*	*f*	*n*	*m*	*f*	*n*	*m*	*f*	*n*	*m*	*f*	*n*	*m*	*f*	*n*	*m*	*f*
NOV (3d)	**PBS**	68	1	0.012	44	0	0.000	59	0	0.000	69	0	0.000	62	0	0.000	61	0	0.000	37	0	0.000	78	0	0.000
	10μM	81	2	0.019	41	0	0.000	62	0	0.000	84	0	0.000	62	0	0.000	47	1	0.015	45	0	0.000	89	0	0.000
	30μM	86	3	0.026	35	0	0.000	33	0	0.000	44	0	0.000	45	0	0.000	29	0	0.000	21	2	0.068	44	0	0.000
NOV (6d)	**PBS**	99	0	0.000	48	0	0.000	80	0	0.000	96	0	0.000	84	0	0.000	81	0	0.000	40	0	0.000	94	0	0.000
	10μM	55	2	0.030	40	0	0.000	53	0	0.000	52	0	0.000	64	0	0.000	39	0	0.000	29	0	0.000	46	0	0.000
	30μM	42	4	0.058	38	2	0.026	33	0	0.000	65	0	0.000	41	0	0.000	26	3	0.093	30	5	0.100	27	6	0.120
NOV (9d)	**PBS**	74	2	0.020	26	0	0.000	37	0	0.000	51	0	0.000	56	0	0.000	28	0	0.000	28	0	0.000	67	0	0.000
	10μM	44	3	0.057	30	7	0.135	30	0	0.000	34	0	0.000	40	0	0.000	28	2	0.058	40	2	0.023	50	6	0.083
	30μM	33	3	0.066	31	3	0.057	40	0	0.000	26	0	0.000	54	0	0.000	30	6	0.150	26	5	0.120	33	6	0.137
	Total n = 9**	**582**	**20**	**0.032**	**333**	**12**	**0.021**	**427**	**0**	**0.000**	**521**	**0**	**0.000**	**508**	**0**	**0.000**	**369**	**12**	**0.017**	**296**	**14**	**0.038**	**528**	**18**	**0.038**
SKOV-3 (3d)	**PBS**	67	0	0.000	37	0	0.000	58	2	0.028	92	0	0.000	71	0	0.000	46	0	0.000	52	0	0.000	31	0	0.000
	10μM	96	2	0.023	47	0	0.000	51	3	0.048	95	0	0.000	81	0	0.000	47	0	0.000	74	0	0.000	48	1	0.005
	30μM	89	3	0.051	42	0	0.000	54	3	0.045	99	1	0.007	60	0	0.000	47	0	0.000	65	0	0.000	44	2	0.013
SKOV-3 (6d)	**PBS**	94	2	0.015	46	1	0.006	48	2	0.035	89	2	0.016	66	0	0.000	45	0	0.000	72	0	0.000	46	1	0.005
	10μM	69	5	0.056	43	4	0.036	41	5	0.100	96	14	0.066	42	0	0.000	42	0	0.000	51	1	0.013	43	2	0.015
	30μM	68	6	0.068	29	2	0.043	54	10	0.140	81	2	0.018	48	1	0.018	45	0	0.000	66	0	0.000	34	4	0.038
SKOV-3 (9d)	**PBS**	83	1	0.009	38	1	0.013	64	2	0.032	76	2	0.020	63	0	0.000	48	0	0.000	73	0	0.000	42	1	0.009
	10μM	42	2	0.035	35	5	0.075	48	15	0.220	60	4	0.053	60	1	0.014	41	0	0.000	25	2	0.048	31	2	0.035
	30μM	82	5	0.045	43	4	0.037	72	16	0.160	68	2	0.023	48	1	0.018	47	0	0.000	54	0	0.000	43	1	0.023
	Total n = 9**	**690**	**26**	**0.034**	**360**	**17**	**0.025**	**490**	**58**	**0.090**	**756**	**25**	**0.023**	**539**	**3**	**0.004**	**408**	**0**	**0.000**	**532**	**3**	**0.007**	**362**	**14**	**0.016**

*[Number of estimated alleles (n), number of mutant alleles (m), mutation frequency (f) calculated using SP-PCR

**Total is sum of the estimated alleles and mutant alleles at each locus for each cell line

Table 3.3 Summary list of 8 informative markers and genes related.

MARKER	CHROMOSOL OCATION	REPEAT MOTIF	MARKER LOCATION	GENE	GENE LOCATION	GENE FUNCTION
D2S123	2p16.3	(CA)21	Chr2: 51,141,941-51,142,151	NRXN1	intron 5-6	Neurexins function in the vertebrate nervous system as cell adhesion molecules and receptors.
				MSH2	3' downstream 3.5Mb	MSH2 mismatch repair gene
				MSH6	3' downstream 3.3Mb	MutS protein helps in the recognition of mismatched nucleotides, prior to their repair
BAT26	2p22-p21	(A)26	Chr2: 47,494,991-47,495,112	EPCAM (TACSTD1)	5' upstream 0.1 Mb	This gene encodes a carcinoma-associated antigen expressed on most normal epithelial cells
				MSH2	5' upstream 0.2 Mb	MSH2 mismatch repair gene
				MSH6	5' upstream 0.4 Mb	MutS protein helps in the recognition of mismatched nucleotides, prior to their repair
DXS9902	Xp22.31	(AGAT)10	Chr X: 15,233,537+15,233,708	ASB9	5' upstream 0.02 Mb	Encodes a member of the ankyrin repeat and suppressor of cytokine signaling (SOCS) box protein family
				ASB11	5' upstream 0.07 Mb	The protein encoded by this gene is a member of the ankyrin repeat and SOCS box-containing (ASB) family of proteins
				PIGA	5' upstream 0.1 Mb	This gene encodes a protein required for synthesis of N-acetylglucosaminyl phosphatidylinositol (GlcNAc-PI)
				PIR	5' upstream 0.16 Mb	This gene encodes a member of the cupin superfamily. The encoded protein is an Fe(II)-containing nuclear protein expressed in all tissues of the body
				VEGF-D (FIGF)	5' upstream 0.12 Mb	The protein encoded by this gene is a member of the platelet-derived growth factor/vascular endothelial growth factor (PDGF/VEGF) family and is active in angiogenesis, lymphangiogenesis, and endothelial cell growth.

Table 3.3 continued

DXS6801	Xq21.32	(ATCT)10	Chr X: 92,511,172+ 92,511,301	FAM 133A	3' downstream 0.4 Mb	Encodes a protein that is similar to ubiquitin-specific proteases
				PCDH11X	3' downstream 1.5 Mb	The protein is thought to play a fundamental role in cell-cell recognition essential for the segmental development and function of the central nervous system
				PABPC5	3' downstream 1.9 Mb	RNA and nucleotide binding
				CRYBB2P1	3' downstream 2 Mb	RNA and nucleotide binding
BAT60	8q21.1	(A)60	Chr 8: 83,732,830 + 83,733,122	E2F	5' upstream 2.3Mb	Regulation of cellular proliferation and tumor biology in ovarian cancer.
				CA2	5' upstream 2.6Mb	Carbonic Anhydrase II isozyme control pH homeostasis in tumors that appears to modulate the behaviour of cancer cells
				CA13	5' upstream 2.4 Mb	Carbonic Anhydrase XIII isozyme control pH homeostasis in tumors that appears to modulate the behaviour of cancer cells
				CA1	5' upstream 2.5 Mb	Carbonic Anhydrase I isozyme control pH homeostasis in tumors that appears to modulate the behaviour of cancer cells
				CA3	5' upstream 2.6 Mb	Carbonic Anhydrase III isozyme control pH homeostasis in tumors that appears to modulate the behaviour of cancer cells
				CHMP4C	3' downstream 1.2 Mb	Complex involved in degradation of surface receptor proteins and formation of endocytic multivesicular bodies (MVBs)
				SNX16	3' downstream 1 Mb	A member of the sorting nexin family. Members of this family contain a phox (PX) domain
				FABP9/4/12/5	3' downstream 1 Mb	FABPs roles include fatty acid uptake, transport, and metabolism
				PMP2	3' downstream 1 Mb	Cytoplasmic lipid binding protein of peripheral myelin

Table 3.3 continued

DXS6800	Xq23-q26	(AGAT)14	ChrX: 78,680,410+78,680,603	ITM2A	3' downstream 0.07 Mb	Involved in osteo- and chondrogenic differentiation
				GPR174	3' downstream 0.28 Mb	G protein coupled receptor that binds an extracellular ligand and transmits the signal to a heterotrimeric G-protein complex.
				TBX22	5' upstream 0.52 Mb	T-box genes encode transcription factors involved in the regulation of developmental processes.
DXS7424	Xq21.33-q22	(AAT)17	Chr X: 100,618816+100,618,983	TIMM8A	3' downstream 0.01 Mb	Import and insertion of hydrophobic membrane proteins from the cytoplasm into the mitochondrial inner membrane
				TAF7L	3' downstream 0.1 Mb	TATA box binding protein-associated factor, RNA polymerase II.
				GLA	5' upstream 0.04Mb	This enzyme predominantly hydrolyzes ceramide trihexoside, and it can catalyze the hydrolysis of melibiose into galactose and glucose
				RPL36A	5' upstream 0.03 Mb	Cytoplasmic ribosomes
				HNRNPH2	5' upstream 0.05 Mb	Associated with pre-mRNAs in the nucleus and appear to influence pre-mRNA processing and other aspects of mRNA metabolism and transport.
				STAG3L4	3' downstream 1.7 Mb	A genome-wide association study of breast and prostate cancer in the NHLBI's Framingham Heart Study
D7S3046	7q21.1	(GATA)12	Chr7: 68552322+68552658	AUTS2	5' upstream 0.5 Mb	Genetic utility of broadly defined bipolar schizoaffective disorder as a diagnostic concept.
				SBDS	3' downstream 2.1 Mb	Microtubule binding, protein binding, and rRNA binding.
				C7orf42	3' downstream 2.2 Mb	Trasmembrane cellular component
				KCTD7	3' downstream 2.2 Mb	Progressive myoclonic epilepsy family
				RABGEF1 E17	3' downstream 2.2 Mb	RABGEF1 forms a complex with rabaptin-5 (RABPT5; MIM 603616) that is required for endocytic membrane fusion, and it serves as a specific guanine nucleotide exchange factor (GEF)

Notes: It shows chromosome location, repeat motifs, marker location, related genes, marker location on gene, and gene function from NCBI, NLM, NIH databases or by reference papers.

Table 3.4 Potential biomarker panel for ovarian cancer.

MARKER	NOV			SKOV-3		
	n	***m***	***f***	***n***	***m***	***f***
D2S123	582	20	*0.032*	690	26	*0.034*
BAT-26	333	12	*0.021*	360	17	*0.025*
DXS9902	427	0	0.000	490	58	0.090
BAT-60	521	0	0.000	756	25	0.023
DXS7424	508	0	0.000	539	3	0.004
Total n = 5	2371	32	**0.0106**	2835	129	**0.0352**

Notes: Mutated allele frequencies of 5 markers from human ovarian normal (NOV) and human ovarian tumor (SKOV-3) cell lines. Values in bold indicate total mutation frequencies for the five markers that showed significant differences between ovarian normal and ovarian tumor cells ($p = 0.05$, t-test). Values in italic indicate total mutation frequency for these two markers that did not show significant differences between both cell lines. Number of estimated alleles (n), number of mutant alleles (m), and mutation frequency (f) were calculated by SP-PCR software version 1.0 (M.D. Anderson Cancer Center Houston, TX).

3.6 References

Abedini MR, Muller EJ, Bergeron R, Gray DA, and Tsang BK. (2010) Akt promotes chemoresistance in human ovarian cancer cells by modulating cisplatin-induced, p53-dependent ubiquitination of FLICE-like inhibitory protein. Oncogene 29:11-25.

Ahuja N, Li Q, Mohan AL, Baylin SB, and Issa JP. (1998) Aging and DNA methylation in colorectal mucosa and cancer. Cancer Res 58:5489-5494.

American Cancer Society. Cancer Facts and Figures 2009. Atlanta, GA: American Cancer Society, Inc.; 2009. Available at: http://www.cancer.org/docroot/CRI/content/. Accessed February 02, 2010.

Armour JA (2006) Tandemly repeated DNA: why should anyone care? Mutat Res 598: 6-14.

Bacher JW, Abdel Megid WM, Kent-First MG, and Halberg RB. (2005) Use of mononucleotide repeat markers for detection of microsatellite instability in mouse tumors. Mol Carcinog 44:285-292.

Bacher JW, Flanagan LA, Smalley RL, Nassif NA, Burgart LJ, Halberg RB, Megid WM, and Thibodeau SN. (2004) Development of a fluorescent multiplex assay for detection of MSI-High tumors. Dis Markers 20:237-250.

Bacon AL, Farrington SM, and Dunlop MG. (2000) Sequence interruptions confer differential stability at microsatellite alleles in mismatch repair-deficient cells. Hum Mol Genet 9:2707-2713.

Barbosa RH, Vargas FR, Lucena E, Bonvicino CR, and Seuánez HN. (2009) Constitutive RB1 mutation in a child conceived by in vitro fertilization: implications for genetic counseling. BMC Med Genet 10:75-79.

Berg KD, Glaser CL, Thompson RE, Hamilton SR, Griffin CA, and Eshleman JR. (2000) Detection of microsatellite instability by fluorescence multiplex polymerase chain reaction. J Mol Diagn 2:20-8.

Boland CR, Thibodeau SN, Hamilton SR, Sidransky D, Eshleman JR, Burt RW, Meltzer SJ, Rodriguez-Bigas MA, Fodde R, Ranzani GN, and Srivastava S. (1998) A National Cancer Institute Workshop on Microsatellite Instability for cancer detection and familial predisposition: development of international criteria for the determination of microsatellite instability in colorectal cancer. Cancer Res 58:5248-5257.

Boland CR. (2008) The molecular biology of gastrointestinal cancer: implications for diagnosis and therapy. Gastrointest Endosc Clin N Am 18:401-413.

Bourguignon LY, Peyrollier K, Xia W, and Gilad E. (2008) Hyaluronan-CD44 interaction activates stem cell marker Nanog, Stat-3-mediated MDR1 gene expression, and ankyrin-regulated multidrug efflux in breast and ovarian tumor cells. J Biol Chem 283:17635-17651.

Brinkmann B, Klintschar M, Neuhuber F, Hühne J, and Rolf B. (1998) Mutation rate in human microsatellites: influence of the structure and length of the tandem repeat. Am J Hum Genet 62:1408-1415.

Brown GJ, St John DJ, Macrae FA, and Aittomäki K. (2001) Cancer risk in young women at risk of hereditary nonpolyposis colorectal cancer: implications for gynecologic surveillance. Gynecol Oncol 80:346-349.

Butler JM, Schoske R, Vallone PM, Kline MC, Redd AJ, and Hammer MF. (2002) A novel multiplex for simultaneous amplification of 20 Y chromosome STR markers. Forensic Sci Int 129:10-24.

Cai KQ, Caslini C, Capo-chichi CD, Slater C, Smith ER, Wu H, Klein-Szanto AJ, Godwin AK, and Xu XX. (2009) Loss of GATA4 and GATA6 expression specifies ovarian cancer histological subtypes and precedes neoplastic transformation of ovarian surface epithelia. PLoS One 4: e6454-e6459.

Coletta RD, Christensen KL, Micalizzi DS, Jedlicka P, Varella-Garcia M, and Ford HL. (2008) Six1 overexpression in mammary cells induces genomic instability and is sufficient for malignant transformation. Cancer Res 68:2204-2213.

Coolbaugh-Murphy M, Maleki A, Ramagli L, Frazier M, Lichtiger B, Monckton DG, Siciliano MJ, and Brown BW (2004) Estimating mutant microsatellite allele frequencies in somatic cells by small-pool PCR. Genomics 84: 419-430.

Coolbaugh-Murphy MI, Xu J, Ramagli LS, Brown BW, and Siciliano MJ (2005) Microsatellite instability (MSI) increases with age in normal somatic cells. Mech Ageing Dev 126:1051-1059.

Daley D, Lewis S, Platzer P, MacMillen M, Willis J, Elston RC, Markowitz SD, and Wiesner GL. (2008) Identification of susceptibility genes for cancer in a genome-wide scan: results from the colon neoplasia sibling study. Am J Hum Genet 82:723-736.

Davis TW, Wilson-Van Patten C, Meyers M, Kunugi KA, Cuthill S, Reznikoff C, Garces C, Boland CR, Kinsella TJ, Fishel R, and Boothman DA. (1998) Defective

expression of the DNA mismatch repair protein, MLH1, alters G2-M cell cycle checkpoint arrest following ionizing radiation. Cancer Res 58:767-778.

Dubrova YE. (2005) Radiation-induced mutation at tandem repeat DNA Loci in the mouse germline: spectra and doubling doses. Radiat Res 163: 200-207.

Duval A, and Hamelin R. (2002) Mutations at coding repeat sequences in mismatch repair-deficient human cancers: toward a new concept of target genes for instability. Cancer Res 62:2447-2454.

Ehrlich M. (2006) Cancer-linked DNA hypomethylation and its relationship to hypermethylation. Curr Top Microbiol Immunol 310:251-74.

Esteller M, Fraga MF, Guo M, Garcia-Foncillas J, Hedenfalk I, Godwin AK, Trojan J, Vaurs-Barrière C, Bignon YJ, Ramus S, Benitez J, Caldes T, Akiyama Y, Yuasa Y, Launonen V, Canal MJ, Rodriguez R, Capella G, Peinado MA, Borg A, Aaltonen LA, Ponder BA, Baylin SB, and Herman JG. (2001) DNA methylation patterns in hereditary human cancers mimic sporadic tumorigenesis. Hum Mol Genet 10: 3001-3007.

Friedrichsen DM, Stanford JL, Isaacs SD, Janer M, Chang BL, Deutsch K, Gillanders E, Kolb S, Wiley KE, Badzioch MD, Zheng SL, Walsh PC, Jarvik GP, Hood L, Trent JM, Isaacs WB, Ostrander EA, and Xu J. (2004) Identification of a prostate cancer susceptibility locus on chromosome 7q11-21 in Jewish families. Proc Natl Acad Sci USA 101:1939-1944.

Funato T, Uehara S, Takahashi M, Kozawa K, Satoh J, Sasaki T, and Kaku M. (2002) Microsatellite instability in gonadal tumors of XY pure gonadal dysgenesis patients. Int J Gynecol Cancer 12:192-197.

Gao R, Matsuura T, Coolbaugh M, Zühlke C, Nakamura K, Rasmussen A, Siciliano MJ, Ashizawa T, and Lin X (2008) Instability of expanded CAG/CAA repeats in spinocerebellar ataxia type 17. Eur J Hum Genet 16: 215-222.

Geisler JP, Goodheart MJ, Sood AK, Holmes RJ, Hatterman-Zogg MA, and Buller RE. (2003) Mismatch repair gene expression defects contribute to microsatellite instability in ovarian carcinoma. Cancer 98:2199-2206

Goddard KA, Witte JS, Suarez BK, Catalona WJ, and Olson JM. (2001) Model-free linkage analysis with covariates confirms linkage of prostate cancer to chromosomes 1 and 4. Am J Hum Gene 68:1197-1206.

Goel A, Nagasaka T, Hamelin R, and Boland CR. (2010) An optimized pentaplex PCR for detecting DNA mismatch repair-deficient colorectal cancers. PLoS One 5:9393-9397.

Gong X, Delorme R, Fauchereau F, Durand CM, Chaste P, Betancur C, Goubran-Botros H, Nygren G, Anckarsäter H, Rastam M, Gillberg IC, Kopp S, Mouren-Simeoni MC, Gillberg C, Leboyer M, and Bourgeron T. (2009) An investigation of ribosomal protein L10 gene in autism spectrum disorders. BMC Med Genet 10:7-11.

Goddard KA, Witte JS, Suarez BK, Catalona WJ, and Olson JM. (2001) Model-Free Linkage Analysis with Covariates Confirms Linkage of Prostate Cancer to Chromosomes 1 and 4. Am J Hum Gene 68:1197-1206.

Halliwell B, Gutteridge JM, and Cross CE. (1992) Free radicals, antioxidants, and human disease. J Lab Clin Med 19: 598-620.

Hanson H, and Hodgson S. (2010) Cancer genetics and reproduction. Best Pract Res Clin Obstet Gynecol 2010 24:3-18.

Helleman J, van Staveren IL, Dinjens WN, van Kuijk PF, Ritstier K, Ewing PC, van der Burg ME, Stoter G, and Berns EM. (2006) Mismatch repair and treatment resistance in ovarian cancer. BMC Cancer 6:201-206.

Huan Z, Nakayama K, Nakayama N, Ishibashi M, Yeasmin S, Katagiri A, Purwana IN, Iida K, Maruyama R, Fukumoto M, and Miyazaki K. (2008) Genetic classification of ovarian carcinoma based on microsatellite analysis: relationship to clinicopathological features and patient survival. Oncol Rep 19:775-781.

Hung WC, and Chaung LY. (1998) The farnesyltransferase inhibitor, FPT inhibitor III upregulates Bax and Bcl-xs expression and induces apoptosis in human ovarian cancer cells. Int J Oncol 12:137-140.

Idury RM, and Cardon LR. (1997) A simple method for automated allele binning in microsatellite markers. Genome Res 7:1104-1109.

Ionov Y, Peinado MA, Malkhosyan S, Shibata D, and Perucho M. (1993) Ubiquitous somatic mutations in simple repeated sequences reveal a new mechanism for colonic carcinogenesis. Nature 363:558-561.

Izutsu N, Maesawa C, Shibazaki M, Oikawa H, Shoji T, Sugiyama T, and Masuda T. (2008) Epigenetic modification is involved in aberrant expression of class III beta-tubulin, TUBB3, in ovarian cancer cells. Int J Oncol 32:1227-1235.

Jemal A, Thun MJ, Ries LA, Howe HL, Weir HK, Center MM, Ward E, Wu XC, Eheman C, Anderson R, Ajani UA, Kohler B, and Edwards BK. (2008) Annual report to the nation on the status of cancer, 1975-2005, featuring trends in lung cancer, tobacco use, and tobacco control. J Natl Cancer Inst 100:1672-1694.

Jirtle RL, Sander M, and Barrett JC. (2000) Genomic imprinting and environmental disease susceptibility. Environ Health Perspect 108:271-278.

Kavanagh JJ, Tresukosol D, De Leon CG, Edwards CL, Freedman RS, Hord M, Howell E, Lenzi R, Krakoff IH, and Kudelka AP. (1995) Phase II study of prolonged oral etoposide in refractory ovarian cancer. Int J Gynecol Cancer 5:351-354.

Li CY, Little JB, Hu K, Zhang W, Zhang L, Dewhirst MW, and Huang Q. (2001) Persistent genetic instability in cancer cells induced by non-DNA-damaging stress exposures. Cancer Res 61:428-432.

Lindahl T. (1993) Instability and decay of the primary structure of DNA. Nature 362:709-715.

Lu W, Ogasawara MA, and Huang P. (2007) Models of reactive oxygen species in cancer. Drug Discov Today Dis Models 4:67-73.

Mead LJ, Jenkins MA, Young J, Royce SG, Smith L, St John DJ, Macrae F, Giles GG, Hopper JL, and Southey MC. (2007) Microsatellite instability markers for identifying early-onset colorectal cancers caused by germ-line mutations in DNA mismatch repair genes. Clin Cancer Res 13:2865-2869.

Megid WA, Ensenberger MG, Halberg RB, Stanhope SA, Kent-First MG, Prolla TA, and Bacher JW. (2007) A novel method for biodosimetry. Radiat Environ Biophys 46:147-154.

Mulero JJ, Chang CW, Calandro LM, Green RL, Li Y, Johnson CL, and Hennessy LK. (2006) Development and validation of the AmpFlSTR Yfiler PCR amplification kit: a male specific, single amplification 17 Y-STR multiplex system. J Forensic Sci 51:64-75.

Murphy KM, Zhang S, Geiger T, Hafez MJ, Bacher J, Berg KD, and Eshleman JR. (2006) Comparison of the microsatellite instability analysis system and the Bethesda panel for the determination of microsatellite instability in colorectal cancers. J Mol Diagn 8:305-311.

Nagarajan RP, Patzel KA, Martin M, Yasui DH, Swanberg SE, Hertz-Picciotto I, Hansen RL, Van de Water J, Pessah IN, Jiang R, Robinson WP, and LaSalle JM. (2008) MECP2 promoter methylation and X chromosome inactivation in autism. Autism Res 1:169-178.

Nakayama K, Takebayashi Y, Hata K, Fujiwaki R, Iida K, Fukumoto M, and Miyazaki K. (2004) Allelic loss at 19q12 and Xq11-12 predict an adverse clinical outcome in patients with mucinous ovarian tumours of low malignant potential. Br J Cancer. 90:1204-1210.

Parsons TJ, Huel R, Davoren J, Katzmarzyk C, Milos A, Selmanović A, Smajlović L, Coble MD, and Rizvić A. (2007) Application of novel "mini-amplicon" STR multiplexes to high volume casework on degraded skeletal remains. Forensic Sci Int Genet 1:175-179.

Perucho M. (1996) Microsatellite instability: the mutator that mutates the other mutator. Nat Med 2:630-631.

Prat J, Ribé A, and Gallardo A. (2005) Hereditary ovarian cancer. Hum Pathol 36:861-870.

Prolla TA, Baker SM, Harris AC, Tsao JL, Yao X, Bronner CE, Zheng B, Gordon M, Reneker J, Arnheim N, Shibata D, Bradley A, and Liskay RM. (1998) Tumour susceptibility and spontaneous mutation in mice deficient in Mlh1, Pms1 and Pms2 DNA mismatch repair. Nat Genet 18:276-279.

Ramocki MB, Peters SU, Tavyev YJ, Zhang F, Carvalho CM, Schaaf CP, Richman R, Fang P, Glaze DG, Lupski JR, and Zoghbi HY. (2009) Autism and other neuropsychiatric symptoms are prevalent in individuals with MeCP2 duplication syndrome. Ann Neurol 66:771-782.

Schweppe RE, Klopper JP, Korch C, Pugazhenthi U, Benezra M, Knauf JA, Fagin JA, Marlow LA, Copland JA, Smallridge RC, and Haugen BR. (2008) Deoxyribonucleic acid profiling analysis of 40 human thyroid cancer cell lines reveals cross-contamination resulting in cell line redundancy and misidentification. J Clin Endocrinol Metab 93:4331-4341.

Sieben NL, Kolkman-Uljee SM, Flanagan AM, le Cessie S, Cleton-Jansen AM, Cornelisse CJ, and Fleuren GJ. (2003) Molecular genetic evidence for monoclonal origin of bilateral ovarian serous borderline tumors. Am J Pathol 162:1095-1101.

Sirchia SM, Tabano S, Monti L, Recalcati MP, Gariboldi M, Grati FR, Porta G, Finelli P, Radice P, and Miozzo M. (2009) Misbehaviour of XIST RNA in breast cancer cells. PLoS One 4:5559-5562.

Sommers CM, Mc Carry BE, Malek F, and Quinn JS. (2004) Reduction of particulae air pollution lowers the risk of heritable mutations in mice. Science 304:1008-1010.

Sood AK, Holmes R, Hendrix MJ, and Buller RE. (2001) Application of the National Cancer Institute international criteria for determination of microsatellite instability in ovarian cancer. Cancer Res 61:4371-4374.

Strand M, Prolla TA, Liskay RM, and Petes TD. (1993) Destabilization of tracts of simple repetitive DNA in yeast by mutations affecting DNA mismatch repair. Nature 365:274-276.

Suraweera N, Duval A, Reperant M, Vaury C, Furlan D, Leroy K, Seruca R, Iacopetta B, and Hamelin R. (2002) Evaluation of tumor microsatellite instability using five quasimonomorphic mononucleotide repeats and pentaplex PCR. Gastroenterology 123:1804-1811.

Toyota M, and Issa JP. (1999) CpG island methylator phenotypes in aging and cancer. Semin Cancer Biol 9:349-357.

Trimeche M, Braham H, Ziadi S, Amara K, Hachana M, and Korbi S. (2008) Investigation of allelic imbalances on chromosome 3p in nasopharyngeal carcinoma in Tunisia: high frequency of microsatellite instability in patients with early-onset of the disease. Oral Oncol 44:775-783.

Umar A, Boland CR, Terdiman JP, Syngal S, de la Chapelle A, Rüschoff J, Fishel R, Lindor NM, Burgart LJ, Hamelin R, Hamilton SR, Hiatt RA, Jass J, Lindblom A, Lynch HT, Peltomaki P, Ramsey SD, Rodriguez-Bigas MA, Vasen HF, Hawk ET, Barrett JC, Freedman AN, and Srivastava S. (2004) Revised Bethesda Guidelines for hereditary nonpolyposis colorectal cancer (Lynch syndrome) and microsatellite instability. J Natl Cancer Inst 96:261-268.

Umar A. (2004) Lynch syndrome (HNPCC) and microsatellite instability. Dis Markers 20:179-180.

Veigl ML, Katsuri L, Olechnowicz J, Ma AH, Lutterbaugh JD, Periyasamy S, Li GM, Drummond J, Modrich PL, Sedwick WD, and Markowitz SD. (1998) Biallelic inactivation of hMLH1 by epigenetic gene silencing, a novel mechanism causing human MSI cancers. Proc Natl Acad Sci USA 95:8698-8702.

Vilariño-Güell C, Smith AG, and Dubrova YE. (2003) Germline mutation induction at mouse repeat DNA loci by chemical mutagens. Mutat Res 526:63-73.

Weber F, Shen L, Fukino K, Patocs A, Mutter GL, Caldes T, and Eng C. (2006) Total-genome analysis of BRCA1/2-related invasive carcinomas of the breast identifies tumor stroma as potential landscaper for neoplastic initiation. Am J Hum Genet 78:961-972.

Yauk CL, Berndt ML, Williams A, Rowan-Carroll A, Douglas GR, and Stämpfli MR. (2007) Mainstream tobacco smoke causes paternal germ-line DNA mutation. Cancer Res 67:5103-5106.

Zhang H, Zhang S, Cui J, Zhang A, Shen L, and Yu H. (2008) Expression and promoter methylation status of mismatch repair gene hMLH1 and hMSH2 in epithelial ovarian cancer. Aust N Z J Obstet Gynecol. 48:505-509.

Zhang Y, Monckton DG, Siciliano MJ, Connor TH, and Meistrich ML (2002) Detection of radiation and cyclophosphamide-induced mutations in individual mouse sperm at a human expanded trinucleotide repeat locus transgene. Mutat Res 516:121-138.

Zubenko GS, Hughes HB 3rd, Zubenko WN, and Maher BS. (2007) Genome survey for loci that influence successful aging: results at 10-cM resolution. Am J Geriatr Psychiatry 15:184-193.

CHAPTER IV

DEREGULATION OF BRCA1 TUMOR SUPPRESOR GENE LEADS TO OVARIAN TUMOR SURVIVAL BY ACCUMULATION OF MICROSATELLITE INSTABILITY

4.1 Abstract

Ovarian cancer susceptibility through *BRCA1* germline mutations plays a critical role in cell stress responses inducing accumulation of DNA damage by modulation of cell survival. Deregulation of tumor suppressor pathways has been described as a cause of progression and metastasis of this type of tumor. We used $BRCA1^{+/+}$ and $BRCA1^{-/-}$ human cell lines to evaluate ovarian cell stress responses after DNA damage caused by oxidative stress (OS). Ovarian cancer cells were treated with different concentrations of hydrogen peroxide as a DNA damage inducer. We analyzed genomic integrity by determining the microsatellite instability (MSI) frequencies in 33 markers located across the genome. We observed significant MSI frequencies in 4 markers (*MONO27, PENTAD, DXS7423* and *DXS7133)*. Genes related to these markers deregulate the tumor suppressor molecules such as *BRCA1, BCL2,* and *p53*. These results suggest that MSI present in important transcription factors can deregulate tumor suppressor genes, thereby modulating cell survival and apoptosis homeostasis during cellular stress responses and contribute to the aggressiveness of ovarian tumorigenesis.

4.2 Introduction

Ovarian cancer is a deadly disease that has a considerable number of new cases in the United States each year. Indeed, the National Cancer Institute has reported 21,880 new cases and 13,850 deaths were expected during 2010 (Jemal *et al.*, 2010). The lifetime risk for developing ovarian cancer in the general population is 1.6%. This number increases to approximately 5% when a woman has one first-degree relative with the disease and 7% when a woman has two first-degree relatives with ovarian cancer. Therefore, there is a strong risk factor for the development of ovarian cancer in families with a history of ovarian cancer (Werness and Eltabbakh, 2001; Pharoah and Ponder, 2002).

Currently, cases of hereditary ovarian cancer are classified as syndromes. There are two major syndromes associated with ovarian cancer: hereditary breast-ovarian cancer (HBOC) syndrome and Lynch syndrome. HBOC (referred to as hereditary ovarian cancer -HOC), is associated with germ-line mutations of *BRCA1* and *BCRA2* and account for 90% of the diagnosed familial ovarian cancer cases. Lynch syndrome (refered to as hereditary non-polyposis colon cancer -HPNCC), accounts for the remaining 10% of the diagnosed familial ovarian cancer cases, and this syndrome results when germline mutations occur in DNA mismatch repair (MMR) genes, such as *hMLH1* and *hMSH2* (Risch *et al.*, 2001; Lynch *et al.*, 1997; Boyd , 2003).

It is well understood that genomic DNA damage occurs frequently in actively dividing cells and that there is a relationship between genomic damage and the onset of tumorigenesis. DNA damage can typically originate from normal endogenous cell processes such as DNA replication, metabolic production of free radicals, or from deleterious exogenous agents such as ultraviolet light, ionizing radiation, toxins,

chemicals, and pollutants (Hoeijmakers, 2009; Mena *et al.*, 2009). All mentioned deleterious agents can affect basic cell processes, which could be the first step for malignant cell transformation. Cells maintain genomic integrity via several protective molecular mechanisms such as the capacity of cells to sense specific regions where DNA damage has occurred, activation of molecular DNA repair machinery, and triggering all cell cycle checkpoint genes (Fry *et al.*, 2005). If any of these mechanisms have been impaired, it correlates with genomic instability (GI), mutagenesis, and cancer progression (Hoeijmakers, 2001). Activation of proto-oncogenes and inactivation of tumor suppressor genes are the most common alterations related to the development and progression of any type of cancer. An example of GI, microsatellite instability (MSI) noted in tumor suppressor genes and oncogenes resulted in specific mutations in these genes, giving rise to cancer development; a few examples are described below. Microsatellites are short tandem repeats of DNA that contain a 1-5 base pair repeat motif sequence that can be repeated from 10 – 30 times (Brinkmann *et al.*, 1998). Mutations in microsatellites, or MSI, are characterized by expansion or contraction of the repeat motif sequence. Accumulation of MSI is associated with different types of cancer such as endometrium, colon, and prostate. In ovarian cancer, an increased accumulation of MSI leads to a gradual decline in the activity of tumor suppressor genes such as *BRCA1/BRCA2* (Narod *et al.*, 1993; Neuhausen and Marshall, 1994; Rice *et al.*, 1998), *PTEN* (Li *et al.*, 1997), as well as the improper activity of oncogenes such as *c-myc* (Rodriguez-Pinilla *et al.*, 2007) and *CCND1* (Simpson *et al.*, 1997). Reactive oxygen species (ROS) exposure is a critical source of MSI and has been indicated as a critical factor of tumorigenesis (Van Loon., 2010).

The multiple-functional protein complex called the tumor suppressor breast and ovarian cancer type 1 susceptibility protein (*BRCA1*) has been involved in promotion of cell cycle arrest, apoptosis, and recognition response of genomic damage (Miki *et al.*, 1994; Liu *et al.*, 2010). The *BRCA1* gene was mapped and cloned for the first time in September 1994 (Miki *et al.*, 1994). This particular gene is located on chromosome 17 at the 17q23 region, and it has been shown that mutations leading to loss of function occur when there is premature truncation of the protein product (Huen *et al.*, 2010). It has been well established that the ability of the *BRCA1* protein to form complex networks with other regulatory proteins is essential for numerous key cellular processes such as cell cycle control, DNA damage recognition or repair, chromatin remodeling, protein ubiquitylation, and transcriptional regulation of gene expression (Linger and Kruk, 2010). *BRCA1* has been called the master regulator of genomic integrity due to the ability to function in different roles in order to maintain cell survival homeostasis (Huen *et al.*, 2010). Different studies that used *BRCA1* defective cells have confirmed GI through deficient DNA repair by homologous recombination and impaired cell cycle checkpoint functions (DelloRusso *et al.*, 2007). Although it is well established that aberrant mutations in this locus leads to its loss of function, the events that initiate mutations as a pathway to cancer formation is not clear. Some studies have identified CpG methylation within the *BRCA1* gene promoter and loss of heterozygosity (LOH) of microsatellite markers located in the chromosomal 17q region (Rice *et al.*, 1998). Therefore, promoter CpG methylation and LOH can inhibit *BRCA1* gene function leading to high risk of ovarian cancer. So far, novel suppressor molecules and genetic events that work independently with *BRCA1* pathway have not been well elucidated in ovarian cancer.

We hypothesize that ROS induced genomic instability is marked by the accumulation of MSI in target sequences of DNA, leading to oxidative stress and the down-regulation of tumor suppressor pathways leading to ovarian tumor progression. In the present study, we applied efficient and sensitive procedures for quantifying MSI by single cell PCR methods that allowed for the identification of low-frequency mutant alleles as well as the wild type alleles in each pool of the DNA sample. We used different microsatellites along the genome to compare and determine MSI frequencies after ROS exposure. The human ovarian cancer cell lines UWB1.289 *BRCA1* null or (-) and UWB1.289 *BRCA1*+ were exposed to different concentrations of hydrogen peroxide (H_2O_2) as a source of ROS. Our results show that the *BRCA1* tumor suppressor gene plays a critical role in anti-apoptotic signals that modulate cell survival and accumulation of DNA damage.

4.3 Materials and Methods

4.3.1 Cell Lines

The human ovarian cancer cell lines *UWB1.289 BRCA1* null and *UWB1.289 BRCA1*+ were purchased from American Type Culture Collection, (ATCC, Rockville, MD). All cells were maintained in T-25 culture flasks (Falcon, Becton Dickinson Labware, NJ). The culture media consisted of 50% RPMI-1640 Medium (Gibco, Invitrogen Corporation Carlsbad, CA), 50% MEBM (Mammary Epithelium Basal Medium) (Clonetics, Lonza, Walkersville, MD) supplemented with 2 ml of bovine pituitary extract (BPE), 0.5 ml epidermal growth factor human recombinant (rhEGF), 0.5 ml insulin, 0.5 ml hydrocortisone, 0.5 ml gentamicin sulphate – amphotericin-B (Clonetics, Lonza, Walkersville, MD), and 3% heat-inactivated fetal bovine serum (Gibco, Invitrogen Corporation, Carlsbad, CA). Gentamicin B1 (G-418) was added at a final concentration of 200 ug/ml to UWB1.289 *BRCA1*+ culture media (Clontech Inc., Mountain View, CA). Cells were maintained at 37ºC in a humidified atmosphere with 5% CO_2. Medium was changed every 72 hours.

4.3.2 *In vitro* exposure to ROS (H_2O_2)

Initial cell cultures were plated in triplicate at a density of 1 x 10^5 cells/cm^2. When the initial culture reached 80% confluency, cells were trypsinized and treated with 0, 10, and 30 μM concentrations of H_2O_2 (Fisher Scientific Houston, TX) in 1X PBS (GibcoBRL, Gaithersburg, MD). Titration curves for H_2O_2 were determined in previous studies, and the concentrations of H_2O_2 were designed to achieve 80% cell viability after initial exposure (data unpublished). These cells were treated with H_2O_2 or 1X PBS for 1 hour at 37ºC in a humidified atmosphere with 5% CO_2. Cells were then centrifuged at

125 X g for 5 min. The supernatant was discarded, and cells were washed twice with fresh 1X PBS. Both control and treated cells were resuspended in 1 ml of Dulbecco′s Modified Eagle′s Medium (DMEM), and an aliquot of cells was used to measure proliferation and caspase 3/7 activity. After H_2O_2 exposure, the remaining aliquot for each sample group was plated in triplicate at a density of 1 x 10^5 cells/ml and cultured at 37ºC in a humidified atmosphere with 5% CO_2.

4.3.3 Cell counting and apoptosis

Both *BRCA1*$^{+/+}$ and *BRCA1*$^{-/-}$ tumorous human ovarian cells were harvested, and an aliquot (10 µl) of each sample was manually counted in a hemocytometer chamber under a microscope to determine the number of cells per ml at days 0, 3, 6, and 9 post-H_2O_2 exposure. On day 0, the sample was taken right after H_2O_2 exposure (1 hour). In addition, caspase-3/7 activation assay was performed using a Caspase-Glo™ 3/7 assay kit (Promega, Madison, WI) according to the manufacturer's instructions. Briefly, human ovarian cancer cells (*BRCA1 null* and *BRCA*1+) were seeded in 96-well plates at a density of 1 × 10^4 cells/well. Caspase-Glo 3/7 reagent (100 µl) was then added to each well, including medium alone, untreated control cells or cells treated with H_2O_2. The plate was then incubated at room temperature for 2 hours, and the luminescence of each sample was measured with a Lmax Luminometer (Molecular Devices Corporation, Sunnyvale, CA, USA). All samples were assayed in triplicate. Luminescence was expressed as relative light units (RLU) which according to the manufacturer's protocol is proportional to the amount of caspase activity present in the sample.

4.3.4 Single cell PCR

Genomic DNA was purified from the cultured human cells with the ChargeSwitch® Genomic DNA Purification Kit following the manufacturer's protocol (Invitrogen Corporation, Carlsbad, CA). DNA was used as a template in a multiplex PCR. Previously, individual standardization of each microsatellite marker was established by PCR methods (Mulero *et al.*, 2006; Parsons *et al.*, 2007; Butler *et al.*, 2002; Berg *et al.*, 2000). DNA genotyping was performed to identify the wild type alleles in samples of DNA concentration of 0.1 ng/µl DNA and single cell equivalent concentration of 12.5-50 pg/µl. PCR was then performed for 33 labeled microsatellites with different fluorescent dyes (6'FAM-blue, HEX-green, or NED-yellow) (IDT, Coralville, IA) to allow for resolution and quality control with automatic detection by fragment analysis in an AB 3130XL Genetic Analyzer (Applied Biosystems, Foster City, CA) in the presence of Gene Scan 500 LIZ Ladder (Applied Biosystems, Foster City, CA) following the manufacturer's protocol. Out of the 33 markers used, five markers were from the National Cancer Institute guidelines, eight have been used in previous studies of ovarian cancer, twelve have been evaluated in other type of cancers colon, lung, melanoma, and prostate, and seven additional markers that were selected by their location on the X chromosome in critical regions that have been shown to be related with autism spectrum disorder (*ASD*) and mental retardation related to the *FRAXA* gene (Table 4.1) (Weber *et al.*, 2009; Sirchia *et al.*, 2009; Ramocki *et al.*, 2009; Gong *et al.*, 2009; Barbosa *et al.*, 2009; Trimeche *et al.*, 2008; Schweppe *et al.*, 2008; Nagarajan *et al.*, 2008; Boland et al, 2008; Prat *et al.*, 2005, Umar *et al.*, 2004; Nakayama *et al.*, 2004; Friedrichsen *et al.*, 2004; Sieben *et al.*, 2003; Funato *et al.*, 2002; Goddard *et al.*, 2001; Jirtle *et al.*, 2000).

DNA concentrations were measured with a Nanodrop ® ND-1000 spectrophotometer, and then, DNA serial dilutions were made at 0.1 ng/ µl, 0.05 ng/ µl, and 0.025 ng/ul. Using these serial DNA dilutions, Poisson analysis of the amplified alleles was performed to calculate the correct genomic equivalent value for each sample in order to obtain less than one diploid genome equivalents of DNA (sample genome equivalents range between 12.5-50 pg/µl). Estimates between 0.5-2 diploid genome-equivalents do not require large numbers of single cell PCR replicates for accurate data analysis (Coolbaugh-Murphy *et al.*, 2005; Coolbaugh-Murphy *et al.*, 2004). We were then able to use less than a single diploid genome-equivalent of DNA to perform single cell PCR analysis with 48 single cell replicates for each marker. This concentration of DNA allowed sufficient sensitivity to distinguish between wild type and mutated alleles at their appropriate frequency.

PCR amplifications were performed in a total reaction volume of 10 µl containing 1 X of buffer D [800 mM Tris HCl, 200 mM $(NH_4)_2SO_4$, 0.2% w/v Tween 20] (US DNA, Fort Worth, TX), 2.5 mM $MgCl_2$ (US DNA, Fort Worth, TX), 1 X of Solution L (US DNA, Fort Worth, TX), 1.25 U Hot-MultiTaq DNA polymerase (5 U/µl; US DNA, Fort Worth, TX), 4% DMSO (Sigma Aldrich, Saint Louis, MO), 0.4 mg/µL bovine albumin serum (Thermo Scientific, Rockford, IL), 300 µM dNTPs (Applied Biosystems, Foster City, CA), and 0.5 and 1.8 µM mixed primer (forward and reverse) respectively. Solution L (1X) was used as a PCR additive that facilitated amplification of difficult templates. PCR was performed on a PE 9600 thermocycler using a ramping cycling protocol: 1 cycle of 95 ºC for 11 minutes; 1 cycle of 96 ºC for 1 minute; 10 cycles of [94 ºC for 30 seconds, ramp 68 seconds to 58 ºC (hold for 30 seconds), ramp 50 seconds to 70 ºC (hold for 60 seconds)]; 25 cycles of [90 ºC for 30 seconds, ramp 60 seconds to 58

ºC (hold for 30 seconds), ramp 50 seconds to 70 ºC (hold for 60 seconds)]; 1 cycle of 60ºC for 30 minutes for final extension; and hold at 4ºC. Negative controls and reaction mixtures were included in each PCR to monitor for contamination.

Products amplified by single cell PCR were separated and detected by fragment analysis on an AB 3130XL Genetic Analyzer (Applied Biosystems, Foster City, CA) in the presence of Gene Scan 500 LIZ Ladder (Applied Biosystems, Foster City, CA) following the manufacturer's protocol. Wild type and mutated alleles were quantified by the GeneMapper version 4.0 software package (Applied Biosystems, Foster City, CA). Presence of wild type and/or mutant alleles was scored in each single cell (replicate). An average of 48 replicates per sample were amplified and scored for both control and experimental groups.

4.3.5 Genomic instability statistical analysis

We amplified less than a single diploid genome-equivalent of DNA with single cell PCR methods to estimate oxidative stress-induced mutation frequencies in specific microsatellite repeat markers. DNA concentrations were adjusted to obtain 0.5-2.0 genome equivalents, on average, per single cell PCR reaction. The average number of amplifiable DNA molecules (λ) in each PCR reaction was calculated using the Poisson distribution: $\lambda = -\ln(K_1/K)$, where K_1 = the total number of alleles expected minus the number of alleles observed, and K = the total number of alleles expected (Coolbaugh-Murphy *et al.*, 2004; Zhang *et al.*, 2002).

As mentioned, we previously determined the size of the wild type allele from each microsatellite marker. Repeat motif shifts from the standardized wild type alleles are considered mutant alleles (Coolbaugh-Murphy *et al.*, 2005; Coolbaugh-Murphy *et al.*,

2004). Mutant allele cutoff levels were determined by a repeat shift greater than 3 repeats or less than 3 repeats for mononucleotide markers (e.g. *BAT26, BAT60*), a shift greater than 2 repeats or less than 3 repeats for dinucleotide markers (e.g. *D2S123*), and a shift greater than 1 repeat or less than 2 repeats for trinucleotide (e.g. *DXS7424)*, tetranucleotide (e.g. *DXS9902, DXS6801*, *DXS6800),* and pentanucleotide (e.g. *PENTA-C, PENTA- D*) markers (see Figure 3.3 on chapter 3) (Goel *et al.*, 2010; Gao *et al.*, 2008; Daley *et al.*, 2008; Helleman *et al.*, 2006; Bacher *et al.*, 2005; Bacher *et al.*, 2004; Geisler *et al.*, 2003; Bacon *et al.*, 2000; Idury and Cardon, 1997).

Mutation frequencies for each marker by sample type, dose, and time were calculated by SP-PCR software version 2.0 (M.D. Anderson Cancer Center, Houston, TX). Maximum likelihood estimates of the mean number of mutant alleles and wild type allele in each pool, as well as their bootstrap standard deviations were also calculated by SP-PCR software version 2.0 (M.D. Anderson Cancer Center, Houston, TX). These analysis methods have been described (Coolbaugh-Murphy *et al.*, 2004). Differences in the estimation of mutation frequencies were calculated with a two tailed *t*-test using raw mutation frequencies. A three way cross class ANOVA, assuming no third factor interaction, and appropriate LSD multiple comparison (*t*-test) outputs were also produced. Results were considered statistically significant with a $p<0.05$ (using Procedure GLM from statistical package SAS/win 9.2, SAS Institute Inc., Cary, NC).

4.4 Results

4.4.1 *BRCA1* $^{+/+}$ and *BRCA1* $^{-/-}$ cell lines displayed changes in proliferation after ROS exposure

The *BRCA1* $^{+/+}$ and *BRCA1* $^{-/-}$ cell lines exhibited similar change in their morphology, post-exposure to 10 μM and 30 μM of H_2O_2. Following exposure to H_2O_2, the edges of cell cytoplasm began to appear more rounded, and this change was accompanied by the detachment of the cell from the bottom of the culture flask. The cells that were not exposed to H_2O_2 did not exhibit a change in their morphology, and they remained attached to the bottom of the culture flask throughout the duration of the experiment. Cells that were not exposed to hydrogen peroxide (H_2O_2) showed increased proliferation, while cells that were exposed to H_2O_2 displayed a marked decrease in proliferation.

The proliferation of cells exposed to H_2O_2 was significantly affected with a marked decrease in proliferation as the concentration of treatment increased, displaying a quiescent state after 3 days post-exposure until 9 days of treatment time ($p=0.0001$, Figure 4.1). On day 3, *BRCA1* $^{+/+}$ and *BRCA1* $^{-/-}$ cell lines post-H_2O_2 exposure showed significantly decreased numbers of viable cells ($p<0.05$). On day 6, *BRCA1* $^{+/+}$ cell line exposed to low H_2O_2 concentration (10 μM) showed a slightly increased proliferation and did not displayed any increases until day 9 post-exposure. In comparison to *BRCA1* $^{+/+}$ cells, the *BRCA1* $^{-/-}$ cell line exposed to a low concentration of H_2O_2 (10 μM) did not show significant changes in proliferation until 9 days post-exposure. *BRCA1* $^{+/+}$ and *BRCA1* $^{-/-}$ cell lines at the high concentration of H_2O_2 did not show marked differences in proliferation (Figure 4.1).

4.4.2 Apoptosis was induced in *BRCA1*$^{+/+}$ and *BRCA1* $^{-/-}$ cell lines as a cause of oxidative stress exposure

Detection of the pro-apoptotic cell proteins caspase 3 and 7 was determined after exposure to ROS damage. There were no significant differences observed in the rate of apoptosis between *BRCA1* (+) and *BRCA1* (-) cell lines. However, high significant differences were observed between H_2O_2 exposure concentrations and days post-exposure. Cells that remained unexposed to H_2O_2 did not display any significant change in the apoptosis rate. In contrast, cells that were exposed to the low concentrations (10 μM) of H_2O_2 showed a significant difference in the rate of apoptosis when compared to the cells that were exposed to the high concentrations (30 μM) of H_2O_2 ($p=0.0005$, Figure 4.2). At 3 days post-exposure for both low and high concentrations (10 μM and 30 μM, respectively), caspase activity increased in *BRCA1*$^{+/+}$ and *BRCA1* $^{-/-}$ cells approximately 2-3 fold when compared to the cells that were left untreated ($p=0.0002$, Figure 4.2). At 6 days post-exposure, the rate of apoptosis in both *BRCA1*$^{+/+}$ and *BRCA1* $^{-/-}$ cell lines decreased for both low and high concentrations of H_2O_2. At 9 days post-exposure, *BRCA1*$^{+/+}$ ovarian cancer cells displayed higher levels of apoptosis in comparison with *BRCA1* $^{-/-}$ ovarian cancer cells (Figure 4.2).

4.4.3 MSI was present in *BRCA1 (+)* and *BRCA1 (-)* cell lines

The BRCA1 gene is a regulator of cell cycle, genomic integrity and apoptosis. We asked whether BRCA1 null cells induce MSI after ROS accumulation. We analyzed MSI in BRCA1$^{+/+}$ and BRCA1 $^{-/-}$ cell lines post-exposure to H_2O_2 using different markers localized on autosomes and sex chromosomes (Table 4.1). Normal and mutant allele sizes were estimated using an internal size standard. Alleles with a different size from the wild type allele, per our previously-mentioned scoring rules, were identified as a

mutation. The total number of normal and mutated alleles was counted, and mutation frequencies per marker were calculated by SPPCR software. Not all analyzed markers showed significant mutation frequencies after ROS exposure. After statistical analysis, our results indicated that MSI was significantly induced in 4 out of the 33 chosen markers (Table 4.2). Significant mutation frequencies were observed in DXS7423, PENTA-D, and MONO27 ($p<0.05$, Figure 4.3; Table 4.2), and DXS7133 showed less significant mutation frequencies ($p<0.1$, Figure 4.3; Table 4.2). This result indicates that MSI is detectable in BRCA1$^{+/+}$ and BRCA1 $^{-/-}$ cell lines as a signal of ROS accumulation.

4.4.4 Mutation frequencies increased in *BRCA1*$^{+/+}$ and *BRCA1* $^{-/-}$ cell lines in response to ROS damage

Accumulation of unrepaired DNA damage over time leads to an abnormal tumor suppression signal inducing cell malignant transformation (Coletta *et al.*, 2008). *BRCA1* is a tumor suppressor gene responsible for DNA damage responses. In order to determine DNA damage after exposure to H_2O_2, we measured MSI at 3, 6, and 9 days post-exposure of H_2O_2 (0, 10 and 30 μM). Nine days-exposure was selected to allow for DNA damage tolerance, cell repair, or apoptosis in *BRCA1*$^{+/+}$ and *BRCA1*$^{-/-}$ cell lines. We observed MSI in *MONO27* and *PENTA-D* markers that increased as a function of time and concentration of treatment in *BRCA1*$^{+/+}$ and *BRCA1*$^{-/-}$ cells lines after ROS exposure. These markers showed high mutation frequencies at different points of time post-exposure and in different treatment doses. MSI was not observed for marker *MONO27* in *BRCA1*$^{+/+}$ and *BRCA1*$^{-/-}$ untreated cells. The *BRCA1*$^{-/-}$ cells that were exposed to the low concentration (10 μM) of H_2O_2 showed accumulation of mutation frequencies after 6 days of treatment. In contrast, the *BRCA1*$^{-/-}$ cells that were exposed to high concentrations (30 μM) of H_2O_2 showed higher mean values of mutation

frequencies ($p<0.05$). The *BRCA1*$^{+/+}$ cell line only showed an increased of mutation frequencies after 3 days post-exposure, but MSI was not detected after 6 days of treatment (Figure 4.4, 4.5 A).

The *PENTA-D* marker was stable for both *BRCA1*$^{+/+}$ and *BRCA1*$^{-/-}$ untreated cells. The *BRCA1*$^{-/-}$ cell line showed an increase of mutation frequencies after 6 days of treatment at both low and high concentrations of H_2O_2 (10 μM and 30 μM). In contrast, *BRCA1*$^{+/+}$ cell line only showed an increase in mutation frequency in the high concentration of H_2O_2 after 6 days post-exposure. Our results suggest that MSI increase after ROS damage accumulation in *BRCA1*$^{+/+}$ and *BRCA1*$^{-/-}$ cell lines as a function of time (Figure 4.4, 4.5 B).

4.4.5 *BRCA1*$^{+/+}$ and *BRCA1*$^{-/-}$ cells showed sensitivity to ROS exposure in a linear dose response

Stress response signals after ROS damage affect the DNA integrity of the cells. We asked whether *BRCA1*$^{+/+}$ and *BRCA1*$^{-/-}$ cell are sensitive to ROS damage by measuring MSI mutation frequencies 3, 6 and 9 days post H_2O_2 exposure. We found that two X chromosome markers showed high mutation frequencies in a linear dose response manner (*DXS7423* and *DXS7133*) (Figure 4.5). *DXS7423* was stable in untreated *BRCA1*$^{+/+}$ and *BRCA1*$^{-/-}$ cells. After H_2O_2 exposure, *BRCA1*$^{+/+}$ displayed progressively increased mutation frequencies over time at both low and high concentrations of H_2O_2 (10 and 30 μM). Surprisingly, we found that *BRCA1*$^{+/+}$ cells at the high exposure concentration displayed higher MSI at 6 days post-exposure, but then had an abrupt drop of MSI in comparison with the low concentration of H_2O_2. In contrast, *BRCA1*$^{-/-}$ displayed higher mean mutation frequencies over time at the high concentration (30 μM) of H_2O_2 but not at the low concentration (10 μM) (Figure 4.4, 4.6A). *DXS7133* was

stable in untreated *BRCA1*$^{+/+}$ and *BRCA1*$^{-/-}$. Mutation frequencies observed in the marker *DXS 7133* for the *BRCA1*$^{+/+}$ cell line displayed similar patterns as previously mentioned for marker (*DXS7423*). *BRCA1*$^{+/+}$ cells showed increased mutation frequencies for the marker *DXS7133* over time at the low concentration (10 μM) of H_2O_2, but in the high concentration (30 μM), these cells showed higher mutation frequencies 3 days post-exposure that increased at 6 days but dropped at 9 days post-exposure. The *BRCA1*$^{-/-}$ cell line exhibited different patterns of mean mutation frequencies at both 10 and 30 μM of H_2O_2 exposure. At the low concentration (10 μM) of H_2O_2, *BRCA1*$^{-/-}$ cells showed high MSI at 3 days post-exposure, could not be detected at 6 days post-exposure, and showed low MSI 9 days post-exposure. In contrast, at the high concentration (30 μM) of H_2O_2, *BRCA1*$^{-/-}$ cells showed mutation frequencies that increased progressively over time (p-value=0.006, Figure 4.4, 4.6B).

4.5 Discussion

The tumor suppressor breast and ovarian cancer type 1 (*BRCA1)* gene is an essential regulator for many cell processes such as DNA repair, apoptosis, and cancer formation (Linger and Kruk, 2010). Familial risk of breast and ovarian cancer as a consequence of the *BRCA1* gene mutation has been widely studied (Mavaddat *et al.*, 2010). However, the additional genetic events that are required for the development of breast and ovarian cancer remain unclear. It is known that carcinogenesis is a multistep process and is associated with loss of DNA integrity as a result of chromosomal and microsatellite instability. Detection of target sequences sensitive to stress used in early detection of hereditary ovarian cancer, therapy response, and prognosis. This study shows how *BRCA1* gene deficiency induces sensitivity to DNA damage after ROS exposure in *BRCA1 null* cells compared to *BRCA1* proficient cells.

The regulation of transcription is the signal that allows *BRCA1* gene functionality in cell cycle, DNA damage response, and tumor suppression. Post-transcriptional protein modifications give rise to either activated or repressed signals that modulate protein functions in cells. The *BRCA1* protein is targeted by many post-transcriptional processes such as methylation, histone modification, phosphorylation, and ubiquitinization that are involved in normal regulation of the protein itself and affect downstream elements. In addition, the *BRCA1* gene works as a cofactor of transcription by protein-protein interaction that address participation in cell cycle, DNA repair, and chromatin modification pathways (Guendel *et al.*, 2010; Liu *et al.*, 2010; Zhang and Powell, 2005; Miyamoto *et al.*, 2002; Venkitaraman *et al.*, 2001).

In previous studies, the *BRCA1* null cell line has shown an increase in radiation sensitivity at high doses of ionizing radiation. In contrast, *BRCA1*$^{+/+}$ cells have displayed a partial decrease in radiation sensitivity (DelloRusso *et al.*, 2007). Thus far, our results demonstrate a tolerance for DNA damage in *BRCA1*$^{+/+}$ cells that displayed quiescent status between 3 to 6 days post-exposure to low and high concentrations of H_2O_2. Once DNA damage is established and not repaired, *BRCA1* proficient cells undergo apoptosis, while *BRCA1*$^{-/-}$ cells displayed less apoptosis allowing accumulation of mutations. Our findings suggest that the alteration of *BRCA1* gene functionality could negatively affect the cellular susceptibility to programed cell death that preserves cellular genomic DNA integrity.

Loss of genomic DNA stability has been associated as an important part of the progression of tumorigenesis. Instability in single tandem repeats can result in DNA mutations that affect gene modulators of cellular stress responses. Our study identified four microsatellite markers that are localized in, or near, genes that play a role in homeostasis between cell survival and cell death (*MONO27* and *PENTA-D*) (Lam *et al.*, 2009). The markers *DXS7423* and *DXS7133* are involved in occurrence and development of cancer (Vauhkonen *et al.*, 2004). It is known that MSI occurs more frequently in repeat regions localized in critical points of the genome (Fan and Chu, 2007). Repeats located in or close to promoters, introns, exons, CpG islands, or 5' or 3' UTR sequences can accumulate mutations in protein coding genes that control ovarian epithelial cell growth and differentiation (Shah *et al.*, 2010; Fan and Chu, 2007). Specific mutations, caused by MSI, can lead to protein modifications due to transcription errors or epigenetic changes (Armour, 2006; Esteller *et al.*, 2001; Toyota and Issa, 1999; Ahuja *et al.*, 1998). Table 4.3 shows the location, repeat motif and repeat-gene location of the 4 most

sensitive markers. The marker *MONO27* is localized in intron 3-4 of the *MAP4K3* (mitogen activated protein kinase kinase kinase 3) gene. Silencing of the *MAP4K3* gene confers a proliferative advantage to cells and significant resistance to DNA damage induced cell death (Lam *et al.*, 2009). The *PENTA-D* marker is localized in intron 4-5 of the *HSF2BP* (heat shock transcription factor 2 binding protein) gene that modulates *HSF2* (heat shock factor 2) gene. The *H2F2BP* gene can be synthesized in ovarian granulosa cells and plays a role as a mediator and indicator of stress in follicular hormones that coordinate ovarian functions (Sirotkin and Bauer, 2010). The *DXS7423* marker is localized in the 5' upstream region (0.6 Mb) of the *MAGEA8* (melanoma antigen family A, 8) gene. This particular gene is a member of the cancer testis-antigen family which is expressed not only in melanoma cancer cells but also in many tumoral tissues such as prostate, pancreas, ovary and breast (Suyama *et al.*, 2010; Zhang *et al.*, 2010; Grigoriadis *et al.*, 2009; Kim *et al.*, 2006). The *DXS7133* marker is localized in the 5' upstream region (0.44 Mb) of the *GUCY2F* (Guanylate cyclase 2F retinal) gene. Overexpression of this gene has been studied in X-linked retinitis pigmentosa, as well as in breast, lung and pancreatic cancers (Wood *et al.*, 2006).

The key role of tumor suppressor proteins is to maintain genomic stability during cell stress response and avoid cell transformation. It is known that deregulation of tumor suppressor molecules such as *BRCA1*, *BCL2*, and *p53* increase cell survival and prevent apoptosis. Our results show that proteins that target deregulation of these tumor suppressors are unstable and affect downstream pathways. First, the *BRCA1* protein is not directly related with the *MAP4K3* gene. However, the *BRCA1* gene does regulate the *GADD45A* (growth arrest and DNA-damage-inducible, alpha) gene that is responsible for growth arrest after DNA damage. Some authors recognize the *GADD45A* gene as a

"cellular stress sensor" (Lam *et al.*, 2009; Tront *et al.*, 2006; Fornace *et al.*, 1992). The interaction of the *GADD45A* gene with the *MTK* family (mitogen activate kinase) results in activation of the *JNK* (c-Jun NH2-terminal kinase) gene that is responsible for cell growth inhibition or apoptosis. Our results show that MSI in the *MONO27* marker could be a signal for transcription modification of the *MAP4K3* gene. Deregulation of the *MAP4K3* gene inhibits the *JNK* gene activation, conferring partial cell proliferation in response to DNA damage and allowing acummulation of MSI after DNA damage after ROS exposure in *BRCA1* null cells.

Second, the *BCL2* tumor suppressor gene directly regulates heat shock protein (HSP) family with the transcription factor *HSF2BP* gene (Jego *et al.*, 2010). The *PENTA-D* marker located in the intron region of *HSF2BP* displayed high frequencies of MSI in both $BRCA1^{+/+}$ and $BRCA1^{-/-}$ cell lines. The $BRCA1^{+/+}$ cell line was more sensitive to DNA damage from high concentrations of H_2O_2 in comparison to the $BRCA1^{-/-}$ cell line that showed less MSI frequency. The *HSP* family is composed of anti-stress molecules responsible for angiogenesis, metastasis, and resistance of ovarian cancer cells to apoptosis by their accumulation in the nucleus.

Third, tumor specific antigens, such as the melanoma antigen-A 11 (*MAGEA 11*) gene, target deregulation of *p53,* allowing cell growth advantages through resistance to apoptosis, as well as to low chemotherapeutic resistance that gives a survival advantage during cellular stress responses. The *MAGEA* gene expression is related to chemoresistance to etoposide treatment in ovarian tumors (Zhang *et al.*, 2010; Monte *et al.*, 2007; Hofmann and Ruschenburg, 2002). This study reports high instability in *DXS7423* marker that is located downstream of the *MAGEA* gene. $BRCA1^{+/+}$ and

BRCA1$^{-/-}$ cell lines both showed an accumulation of DNA damage after ROS exposure that can facilitate progression of ovarian cancer cells.

In conclusion, we have identified novel genes that play key roles in tumor suppression during DNA damage responses and tumorigenesis. Once MSI occurs on the genes *MAP4K3*, *HSF2BP*, and *MAGEA*, cell proliferation and accumulation of DNA damage was observed and analyzed in the ovarian cancer cell lines by deregulation of tumor suppressor pathways. Validation of novel potential biomarkers that are described in the present study could open a door to understanding ovarian tumorigenesis. Further studies, like gene expression analysis, are needed to delineate additional genetic events that are required for the establishment of predictive tools involved in cancer invasion, treatment resistance, and efficient prognosis of ovarian cancer.

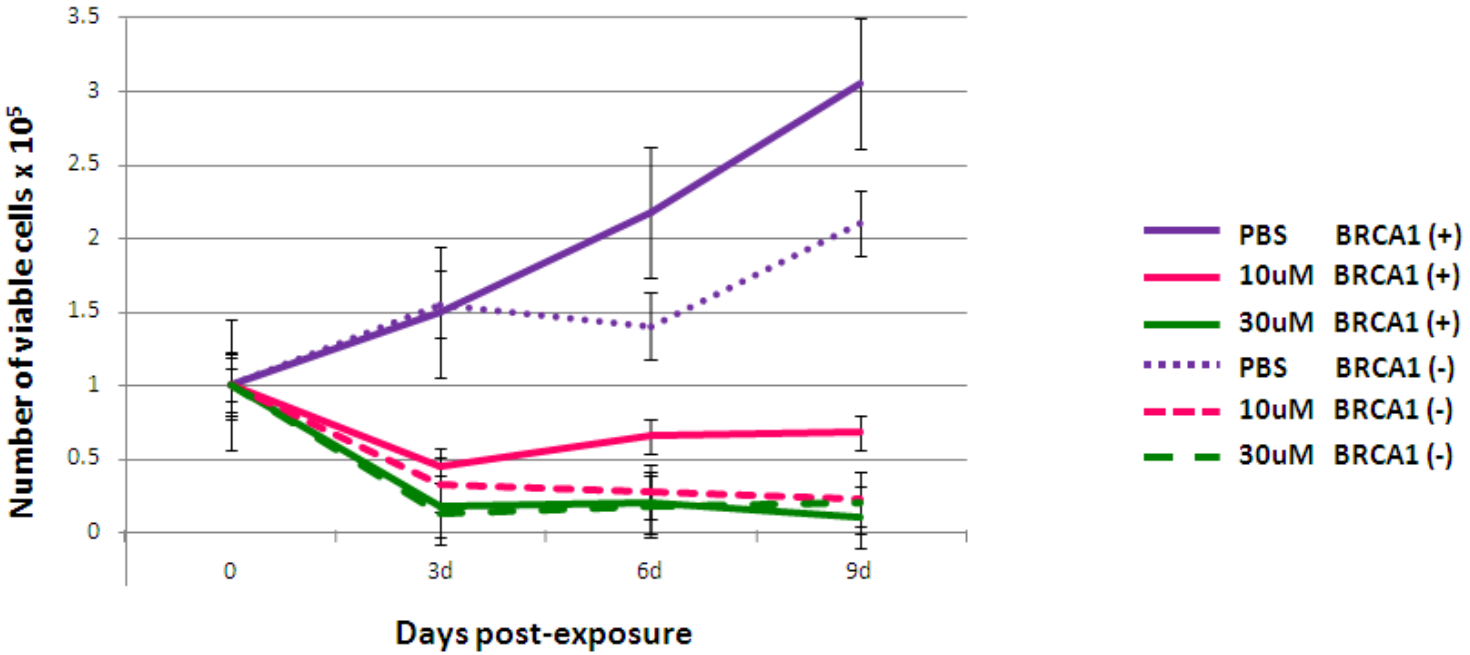

Figure 4.1 Similar kinetics of ovarian cancer cell proliferation

Notes: *BRCA1*$^{+/+}$ and *BRCA1* $^{-/-}$ cell lines displayed similar kinetics of cell proliferation. Cell growth curves of ovarian cancer cells were significantly different after H_2O_2 exposure in comparison to the untreated cancer cells. Cell cultures were treated with three different concentrations of H_2O_2 (0 µM-PBS, 10 µM, and 30 µM) and measured at 0, 3, 6, and 9 days. Cells were harvested and manually counted in a hemocytometer chamber under a light microscope. Total cell counts reflect the total number of cells per ml at 0, 3, 6, and 9 days after H_2O_2 exposure. The values expressed in this figure represent the mean and standard error from triplicate determinations.

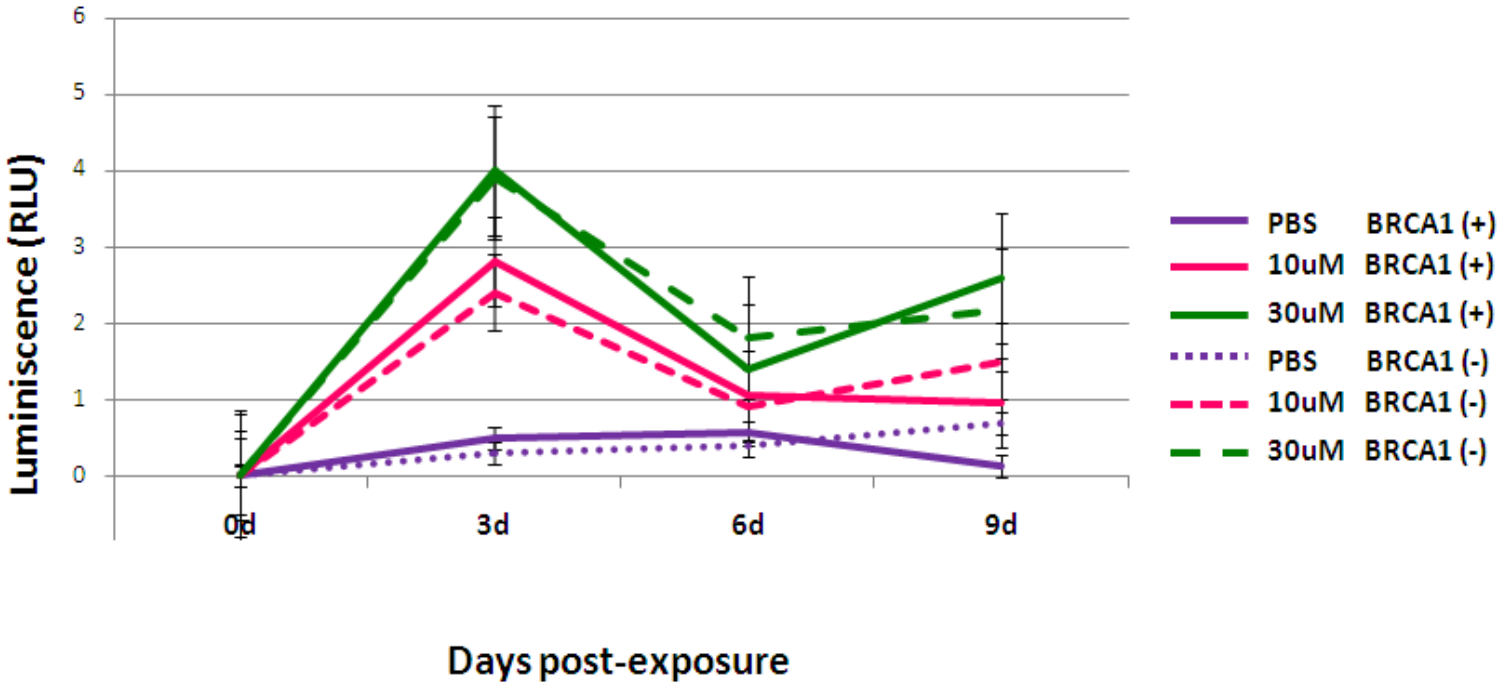

Figure 4.2 Activation of apoptotic pathways as a response to ROS damage

Notes: Caspase 3 and 7 activity was measured at 0, 3, 6, and 9 days post-exposure from *BRCA1* (+) and *BRCA1* (-) cell line cultures treated with three different concentrations of H_2O_2 (0 µM-PBS, 10 µM, and 30 µM). Significant differences were observed between treated ovarian cancer cells and untreated ovarian cancer cells at 3 days ($p=0.03$). Luminescence was expressed as relative light units (RLU) that were proportional to the amount of caspase activity present in the sample. The values expressed in this figure represent the mean and standard error from triplicate determinations.

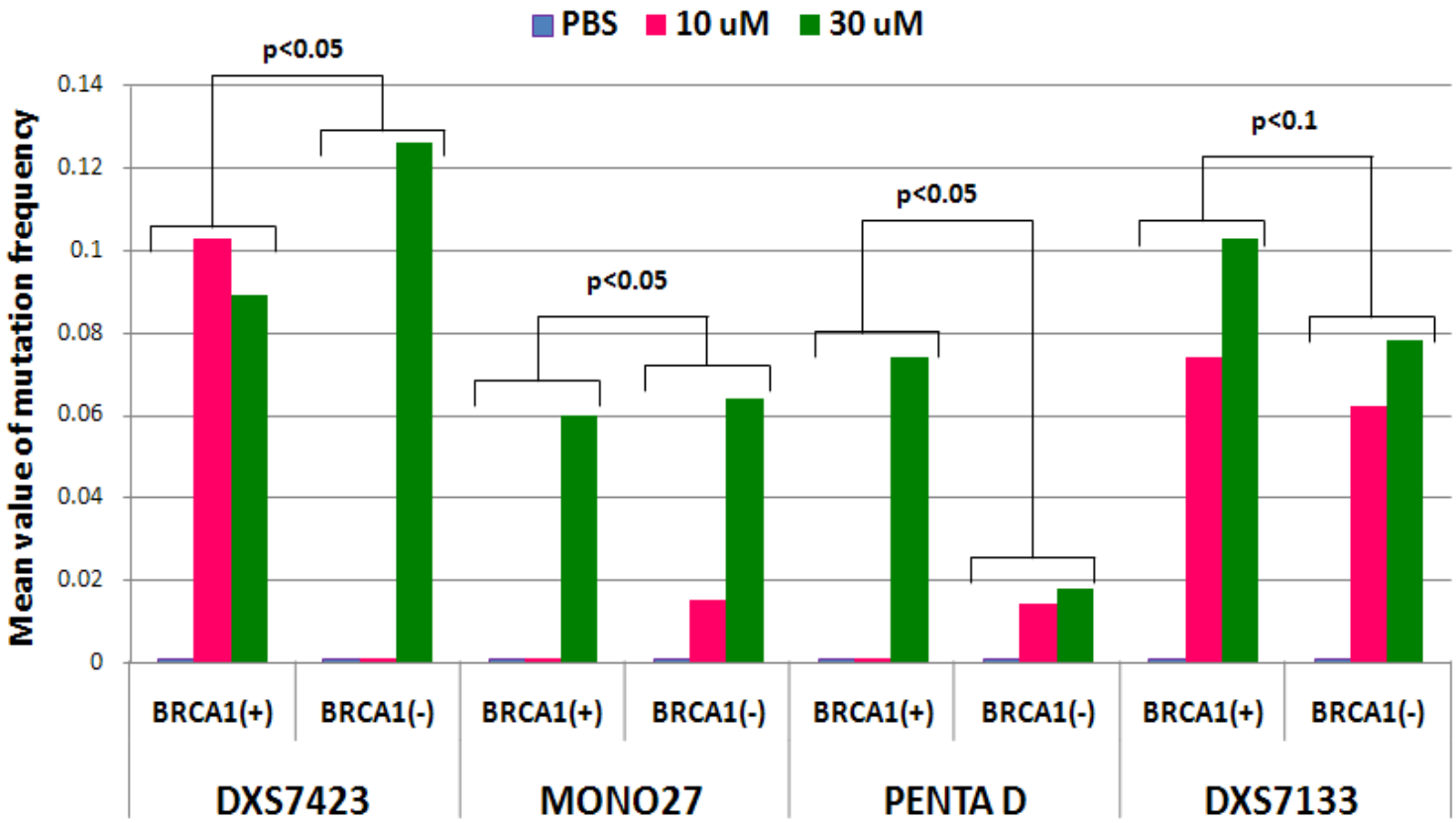

Figure 4.3 Comparison of the mutation frequency in the ovarian cancer H2O2 treated versus ovarian cancer untreated cell lines for 4 informative markers

Notes: (p-values are shown at the top of each bar). Values expressed in the figure represent the mean value of replicates. Mean value of mutation frequency calculated by small pool-PCR (SP-PCR) software version 2.0 (M.D. Anderson Cancer Center, Houston, TX).

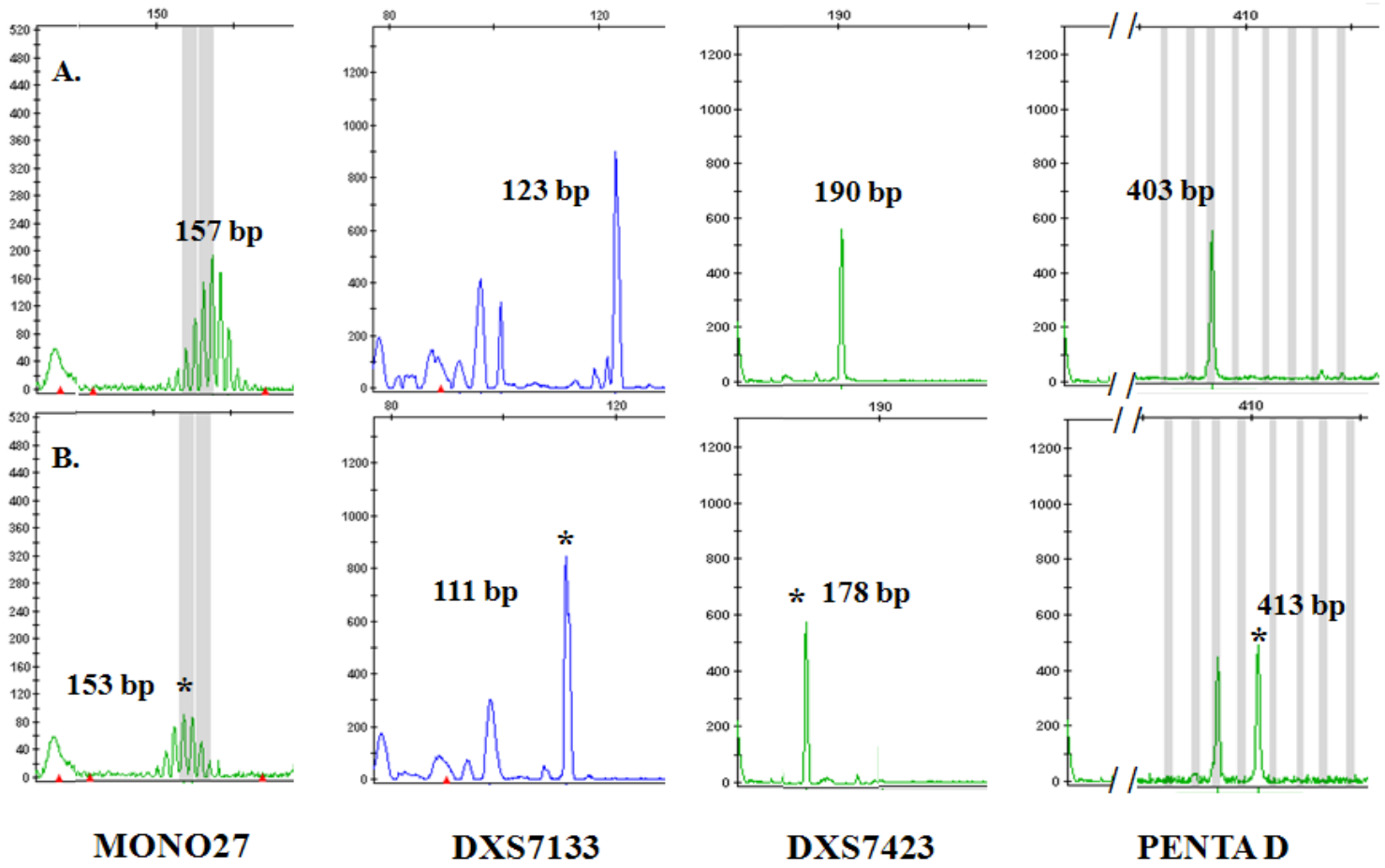

Figure 4.4 Representative microsatellite electropherograms

Notes: PCR fragment sizes listed in number of nucleotide base pairs (bp). Panel A.Wild type allele. Panel B. Single cell PCR amplification product (25-50 pg/ml of DNA) of ROS induced mutant allele. Markers in blue are FAM labeled and markers in green are HEX labeled.

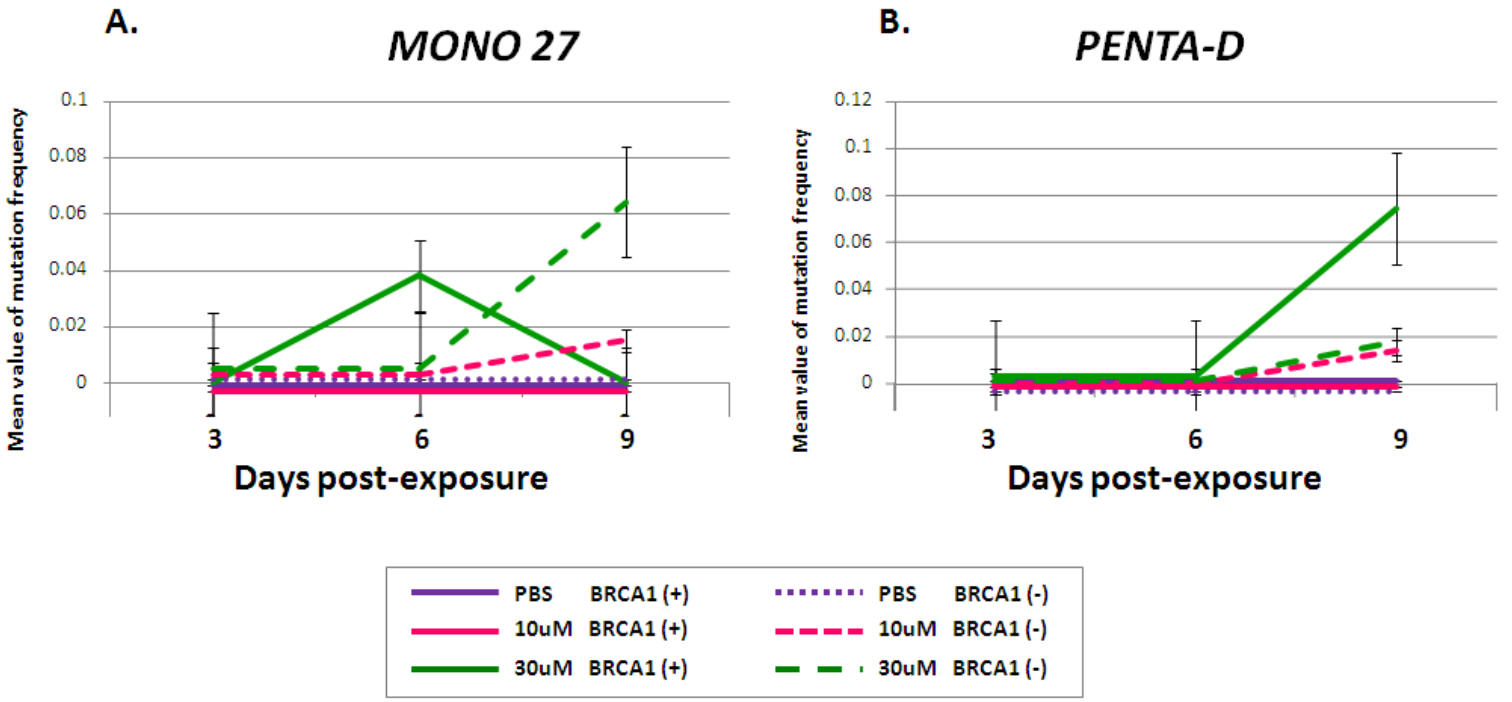

Figure 4.5 Dose and time mutation frequency responses

Notes: Comparison of mutation frequency in the H_2O_2-treated versus untreated *BRCA1* (+) and *BRCA1* (-) ovarian cancer cell lines at 0, 3, 6, and 9 days. Mean values of mutation frequency were calculated by small pool-PCR (SP-PCR) software version 1.0 (M.D. Anderson Cancer Center, Houston, TX)

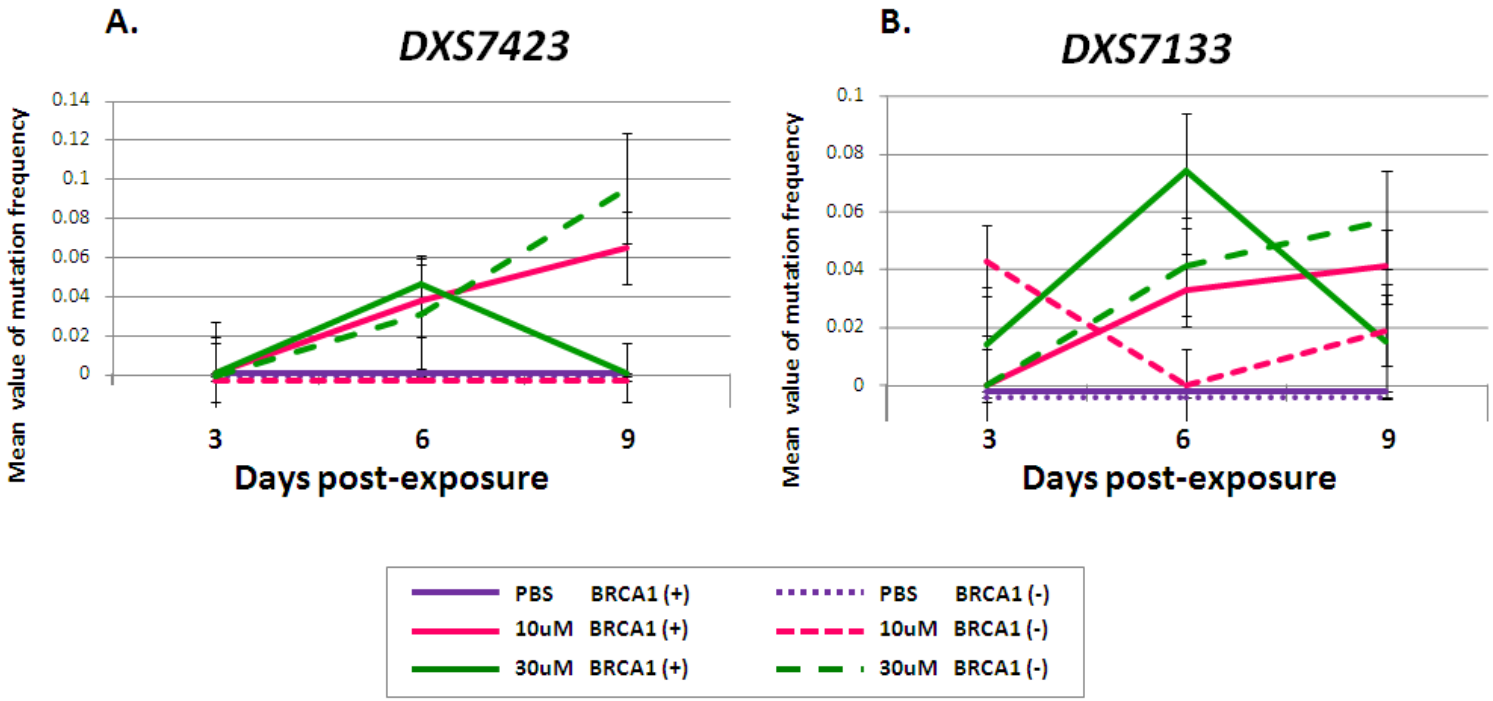

Figure 4.6 Variation of mutation frequency over time

Notes: Comparison of mutation frequency in the H_2O_2-treated versus untreated *BRCA1* (+) and *BRCA1* (-) ovarian cancer cell lines at 3, 6, and 9 days. On markers *DXS7423* (panel A) and *DXS7133* (panel B), ovarian tumor cells displayed sensitivity to ROS in linear dose response over time unrelated to *BRCA1* tumor suppressor status. Mean values of mutation frequency were calculated by small pool-PCR (SP-PCR) software version 2.0 (M.D. Anderson Cancer Center, Houston, TX).

Table 4.1 Microsatellite markers for detection of MSI in human ovarian cancer BRCA1 (+/+) and human ovarian cancer BRCA1 (-/-) cell lines.

n.	MARKER	CHROMOSOMAL LOCATION	SIZE RANGE (bp)	REPEAT MOTIF	GENBANK NUMBER	PRIMER SEQUENCES	FLUORESCENT LABELS
1	BAT 26	2p22-p21	100 - 138	(A)26	AC079775	TGACTACTTTTGACTTCAGCCAGT AACCATTCAACATTTTTAACCCTT	FAM (*)
2	D2S123	2p16.3	200 - 232	(CA)21	Z16551	AAACAGGATGCCTGCCTTTA GGACTTTCCACCTATGGGAC	FAM (*)
3	MONO27	2p22.3	142 - 164	(T)27	AC007684	TGTGAACCACCTATGAATTGCAGA ATTGCTTGCAGTGAGCAGAGATCGTT	HEX (*)
4	NR24	2q11.2	124 - 136	(A)24	HSZNF2	CCATTGCTGAATTTTACCTC ATTGTGCCATTGCATTCCAA	HEX (*)
5	D3S1067	3p14.2	80- 96	(CA)21	GDB:188716	TCATCTATCTCCCAACTGTTGAG GAGCACTACCTGTTTAAGATAGG	FAM (**)
6	BAT 25	4q11-q12	114 - 124	(A)25	L04143	TCGCCTCCAAGAATGTAAGT ATTTCTGCATTTTAACTATGGCTC	HEX (*)
7	D7S3046	7q21.1	200 - 260	(GATA)12	G10353	GAGGAGACAGCCAGGGATATA ATTTCTCTATAACCTCTCTCCCTATCT	FAM (**)
8	D7S3070	7q36.1	100 - 152	(GATA)16	G27340	CATTTCTTCTGCCCCCATGA ATTTGACAGCTGAAAAGGTGCAGATG	FAM (**)
9	D7S1808	7p15.2-p15.1	200 - 220	(GGAA)18	G08643	GGAGGAAAAGTCTTAAACGTGAAT ATTGGCCTTGATGTGTTTGTTACT	FAM (**)
10	BAT 60	8q21.1	255 - 280	(A)60	NT_008183	TCTCATTTGAGTGGTGGAAGTGACTGGT TATTCTTTCGGGATGTAATCTCT	HEX (**)
11	PENTA C	9p13.3-p12	143 - 194	(GTTTT)12	AL138752	CATGGCATTGGGGACATGAACACA CACTGAGCGCTTCTAGGGACTTCT	NED (**)
12	D10S1426	10p11,2	152-180	(GATA)14	G08812	GCCGATCCTGAAGCAATAGC ATTCCCCTTGGTGGTGTCATCCT	FAM (**)
13	NR21	14q11.2	96 - 100	(A)21	XM_033393	CGGAGTCGCTGGCACAGTTCTATT TCGCGTTTACAAACAAGAAAAGTGT	HEX (**)
14	PENTA E	15q26.2	379 - 474	(GAAAA)5	_	ATTACCAACATGAAAGGGTACCAATA TGGGTTATTAATTGAGAAAACTCCTTACAATTT	FAM (**)
15	TP53	17p13.1	103-120	(AC)12	7157	ACTGCCACTCCTTGCCCATTC AGGGATACTATTCAGCCCGAGGTG	FAM (**)
16	D18S51	18q21.3	280 - 340	(AGAA)23	HUMUT574	CATGCCACTGCACTTCACTC CCGACTACCAGCAACAACAC	FAM (**)
17	PENTA D	21q	376 - 449	(GAAAA)13	AP001752	CAGCCTAGGTGACAGAGCAAGACA ATTTGCCTAACCTATGGTCATAAC	FAM (**)
18	DXS101	Xq22.1	150-219	(TTC)18	158931	GTTTTATCCCCGCTACAGGA CTGCATATTCTGCGCATGT	FAM (***)
19	DXS981	Xq11.2	182 - 220	(ATCT)12	57760	TCAGAGGAAAAGAAGTAGACATACT TTCTCTCCACTTTTCAGAGTCA	FAM (***)
20	DXS6797	Xq22.3	250 - 270	(ATCT)12	G08100	TTCCCTCTCTCCCTCTGTCT ACACACACCCAAAACCAGAT	HEX (***)
21	DXS6807	Xp22.3	250-273	(ATCT)8	G09662	TCCATCTTTCTCTGAACCTTCC TGCTTTAGGCTGATGTGAGG	FAM (***)
22	DXS6789	Xq23q26	118-150	(ATGT)9	G08105	GTTGGTACTTAATAAACCCTCTTT AAGAAGTTATTTGATGTCCTATTGT	HEX (***)
23	DXS6801	Xq21.32	126-134	(ATCT)10	G09742	CATTTCCTCTAACAAGTCTCC CAGAGAGTCAGAATCAGTAG	FAM (***)
24	DXS8377	Xq28	203-241	(AAG)29	100294364	CACTTCATGGCTTACCACAG GACCTTTGGAAAGCTAGTGT	FAM (***)
25	DXS9902	Xp22.31	170-186	(AGAT)10	G27261	TGGAGTCTCTGGGTGAAGAG CAGGAGTATGGGATCACCAG	FAM (***)
26	DXS6800	Xq23-q26	197-221	(AGAT)14	G09609	GTGGGACCTTGTGATTGTGTGAG CTGGCTGACACTTAGGGAAA	FAM (***)
27	DXS7130	Xq24	131-191	(ATCT)14	G10303	TCCCCTCTCATCTATCTGACTG CACTCCTGGTGCCAAACTCT	HEX (****)
28	DXS6799	Xq21.33	241-261	(ATCT)15	G08099	ATGAATTCAGAATTATCCTCATACC GAACCAACCTGCTTTTCTGA	FAM (****)
29	DXS6795	Xp22.11	279-291	(ATA)28	G09877	TGTCTGCTAATGAATGATTTGG CCATCCCCTAAACCTCTCAT	HEX (****)
30	DXS7133	Xq22.3	126-127	(ATAG)12	G08113	AGCTTCCTTAGATGGCATTCA GTTTTTAACGGTGTTCATGCTT	FAM (****)
31	DXS6804	Xq23-q24	172-196	(ATCT)13	G08108	CCCAGATATTTTGACCACCA GGCATGTGGTTGCTATAACC	FAM (****)
32	DXS7424	Xq21.33-q22	82-150	(AAT)17	695	AAAACAGGAAGACCCCATC GGCTAAGAAGAATCCCGCACA	HEX (****)
33	DXS7423	Xq28	161-187	(CCAT)11	sWXD2772	GTCTTCCTGTCATCTCCCAAC TAGCTTAGCGCCTGGCACATA	HEX (****)

Table 4.1 continued

Notes: It shows chromosome location, size, repeat motifs, Genbank access number, primer sequences from NCBI, NLM, NIH databases or by reference papers, and dye labels for each marker. (*) Markers included in the National Cancer Institute guidelines. (**) Markers have been evaluated in other type of cancers such as colon, lung, melanoma, and prostate. (***) Markers have been used in previous studies of ovarian cancer. (****) Markers selected by their location on the X chromosome in critical regions that have been shown to be related with autism spectrum disorder (ASD) and mental retardation.

Table 4.2 Frequencies of MSI at four informative microsatellite loci in human ovarian cancer *BRCA1* $^{+/+}$ and human ovarian cancer *BRCA1* $^{-/-}$ cell lines.

Cell line and days post-exposure	H_2O_2 Concentration	LOCI *											
		DXS7423			PENTA-D			MONO27			DXS7133		
		n	*m*	*f*	*n*	*m*	*f*	*n*	*m*	*f*	*n*	*m*	*f*
BRCA1$^{+/+}$ (3d)	PBS	38	0	0	37	0	0	48	0	0	36	0	0
	10µM	45	0	0	39	0	0	48	0	0	40	0	0
	30µM	48	0	0	36	0	0	43	0	0	48	1	0.014
BRCA1$^{+/+}$ (6d)	PBS	35	0	0	20	0	0	18	0	0	40	0	0
	10µM	52	3	0.038	21	0	0	27	0	0	22	1	0.033
	30µM	32	5	0.046	24	0	0	30	3	0.038	26	3	0.074
BRCA1$^{+/+}$ (9d)	PBS	43	0	0	41	0	0	45	0	0	36	0	0
	10µM	31	2	0.065	42	0	0	38	0	0	37	2	0.041
	30µM	38	0	0	26	3	0.074	48	0	0	70	2	0.015
BRCA1$^{-/-}$ (3d)	PBS	42	0	0	42	0	0	44	0	0	42	0	0
	10µM	37	0	0	30	0	0	39	0	0	58	4	0.043
	30µM	39	0	0	46	0	0	46	0	0	33	0	0
BRCA1$^{-/-}$ (6d)	PBS	34	0	0	32	0	0	32	0	0	29	0	0
	10µM	43	0	0	26	0	0	42	0	0	39	0	0
	30µM	32	1	0.031	30	0	0	20	0	0	60	4	0.041
BRCA1$^{-/-}$ (9d)	PBS	38	0	0	44	0	0	29	0	0	34	0	0
	10µM	34	0	0	36	1	0.014	38	1	0.015	31	1	0.019
	30µM	25	3	0.095	32	1	0.018	22	3	0.064	39	3	0.057
p-values			***0.0007***			***0.0009***			***0.0014***			***0.0695***	

*[Number of estimated alleles (n), number of mutant alleles (m), mutation frequency (f) calculated using SP-PCR]

Table 4.3 Summary list of 4 informative markers and related genes

MARKER	CHROMOSOME LOCATION	REPEAT MOTIF	MARKER LOCATION	GENE	GENE LOCATION	GENE FUNCTION
DXS7423	Xq28	(CCAT)11	ChrX:149710903-149711089	MAGEA 11	3' downstream 0.8 Mb	**(Melanoma antigen family A, 11)** Androgen receptor coregulator expressed in endometrium
				MAGEA 8	3' downstream 0.6 Mb	**(Melanoma antigen family A, 8)** Increases androgen receptor transcriptional activity
				MTM1	5' upstream 0.1 Mb	**(Myotubularin 1)** Process cellular maturation and differentiation
				HMGB3	5'upstream 0.4 Mb	**(High mobility group box 3)** A minor allele of this gene has been implicates in high risk of breast cancer
PENTA-D	21q1	(GAAAA)13	Chr21:45056039-45056234	HSF2BP	Intron 4-5	**(Heat shock factor 2 binding protein)** Heat shock transcription factor; involved in cell stress
				CRYAA	3' downstream 0.4 Mb	**(Crystallin Alpha A)** Major proteins of the vertebrate eye lenses
MONO27	2p22.3	(T)27	Chr2:39572995-39573149	MAP4K3	ntron 3-4	**(Mitogen activated protein kinase kinase kinase 3)** Modulates cell death via post-trascriptional regulation
DXS7133	Xq22.3	(ATAG)12	ChrX:109,041,542-109,041,636	ACLS4	3' downstream 0.16 Mb	**(Long-chain fatty Acyl-CoA Synthetase 4)** Isozyme of the long-chain fatty-acid-coenzyme A ligase family (Alport Syndrome)
				KCNE1L	3' downstream 0.17 Mb	**(Voltage-gated potassium (kv) channles1-like)** Voltage gated potassium (kv) channels; related to mental retardation and Alport Syndrome (AMME syndrome)
				NTX2	3' downstream 0.26 Mb	**(Nuclear transport factor 2-like export factor 2)** Nuclear transport factor 2-like export factor 2; mediates the cell cycle control, and mitotic spindle assembly
				GCY2F	3' downstream 0.31 Mb	**(Guanylate cyclase 2F, retinal)** Guanilate cyclase 2F, retinal; gene associated to X-linked retinitis pigmentosa
				AMMECR1	5' upstream 0.6 Mb	(Alport syndrome, mental retardation, midface hypoplasia, elliptocytosis chromosomal region gene 1)

Notes: It shows chromosome location, repeat motifs, marker location, gene related, marker location on gene, and gene function from NCBI, NLM, NIH databases or by reference papers

4.6 References

Ahuja N, Li Q, Mohan AL, Baylin SB, and Issa JP. (1998) Aging and DNA methylation in colorectal mucosa and cancer. Cancer Res 58:5489-5494.

Armour JA (2006) Tandemly repeated DNA: why should anyone care? Mutat Res 598:6-14.

Bacher JW, Abdel Megid WM, Kent-First MG, and Halberg RB. (2005) Use of mononucleotide repeat markers for detection of microsatellite instability in mouse tumors. Mol Carcinog 44:285-292.

Bacher JW, Flanagan LA, Smalley RL, Nassif NA, Burgart LJ, Halberg RB, Megid WM, and Thibodeau SN. (2004) Development of a fluorescent multiplex assay for detection of MSI-High tumors. Dis Markers 20:237-250.

Bacon AL, Farrington SM, and Dunlop MG. (2000) Sequence interruptions confer differential stability at microsatellite alleles in mismatch repair-deficient cells. Hum Mol Genet 9:2707-2713.

Barbosa RH, Vargas FR, Lucena E, Bonvicino CR, and Seuánez HN. (2009) Constitutive RB1 mutation in a child conceived by in vitro fertilization: implications for genetic counseling. BMC Med Genet 10:75-79.

Berg KD, Glaser CL, Thompson RE, Hamilton SR, Griffin CA, and Eshleman JR. (2000) Detection of microsatellite instability by fluorescence multiplex polymerase chain reaction. J Mol Diagn 2:20-28.

Boland CR. (2008) The molecular biology of gastrointestinal cancer: implications for diagnosis and therapy. Gastrointest Endosc Clin N Am 18:401-413.

Boyd J. (2003) Specific Keynote: hereditary ovarian cancer: what we know. Gynecol Oncol 88: S8-S10.

Brinkmann B, Klintschar M, Neuhuber F, Hühne J, and Rolf B. (1998) Mutation rate in human microsatellites: influence of the structure and length of the tandem repeat. Am J Hum Genet 62:1408-1415.

Butler JM, Schoske R, Vallone PM, Kline MC, Redd AJ, and Hammer MF. (2002) A novel multiplex for simultaneous amplification of 20 Y chromosome STR markers. Forensic Sci Int 129:10-24.

Coletta RD, Christensen KL, Micalizzi DS, Jedlicka P, Varella-Garcia M, and Ford HL. (2008) Six1 overexpression in mammary cells induces genomic instability and is sufficient for malignant transformation. Cancer Res 68:2204-2213.

Coolbaugh-Murphy M, Maleki A, Ramagli L, Frazier M, Lichtiger B, Monckton DG, Siciliano MJ, and Brown BW (2004) Estimating mutant microsatellite allele frequencies in somatic cells by small-pool PCR. Genomics 84:419-430.

Coolbaugh-Murphy MI, Xu J, Ramagli LS, Brown BW, and Siciliano MJ (2005) Microsatellite instability (MSI) increases with age in normal somatic cells. Mech Ageing Dev 126:1051-1059.

Daley D, Lewis S, Platzer P, MacMillen M, Willis J, Elston RC, Markowitz SD, and Wiesner GL. (2008) Identification of susceptibility genes for cancer in a genome-wide scan: results from the colon neoplasia sibling study. Am J Hum Genet 82:723-736.

DelloRusso C, Welcsh P, Wang W, Garcia R, King M, and Swisher E. (2007) Functional characterization of a novel BRCA1-null ovarian cancer cell line in response to ionizing radiation. Mol Cancer Res 5:35-45.

Esteller M, Fraga MF, Guo M, Garcia-Foncillas J, Hedenfalk I, Godwin AK, Trojan J, Vaurs-Barrière C, Bignon YJ, Ramus S, Benitez J, Caldes T, Akiyama Y, Yuasa Y, Launonen V, Canal MJ, Rodriguez R, Capella G, Peinado MA, Borg A, Aaltonen LA, Ponder BA, Baylin SB, and Herman JG. (2001) DNA methylation patterns in hereditary human cancers mimic sporadic tumorigenesis. Hum Mol Genet 10:3001-3007.

Fan H, and Chu JY. (2007) A brief review of short tandem repeat mutation. Genomics Proteomics Bioinformatics 5:7-14.

Fornace A, Jackman J, Hollander MC, Hoffman-Liebermann B, and Liebermann DA. (1992) Genotoxic stress response genes and growth arrest genes: gadd, MyD, and other genes induced by treatments eliciting growth arrest. Ann NY Acad Sci 663:139-154.

Friedrichsen DM, Stanford JL, Isaacs SD, Janer M, Chang BL, Deutsch K, Gillanders E, Kolb S, Wiley KE, Badzioch MD, Zheng SL, Walsh PC, Jarvik GP, Hood L, Trent JM, Isaacs WB, Ostrander EA, and Xu J. (2004) Identification of a prostate cancer susceptibility locus on chromosome 7q11-21 in Jewish families. Proc Natl Acad Sci USA 101:1939-1944.

Fry RC, Begley TJ, and Samson LD. (2005) Genome-wide responses to DNA-damaging agents. Annu Rev Microbiol 461:1071-1078.

Funato T, Uehara S, Takahashi M, Kozawa K, Satoh J, Sasaki T, and Kaku M. (2002) Microsatellite instability in gonadal tumors of XY pure gonadal dysgenesis patients. Int J Gynecol Cancer 12:192-197.

Gao R, Matsuura T, Coolbaugh M, Zühlke C, Nakamura K, Rasmussen A, Siciliano MJ, Ashizawa T, and Lin X (2008) Instability of expanded CAG/CAA repeats in spinocerebellar ataxia type 17. Eur J Hum Genet 16:215-222.

Geisler JP, Goodheart MJ, Sood AK, Holmes RJ, Hatterman-Zogg MA, and Buller RE. (2003) Mismatch repair gene expression defects contribute to microsatellite instability in ovarian carcinoma. Cancer 98:2199-2206.

Goel A, Nagasaka T, Hamelin R, and Boland CR. (2010) An optimized pentaplex PCR for detecting DNA mismatch repair-deficient colorectal cancers. PLoS One 5:9393-9402.

Goddard KA, Witte JS, Suarez BK, Catalona WJ, and Olson JM. (2001) Model-free linkage analysis with covariates confirms linkage of prostate cancer to chromosomes 1 and 4. Am J Hum Gene 68:1197-1206.

Gong X, Delorme R, Fauchereau F, Durand CM, Chaste P, Betancur C, Goubran-Botros H, Nygren G, Anckarsäter H, Rastam M, Gillberg IC, Kopp S, Mouren-Simeoni MC, Gillberg C, Leboyer M, and Bourgeron T. (2009) An investigation of ribosomal protein L10 gene in autism spectrum disorders. BMC Med Genet 10:7-11.

Grigoriadis A, Caballero OL, Hoek KS, da Silva L, Chen YT, Shin SJ, Jungbluth AA, Miller LD, Clouston D, Cebon J, Old LJ, Lakhani SR, Simpson AJ, and Neville AM. (2009) CT-X antigen expression in human breast cancer. Proc Natl Acad Sci USA 106:13493-13498.

Guendel I, Carpio L, Pedati C, Schwartz A, Teal C, Kashanchi F, and Kehn-Hall K. (2010) Methylation of the tumor suppressor protein, BRCA1, influences its transcriptional cofactor function. PLoS One 5:e11379-e11384.

Helleman J, van Staveren IL, Dinjens WN, van Kuijk PF, Ritstier K, Ewing PC, van der Burg ME, Stoter G, and Berns EM. (2006) Mismatch repair and treatment resistance in ovarian cancer. BMC Cancer 6:201-211.

Hoeijmakers JH. (2001) Genome maintenance mechanisms for preventing cancer. Nature 411:366-374.

Hoeijmakers JH. (2009) DNA damage, aging, and cancer N Engl J Med 361:1475-1485.

Hofmann M, and Ruschenburg I. (2002) mRNA detection of tumor-rejection genes BAGE, GAGE, and MAGE in peritoneal fluid from patients with ovarian carcinoma as a potential diagnostic tool. Cancer 96:187-193.

Huen M, Sy S, and Chen J. (2010) *BRCA1* and its toolbox for the maintenance of genome integrity. Nature 11:138-148.

Idury RM, and Cardon LR. (1997) A simple method for automated allele binning in microsatellite markers. Genome Res 7:1104-1109.

Jego G, Hazoumé A, Seigneuric R, and Garrido C. (2010) Targeting heat shock proteins in cancer. Cancer Lett [Epub ahead of print].

Jemal A, Siegel R, Xu J, and Ward E. (2010) Global Cancer Statistics 2010. CA Cancer J Clin [Epub ahead of print]

Jirtle RL, Sander M, and Barrett JC. (2000) Genomic imprinting and environmental disease susceptibility. Environ Health Perspect 108:271-278.

Kim J, Reber HA, Hines OJ, Kazanjian KK, Tran A, Ye X, Amersi FF, Martinez SR, Dry SM, Bilchik AJ, and Hoon DS. (2006) The clinical significance of MAGEA3 expression in pancreatic cancer. Int J Cancer 118:2269-2275.

Lam D, Dickens D, Reid EB, Loh SH, Moisoi N, and Martins LM. (2009) MAP4K3 modulates cell death via the post-transcriptional regulation of BH3-only proteins Proc Natl Acad Sci USA 106:11978-11983

Li J, Yen C, Liaw D, Podyspasnina K, Bose S, Wang SI, Puc J, Miliaresis C, Rodgers L, McCombie R, Bigner SH, Giovanella BC, Ittmann M, Tycko B, Hibshoosh H, Wigler MH, and Parsons R. (1997) PTEN, a putative protein tyrosine phosphatase gene mutated in human brain, breast, and prostate cancer. Science 275:1943-1947.

Linger RJ, and Kruk PA. (2010) BRCA1 16 years later: risk-associated BRCA1 mutations and their functional implications. FEBS J 277:3086-3096.

Liu W, Zong W, Wu G, Fujita T, Li W, Wu J, and Wan Y. (2010) Turnover of BRCA1 involves in radiation-induced apoptosis. PLoS One 5: e14484-e14495.

Lynch HT, Smyrk T, and Lynch J. (1997) An update of HNPCC (Lynch Syndrome) Cancer Genet Cytogenet 93:84-99.

Mavaddat N, Antoniou AC, Easton DF, and Garcia-Closas M. (2010) Genetic susceptibility to breast cancer. Mol Oncol 4:174-191.

Mena S, Ortega A, and Estrella JM. (2009) Oxidative stress in environmental-induced carcinogenesis. Mutat Res 674: 36-44.

Miki Y, Futreal PA, Liu Q, Shattuck-Eidens D, Cochran C, Harshman K, Tavtigian S, Bennett LM, Haugen-Strano A, and Swensen J (1994) *BRCA1* mutations in primary breast and ovarian carcinoma Science 266:66-71.

Miki Y, Swensen J, Shattuck-Eidens D, Futreal PA, Harshman K, Tavtigian S, Liu Q, Cochran Ch, Bennett L, Ding W, Bell R, Rosenthal J, Hussey Ch, Tran T, McClure M, Frye Ch, Hattier T, Phelps R, Haugen-Strano A, Katcher H, Yakumo K, Gholami Z, Shaffer D, Stone S, Bayer S, Wray Ch, Bogden R, Dayananth P, Ward J, Tonin P, Narod S, Bristow PK, Norris F, Helvering L, Morrison P, Rosteck P, Lai M, Barrett J, Lewis C, Neuhausen S, Cannon-Albright L, Goldgar D, Wiseman R, Kamb A, and Skolnick M. (1994) A strong candidate for the breast and ovarian cancer susceptibility gene *BRCA1*. Science 266:66-71.

Miyamoto K, Fukutomi T, Asada K, Wakazono K, Tsuda H, Asahara T, Sugimura T, and Ushijima T. (2002) Promoter hypermethylation and post-transcriptional mechanisms for reduced BRCA1 immunoreactivity in sporadic human breast cancers. Jpn J Clin Oncol 32:79-84.

Monte M, Simonatto M, Peche LY, Bublik DR, Gobessi S, Pierotti MA, Rodolfo M, and Schneider C. (2007) MAGE-A tumor antigens target p53 transactivation function through histone deacetylase recruitment and confer resistance to chemotherapeutic agents. Proc Natl Acad Sci USA 10330:11160-11165.

Mulero JJ, Chang CW, Calandro LM, Green RL, Li Y, Johnson CL, and Hennessy LK. (2006) Development and validation of the AmpFlSTR Yfiler PCR amplification kit: a male specific, single amplification 17 Y-STR multiplex system. J Forensic Sci 51:64-75.

Narod S, Lynch H, Conway T, Watson P, Feunteun J, and Lenoir G. (1993) Increasing incidence of breast cancer in family with BRCA1 mutation. Lancet 341:1101-1102.

Nagarajan RP, Patzel KA, Martin M, Yasui DH, Swanberg SE, Hertz-Picciotto I, Hansen RL, Van de Water J, Pessah IN, Jiang R, Robinson WP, and LaSalle JM. (2008) MECP2 promoter methylation and X chromosome inactivation in autism. Autism Res 1:169-178.

Nakayama K, Takebayashi Y, Hata K, Fujiwaki R, Iida K, Fukumoto M, and Miyazaki K. (2004) Allelic loss at 19q12 and Xq11-12 predict an adverse clinical outcome in patients with mucinous ovarian tumours of low malignant potential. Br J Cancer 90:1204-1210.

Neuhausen SL, and Marshall CJ. (1994) Loss of heterozygosity in familial tumors from three BRCA1-linked kindreds. Cancer Res 54:6069-6072.

Parsons TJ, Huel R, Davoren J, Katzmarzyk C, Milos A, Selmanović A, Smajlović L, Coble MD, and Rizvić A. (2007) Application of novel "mini-amplicon" STR multiplexes to high volume casework on degraded skeletal remains. Forensic Sci Int Genet 1:175-179.

Pharoah PD, and Ponder BAJ. (2002) The genetics of ovarian cancer. Best Pract Res Clin Obstet Gynecol 16:449-468.

Prat J, Ribé A, and Gallardo A. (2005) Hereditary ovarian cancer. Hum Pathol 36:861-870.

Ramocki MB, Peters SU, Tavyev YJ, Zhang F, Carvalho CM, Schaaf CP, Richman R, Fang P, Glaze DG, Lupski JR, and Zoghbi HY. (2009) Autism and other neuropsychiatric symptoms are prevalent in individuals with MeCP2 duplication syndrome. Ann Neurol 66:771-782.

Rice JC, Massey-Brown KS, and Futscher BW. (1998) Aberrant methylation of the BRCA1 CpG island promoter is associated wuith decreased BRCA1 mRNA in sporadic breast cancer cells. Oncogene 17:1807-1812.

Risch HA, McLaughlin JR, Cole DE, Rosen B, Bradley L, Kwan E, Jack E, Vesprini DJ, Kuperstein G, Abrahamson JL, Fan I, Wong B, and Narod SA. (2001) Prevalence and penetrance of germline BRCA1 and BRCA2 mutations in a population series of 649 women with ovarian cancer. Am JHum Genet 68:700-710.

Rodriguez-Pinilla SM, Jones RL, Lambros MB, Arriola E, Savage K, James M, Pinder SE, and Reis-Filho JS. (2007) MYC amplification in breast cancer: a chromogenic in situ hybridization study. J Clin pathol 60:1017-1023.

Schweppe RE, Klopper JP, Korch C, Pugazhenthi U, Benezra M, Knauf JA, Fagin JA, Marlow LA, Copland JA, Smallridge RC, and Haugen BR. (2008) Deoxyribonucleic acid profiling analysis of 40 human thyroid cancer cell lines reveals cross-contamination resulting in cell line redundancy and misidentification. J Clin Endocrinol Metab 93:4331-4341.

Shah SN, Hile SE, and Eckert KA. (2010) Defective mismatch repair, microsatellite mutation bias, and variability in clinical cancer phenotypes. Cancer Res 70:431-435.

Sieben NL, Kolkman-Uljee SM, Flanagan AM, le Cessie S, Cleton-Jansen AM, Cornelisse CJ, and Fleuren GJ. (2003) Molecular genetic evidence for monoclonal origin of bilateral ovarian serous borderline tumors. Am J Pathol 162:1095-1101.

Simpson JF, Quan DE, O'Malley F, Odom-Maryon T, and Clarke PE. (1997) Amplification of CCND1 and expression of its protein product, cyclin D1, in ductal carcinoma in situ of the breast. Am J Pathol 151:161-168.

Sirchia SM, Tabano S, Monti L, Recalcati MP, Gariboldi M, Grati FR, Porta G, Finelli P, Radice P, and Miozzo M. (2009) Misbehaviour of XIST RNA in breast cancer cells. PLoS One 4:5559-5562.

Sirotkin AV, and Bauer M. (2010) Heat shock proteins in porcine ovary: synthesis, accumulation and regulation by stress and hormones. Cell Stress Chaperones Dec 28. [Epub ahead of print].

Suyama T, Shiraishi T, Zeng Y, Yu W, Parekh N, Vessella RL, Luo J, Getzenberg RH, and Kulkarni P. (2010) Expression of cancer/testis antigens in prostate cancer is associated with disease progression. Prostate 70:1778-1787.

Toyota M, and Issa JP. (1999) CpG island methylator phenotypes in aging and cancer. Semin Cancer Biol 9:349-357.

Trimeche M, Braham H, Ziadi S, Amara K, Hachana M, and Korbi S. (2008) Investigation of allelic imbalances on chromosome 3p in nasopharyngeal carcinoma in Tunisia: high frequency of microsatellite instability in patients with early-onset of the disease. Oral Oncol 44:775-783.

Tront J, Hoffman B, and Lieberman D. (2006) Gadd45a suppresses Ras-driven mammary tumorigenesis by activation of c-jun NH2-terminal kinase and p38stress signaling resulting in apoptosis and senescence. Cancer res 66:8448-8454.

Umar A, Boland CR, Terdiman JP, Syngal S, de la Chapelle A, Rüschoff J, Fishel R, Lindor NM, Burgart LJ, Hamelin R, Hamilton SR, Hiatt RA, Jass J, Lindblom A, Lynch HT, Peltomaki P, Ramsey SD, Rodriguez-Bigas MA, Vasen HF, Hawk ET, Barrett JC, Freedman AN, and Srivastava S. (2004) Revised Bethesda Guidelines for hereditary nonpolyposis colorectal cancer (Lynch syndrome) and microsatellite instability. J Natl Cancer Inst 96:261-268.

Van Loon B, Markkanen E, and Hubscher U. (2010) Oxygen as a friend and enemy: How to combat the mutational potential of 8-oxo-guanine. DNA Repair 9:604-616.

Vauhkonen H, Vauhkonen M, Sipponen P, and Sajantila A. (2004) Correlation between the allelic distribution of STRs in a finnish population and phenotypically different gastrointestinal tumours: a study using four X-chromosomal markers (DXS7423, DXS8377, ARA, DXS101) Ann Hum Genet 68 (Pt 6):555-62.

Venkitaraman AR. (2001) Functions of BRCA1 and BRCA2 in the biological response to DNA damage. J Cell Sci 114(Pt 20):3591-8.

Weber F, Shen L, Fukino K, Patocs A, Mutter GL, Caldes T, and Eng C. (2006) Total-genome analysis of BRCA1/2-related invasive carcinomas of the breast identifies tumor stroma as potential landscaper for neoplastic initiation. Am J Hum Genet 78:961-972.

Wood LD, Calhoun ES, Silliman N, Ptak J, Szabo S, Powell SM, Riggins GJ, Wang TL, Yan H, Gazdar A, Kern SE, Pennacchio L, Kinzler KW, Vogelstein B, and Velculescu VE.(2006) Somatic mutations of GUCY2F, EPHA3, and NTRK3 in human cancers Hum Mutat 27:1060-1061.

Werness BA, and Eltabbakh GH. (2001) Familial ovarian cancer and early ovarian cancer: biologic, pathologic, and clinical features. Int J Gynecol Pathol 20:48-63.

Zhang J, and Powell SN. (2005) The role of the BRCA1 tumor suppressor in DNA double-strand break repair.Mol Cancer Res 3:531-539.

Zhang S, Zhou X, Yu H, and Yu Y. (2010) Expression of tumor-specific antigen MAGE, GAGE and BAGE in ovarian cancer tissues and cell lines. BMC Cancer 10:163-166.

Zhang Y, Monckton DG, Siciliano MJ, Connor TH, and Meistrich ML (2002) Detection of radiation and cyclophosphamide-induced mutations in individual mouse sperm at a human expanded trinucleotide repeat locus transgene. Mutat Res 516:121-138.

CHAPTER V

ACCUMULATION OF MICROSATELLITE INSTABILITY IN SUPEROXIDE DISMUTASE-1 KNOCKOUT MICE: A POSSIBLE PREDICTOR OF GERM CELL DEVELOPMENT OR TUMORIGENESIS

5.1 Abstract

The superoxide dismutase 1 gene (*Sod1*) is one of the cell protective mechanisms to eliminate reactive oxygen species (ROS) damage in order to protect cell components and avoid tumorigenesis. Mouse primordial germinal cells (PGCs) are a population of cells originating from the proximal margin of the epiblast in close proximity to the extra embryonic ectoderm, and from which some cells differentiate into male or female germinal cells. During cell migration across the genital ridge, PGCs display an extensive proliferation rate and they are exposed to ROS damage. In abscense of cell antioxidant mechanisms, PGCs have increased risk to accumulate specific mutations by free radical damage. We hypothetize that during cell migration, *Sod1* knockout PGCs accumulate microsatellite instability (MSI) and this could be a signal for PGC pool selection or a cause of tumor transformation. We dissected and isolated PGCs from *Sod1* $^{+/+}$ (wild type), *Sod1* $^{+/-}$ (heterozygous), and *Sod1*$^{-/-}$ (homozygous) mouse strain (B6; 129S7-*Sod1*$^{tm1Leb/J}$), from the genital ridge at 10.5 days post coitum (dpc) and 18 dpc to determine and quantify MSI in 10 single tandem repeat markers by single cell PCR methods. Our results demonstrate that PGCs from *Sod1* knockout mice accumulated MSI in five markers (*4-4-19844, D13mit16, D13mit78, D19mit68,* and *DXmit249*) located

near important genes involved in cell proliferation and differentiation. Taken together, this study shows that MSI is directly related to *Sod1* gene disruption that could induce abnormal migration characteristics seen in PGC such as invasion and metastasis. In conclusion, MSI could be a signal for PGC pool selection, or cell transformation into tumorigenesis.

5.2 Introduction

Primordial germinal cells (PGCs) are the progenitors of spermatogonia and oogonia in the testis and ovary, respectively (De Felici *et al.*, 2002). PGCs originate from the embryonic primary ectoderm (epiblast), and they are one of the cell types that migrate directly through the developing embryo to their site of histogenesis (Pesce, 2002; Tam and Snow, 1981). Proliferation and migration of PGCs has been widely studied in different animal models such as mouse, rabbit, sheep, and pig (Ledda *et al.*, 2010). Of all mammals studied so far, the mouse has provided the most extensive data for the study of early stages of embryonic development (De Felici, 2000; Labosky, 1999). There is a similarity in development between mouse and human germinal cells. Therefore, the mouse is an outstanding research model for the study of germ cell lineage (McLaren, 2003; Resnic *et al.*, 1992). Our study utilizes mouse PGCs as a model to evaluate the effects of oxidative stress in germ cell development that leads to genomic instability by accumulation of microsatellite instability (MSI). Elevated free radical damage through reactive oxygen species (ROS) accumulation can override DNA repair mechanisms, giving rise to increased cell mutations that induce infertility, cancer development, chronic diseases (including cardiovascular and neurodegenerative diseases), and aging (Essick and Sam, 2010; Agarwal *et al.*, 2005).

In mammalian cells, protection against oxidative DNA damage caused by ROS accumulation is accomplished by a complex defense systems composed of antioxidant enzymes such as the superoxide dismutase family (*Sod1, Sod2*, and *Sod3*) (Carlsson *et al.*, 1995). *Sod1* is also known as copper/zinc superoxide dismutase (Cu/Zn Sod). *Sod2* is also known as manganese superoxide dismutase (Mn-Sod), and *Sod3* is also known as secreted extracellular superoxide dismutase (EC-Sod). All of these *Sod* genes play

critical roles in order to maintain cell oxidative homeostasis and are expressed in the rodent ovary and testis (Matzuk *et al.*, 1998). The *Sod1* gene codes for cytosolic superoxide dismutase, which is important for the catalyzation of superoxide ion (O_2^-) into hydrogen peroxide (H_2O_2), and in presence of catalase, H_2O_2 is reduced to water (Lu *et al.*, 2007). The *SOD1* enzyme has been isolated from a wide range of organisms such as yeast, bacteria, mice, chicken and bovine (Noor *et al.*, 2002). *Sod1* mutant mice display a pleiotropic phenotype that includes neurodegeneration, immunodeficiency, cancer predisposition, and hypersensitivity to ionizing radiation (Peled-Kamar *et al.*, 1995). Although *Sod1* knockout mice are born and develop normally, *Sod1* deficient female mice are subfertile or infertile and display a marked increase in post-implantation embryonic lethality (Ho *et al.*, 1998). All together, *Sod1* deficient mice are prone to infertility and cancer due to an increase of ROS within the ovary affecting its function. This increased ROS to which the *Sod1* knockout mice are exposed, results in inhibition of downstream genetic mechanisms that are responsible for the increased risk of ovarian follicular disfunction and are at a higher risk for cancer development (Ho *et al.*, 1998).

Endogenous production of ROS from different cellular metabolic processes leads to persistent exposure to oxidative damage (Noor *et al.*, 2002). Protective mechanisms against this damage are needed in order to counteract harmful effects in vulnerable cell components such as mitochondria, nucleus, and membrane (Essick and Sam, 2010). However, mutations in the genes responsible for removing superoxide radicals generated in the cytoplasm and nucleus can have a negative impact on genomic DNA integrity, giving rise to defects in cell functionality and cell malignancy transformation (Noor *et al.*, 2002). In order to analyze the role of the *Sod1* gene in genomic homeostasis of mouse PGC development, we dissected and isolated primordial germinal cells from the

genital ridges of *Sod1* $^{+/+}$ (wild type), *Sod1* $^{+/-}$ (heterozygous), and *Sod1*$^{-/-}$ (homozygous) mice. Our results support the hypothesis that accumulation of genomic DNA instability due to oxidative damage, established by MSI, is a main factor that negatively influences cell development and cell migration. MSI was detected in different mouse single tandem repeats in *Sod1* homozygous -/- mouse embryos at 10.5 days post-coitum (dpc). This study suggest that these markers are important novel target sequences that could be used in humans as a screening method to evaluate the disruption of cell stress responses that lead to initiation and progression of ovarian carcinoma.

5.3 Materials and Methods

5.3.1 Animal model

Uteri of pregnant female mice from the heterozygous superoxide dismutase 1 (*Sod1*) knockout strain (B6; 129S7-*Sod1*$^{tm1Leb/J}$) were purchased from The Jackson Laboratory (Bar Harbor, ME). Details related to the generation of the *Sod1* mouse model have been previously described. Briefly, target mutations in the *Sod 1* gene were generated by replacement of exon 1 and 2 with a PGK-hptr expression cassette (Matzuk *et al.*, 1998). In the Jackson Lab facilities, male and female heterozygous mice with the superoxide dismutase 1 (*Sod1*^{tm1Leb}) gene were bred. Females were checked for vaginal plugs and plug-positive females were transferred to necropsy at 10.5 and 18 days post-coitum (dpc). Uteri were removed from euthanized females and shipped to our laboratory at Mississippi State University. A total of two pregnant uteri at 10.5 dpc and two uteruses at 18 dpc were dissected. We obtained male and female mouse fetuses with the three expected genotypes: wild type homozygous *Sod1* $^{+/+}$, heterozygous *Sod1* $^{+/-}$ and homozygous *Sod1* $^{-/-}$.

5.3.2 Isolation and maintenance of primordial germinal cells

From each mouse fetus, the placenta and extra embryonic tissues were removed. Mouse fetuses were transferred into a fresh petri dish filled with D-PBS and the length was measured. Fetus tails were removed for DNA purification, sexing, and genotyping by PCR. Each mouse fetus was dissected following the protocol previously standardized in our lab (Moreno-Ortiz *et al.*, 2009). Briefly, gonadal ridges were removed by cutting away the tissues that support them. Gonadal ridges were transferred to a petri dish filled with fresh PBS to clean away the surrounding somatic cells. Dispersed suspensions of

PGCs from the containing tissues were recovered for isolation of DNA. Characterization of PGCs was achieved using the alkaline phosphatase kit according to the manufacturer's instructions (Millipore, Billerica, MA).

5.3.3 DNA isolation

DNA was prepared from each fetus tail and from primordial germinal cells harvested from gonadal ridges at 10.5 and 18 dpc. DNA was isolated with the Purelink genomic DNA mini kit (Invitrogen Carlsbad, CA) following the manufacturer's protocol. All DNA samples were quantified using a NanoDrop™ ND1000 spectrophotometer (Thermo Scientific, Wilmington, DE).

5.3.4 Sex determination of mouse fetus

Sex determination was achieved by PCR amplifications performed in a total reaction volume of 25µl containing 1X of buffer D (US DNA, Forth Worth, TX), 2.5mM of MgCl (US DNA, Forth Worth, TX), 10mM of dNTPs (Applied Biosystems, Foster City, CA) and 1.25 U/µL of hot multitaq DNA polymerase (5 U/µl; US DNA, Forth Worth, TX). Primers were used as follows: Zfy forward 5'-AAGATAAGCTTACATAATCACATGGA and Zfy reverse 3'-CCTATGAAATCCTTTGCTGCA CATGT, 600bp. The m-DXNds3 forward: GAGTGCCTCATCTATACTTACAG and m-DXNds3 reverse: TCTAGTTCATTGTTGATTAGTTGC, 242 bp (Nagamine CM, 1989). PCR was performed on PE 9600 thermocycler using following cycling protocol: 1 cycle of 95°C for 11 min, 30 cycles of (denaturation for 60 sec at 94°C, annealing for 150 sec at 60°C, and extension for 150 sec at 72°C) final step 1 cycle of 72°C for 2 min and hold at 4°C.

Negative controls were included in each PCR. Amplified products were analyzed with gel electrophoresis at 4% nusieve agarose gel (Clonetics, Lonza, Walkersville, MD).

5.3.5 Genotyping of mouse fetus

Genotyping of mouse fetuses to determine presence of the *Sod1* transgene was achieved by PCR amplifications performed in a total reaction volume of 25 µl containing 1X of buffer D (US DNA, Forth Worth, TX), 2.5mM of MgCl (US DNA, Forth Worth, TX), 10 mM of dNTPs (Applied Biosystems, Foster City, CA) and 1.25 U/µL of hot multitaq DNA polymerase (5 U/µl; US DNA, Forth Worth, TX). Primers used were: Mut781F 5'-TGTTCTCCTCTTCCTCAT CTCC-3', Mut782R 5'-ACCCTTTCCAAATCCTCAGC-3', Wt878F 5'TGAACCAGTTGT GTTGTCAGG-3', and Wt888R 5'-TCCATCACTGGTACAT AGCC-3' (The Jackson Lab, Bar Harbor, ME). PCR reactions were performed on PE 9600 thermocycler using cycle as follows: 1 cycle for 94°C for 3 min, 35 cycles of (94°C for 20 sec, 60°C for 1 min; 72°C for 1 min); 1 cycle 72°C for 2 min, and hold at 4°C. Negative controls were included in each PCR. Amplified products were analyzed with gel electrophoresis at 4% nusieve agarose gel (Clonetics-Lonza, Walkersville, MD).

5.3.6 Mouse single tandem repeat markers selection and standardization

A total of 21 single tandem repeats (STR) were selected from across the mouse genome. Fifteen markers were located on autosomes, and six markers were located on X chromosome (Table 5.1). Fluorescent primers were purchased from IDT (Coralville, IA) at 100 µM/µL. The labeled dyes used were either 6-FAM (blue) or HEX (green). For initial testing, forward and reverse primers were combined for a final primer concentration of 25µM/µL to create a singleplex primer stock. Primers were tested at

concentrations ranging from 0.8-1.5 μM/μL in standard PCR conditions and reagents. Each locus was standardized in separate PCR reactions for optimization and to ensure specificity and sensitivity of the marker.

5.3.7 Single cell PCR

PCR was performed for 10 markers out of 21 total markers because only these 10 markers amplified during standardization. Two markers came from the mouse X chromosome, one marker each from chromosomes 6 and 17, and two markers each from chromosomes 8, 13, and 19 (Table 5.2). DNA serial dilutions were made at 0.1 ng/μL, 0.05 ng/μL, and 0.025 ng/μL. Using these serial DNA dilutions, Poisson analysis of the amplified alleles was performed to calculate the correct genomic equivalent value for each sample in order to obtain less than one diploid genome equivalent of the DNA sample (sample genome equivalents range between 12.5-50 pg/μL) (Coolbaugh-Murphy *et al.*, 2005; Coolbaugh-Murphy *et al.*, 2004). This concentration of DNA allowed sufficient sensitivity to distinguish between wild type and mutated alleles at their appropriate frequency.

PCR amplifications were performed in a total reaction volume of 10 μl containing 1 X of buffer D [800 mM Tris HCl, 200 mM $(NH_4)_2SO_4$, 0.2% w/v Tween 20] (US DNA, Fort Worth, TX), 2.5 mM $MgCl_2$ (US DNA, Fort Worth, TX), 1 X of Solution L (US DNA, Fort Worth, TX), 1.25 U Hot-MultiTaq DNA polymerase (5 U/μl; US DNA, Fort Worth, TX), 4% DMSO (Sigma Aldrich, Saint Louis, MO), 0.4 mg/μL bovine albumin serum (Thermo Scientific, Rockford, IL), 300 μM dNTPs (Applied Biosystems, Foster City, CA), and 0.5 and 1.8 μM mixed primer (forward and reverse) respectively. Solution L (1X) was used as an additive that facilitates amplification of difficult

templates. PCR was performed on a PE 9600 thermocycler using a ramping cycling protocol: 1 cycle of 95 ºC for 11 minutes; 1 cycle of 96 ºC for 1 minute; 10 cycles of [94ºC for 30 seconds, ramp 68 seconds to 58 ºC (hold for 30 seconds), ramp 50 seconds to 70 ºC (hold for 60 seconds)]; 25 cycles of [90 ºC for 30 seconds, ramp 60 seconds to 58 ºC (hold for 30 seconds), ramp 50 seconds to 70 ºC (hold for 60 seconds)]; 1 cycle of 60ºC for 30 minutes for final extension; and hold at 4ºC. Negative controls and reaction mixtures were included in each PCR to monitor for contamination.

Products amplified by single genome equivalent PCR were separated and detected by fragment analysis on an AB 3130XL Genetic Analyzer (Applied Biosystems, Foster City, CA) in the presence of Gene Scan 500 LIZ Ladder (Applied Biosystems, Foster City, CA) following the manufacturer's protocol. Wild type and mutated alleles were quantified with the GeneMapper version 4.0 software package (Applied Biosystems, Foster City, CA). Repeat motif shifts from wild type standardized alleles were considered mutant alleles (Coolbaugh-Murphy *et al.*, 2005; Coolbaugh-Murphy *et al.*, 2004). We followed scoring rules for each marker as we previously mention in Chapters 3 and 4. Presence of wild type and/or mutant alleles was scored for each single cell replicate. An average of 48 replicates per sample were amplified and scored from different samples of mouse PGCs.

5.3.8 Genomic instability statistical analysis

We amplified less than a single diploid genome-equivalent of DNA with single cell PCR methods to estimate oxidative stress-induced mutation frequencies in specific microsatellite repeat markers. DNA concentrations were adjusted to obtain between 0.5-2 genome equivalents, on average, per single cell PCR reaction. The average number of

amplifiable DNA molecules (λ) in each PCR reaction was calculated using the Poisson distribution: $\lambda = -\ln(K_1/K)$, where K_1 = the total number of alleles expected minus the number of alleles observed, and K = the total number of alleles expected (Coolbaugh-Murphy *et al.*, 2004; Zhang *et al.*, 2002).

Mutation frequencies for each marker by sample genotype, sex, and age were calculated by SP-PCR software version 2.0 (M.D. Anderson Cancer Center, Houston, TX). Maximum likelihood estimates of the mean number of mutant alleles and wild type alleles in each replicate, as well as their bootstrap standard deviations, were also calculated by SP-PCR software version 2.0 (M.D. Anderson Cancer Center, Houston, TX). Differences in the estimation of mutation frequencies were calculated with a two tailed *t*-test using raw mutation frequencies. A three way cross class ANOVA, assuming no third factor interaction, and appropriate LSD multiple comparison (*t*-test) outputs were also produced. Results were considered statistically significant with a $p<0.05$ (using Procedure GLM from statistical package SAS/win 9.2, SAS Institute Inc., Cary, NC).

5.4 Results

5.4.1 *Sod1* $^{-/-}$ knockout genotype could be responsible for embryo growth retardation or loss of pregnancy

We obtained two mouse uteri from The Jackson Laboratory at 10.5 dpc and two uteri at 18dpc. Fetal genotypes were determined with PCR using purified DNA samples of mouse fetus tails dissected during the isolation protocol. We were able to genotype the following 37 fetuses: 19 females including 8 *Sod1*$^{+/+}$, 9 *Sod1*$^{+/-}$, and 2 *Sod1* $^{-/-}$, and 18 male fetuses including 3 *Sod1*$^{+/+}$, 11 *Sod* $^{+/-}$, and 4 *Sod1*$^{-/-}$ (Figures 5.1, 5.2, 5.3). Drastic reduction in the physical size of female homozygous *Sod1*$^{-/-}$ mouse fetuses was observed. These results suggest that the reduced number of the female *Sod1*$^{-/-}$ phenotype might be the result of subfertility due to early embryonic resorption or spontaneous miscarriage (Figure 5.3). However, this observation was not statistically significant. The lengths of all dissected fetuses were measured, and we observed that at 10.5 dpc of gestational age, male and female *Sod1*$^{+/+}$ (wild type) and heterozygous *Sod1* $^{+/-}$ mouse fetuses showed an average size of 14 mm. In contrast, female homozygous *Sod1*$^{-/-}$ mouse fetuses showed a slight decrease in average size at 10 mm, and male homozygous *Sod1*-/- mouse fetuses showed an average size of 13 mm. At 18 dpc, all fetuses showed an average size of 21 mm for all genotypes, and no differences between male and female fetuses were observed (Figure 5.4).

5.4.2 Genomic instability in single tandem repeats was present in *Sod1* knockout mice

Cancer has been correlated with accumulation of spontaneous mutations due to oxidative stress in different organs such as brain, testes, ovary, and liver (Elchuri *et al.*, 2005). Mechanism of cellular defense against oxidative stress includes superoxide

dismutase 1 (*Sod1*) which is a key molecule in the redox system (Noor *et al.*, 2002). We asked whether disruption of the *Sod1* function induces accumulation of the spontaneous mutations in PGCs early in embryonic development at 10.5 dpc and later on at 18 dpc. We determined genomic instability by MSI analysis at two different times during mouse embryonic germinal cell development (10.5 dpc and 18 dpc). DNA samples from female and male PGCs of $Sod1^{+/+}$, $Sod1^{+/-}$, and $Sod1^{-/-}$ genotypes were analyzed. We observed statistically significant high frequencies of mutations in five out of 10 microsatellites evaluated (*4-4-19844, D13mit16, D13mit78, D19mit68,* and *DXmit249*) (Figure 5.5) (Table 5.3). These results show that spontaneous mutations can accumulate in microsatellite sequences during embryonic development due to a deficiency in mouse PGCs to oxidative stress response.

5.4.3 Microsatellite instability occurs early in the mouse PGC development

Mouse PGCs migrate out of the hindgut through the dorsal mesentery at 9.5 dpc. PGCs arrive at the genital ridge at 10.5-11.5 dpc. The complete colonization of the genital ridge by PGCs is achieved at 13 dpc. After PGC migration and colonization, the percentage of PGCs gradually decline from 13.5 dpc to 16.5 dpc of mouse embryonic development (Bendel-Stenzel *et al.*, 1998). We suggest that accumulation of MSI could be the signal on the genital ridge for PGC selection before meiotic arrest takes place. Our results report high mean frequencies of MSI in *Sod1* knockout mouse PGC samples, whereas wild type *Sod1* and heterozygous $Sod1^{+/-}$ mouse PGC samples did not show MSI over time. Specifically female PGCs *Sod1* knockout -/- at 10.5 dpc showed a high overall mean frequency of MSI in four unstable markers (f= 0.362) in comparison with the MSI frequency observed just in one unstable marker at 18 dpc (f= 0.012). Our results suggest

that MSI could be a signal for PGC pool selection during early mouse gonad colonization in embryos with abnormal redox mechanisms (Table 5.3).

5.4.4 Oxidative stress response due to superoxide dismutase 1 deficiency differs between sexes

Previous studies have reported that female *Sod1* knockout mice are infertile in comparison with male homozygous mice that are reproductively normal (Ho *et al.*, 1998; Matzuk *et al.*, 1998). We were interested in determining if MSI accumulation is common in female or male PGCs from *Sod1* knockout mouse embryos. Our results showed high MSI frequency in female and male *Sod1* knockout mouse PGCs. Female *Sod1* knockout PGCs showed statistically high MSI frequencies in four markers at 10.5 dpc (*4-4-19844, D13mit16, D13mit78,* and *DXmit249*) and only one marker showed instability at 18 dpc (*D13mit78*). In contrast, male *Sod1* knockout PGCs showed instability frequencies in three markers at 10.5 dpc (*D13mit16, D19mit68,* and *DXmit249*) and no instability was detected at 18 dpc. Female *Sod1* knockout PGCs displayed a significant 3-fold increase in the overall mean mutation frequency compared with male *Sod1* knockout PGCs ($p<0.05$) (Figure 5.6). Mutation frequencies in wild type and heterozygous *Sod1* were stable in both female and male PGCs samples. These observations confirm that MSI could be the cause of female *Sod1* reproductive deficiency.

5.4.5 Microsatellite instability was detected in markers located near genes responsible for cellular stress responses

Upon migration and colonization of genital ridge by PGCs, several molecular pathways are responsible for the establishment of germinal cell pool during the mouse embryonic development (Matsui, 1998). Deregulation of *Sod1* gene is a perfect model to evaluate oxidative stress damage as a cause of disease (Miana-Mena *et al.*, 2010; Van

Remmen *et al.*, 2004). We determined MSI frequencies in two markers in both female and male knockout *Sod1* mice. One marker is located near a gene involved in counteracting the oxidative damage mechanism (*Dxmit249*) and the other marker has been linked to migration and colonization status of PGCs (*D13mit16*). Significant differences in MSI frequencies were obtained with these two markers at 10.5 dpc between female and male PGC samples. High MSI frequencies in both markers were observed in female and male *Sod1* knockout mice compared to female and male wild type and heterozygous +/- *Sod1* mice ($p<0.0001$). *Dxmit249* marker was highly unstable compared to *D13mit16* at 10.5 dpc in female and male *Sod1* knockout mice (Figure 5.7). At 18 dpc both markers were stable. Our results indicate that MSI detected in markers located near genes responsible for the downstream steps in the antioxidant *Sod1* pathway could be the signal for oxidative stress damage.

5.4.6 Embryonic development is disrupted by the presence of MSI in genes responsible for cell lineage commitment

Early during mouse embryonic development, primordial germinal cells are derived from the embryonic primary ectoderm (epiblast) (Pesce M, 2002). Developmental genes responsible for cell lineage commitment are targets for the accumulation of spontaneous mutations generated by deregulation of antioxidative pathways (Huang *et al.*, 1997). We wanted to demonstrate that MSI is present near genes involved in embryonic differentiation pathways. We found that MSI was present in two unstable markers related to key genes that play a role in the morphogenesis stages of the embryo (*D13mit78* and *4-4-19844*). Significant differences in MSI frequency were observed in female *Sod1* knockout PGCs when compared to male *Sod1* knockout PGCs, which were stable for these two markers. The MSI detected in the *D13mit78* marker was

highly significant at 10.5 dpc in the female *Sod1* knockout PGC sample (*f*=0.14 p=0.0001) compared to the MSI frequency of marker *4-4-19844* (*f*=0.074 and p=0.0002) (Figure 5.8). Unstable alleles were not detected in either wild type *Sod1*$^{+/+}$ PGC or heterozygous *Sod1* $^{+/-}$ PGC samples. Taken together, these findings demonstrate that MSI could be a signal that triggers deregulation of genes involved in germ cell lineage commitment.

5.4.7 Male PGCs are sensitive to microsatellite instability in specific markers related to Wnt cofactor genes

The Wnt signaling pathway participates in embryogenesis. This pathway controls cell proliferation and migration of mouse PGC and is thought to be related to specific functions in gonad and germ cell development (Gatcliffe *et al.*, 2008). We detected MSI in one marker (*D19mit68*) that is associated with Wnt cofactor responsible for the intracellular signaling cascade in mouse embryonic development. However, only male *Sod1* knockout PGCs were unstable for this marker, and significant MSI frequency was observed in *D19mit68* at 10.5 dpc (p=0.0067) (Figure 5.9). This marker was stable in both *Sod1* wild type and *Sod1* heterozygous male and female mice of all genotypes. Some non-significant instability was detected in PGCs at 18 dpc in both *Sod1* wild type and *Sod1* heterozygous male and female mice of all genotypes. This result is congruent with the importance of the Wnt signaling cascade function reported by others (Johnson and Rajamannan, 2006). MSI detection in this marker could be a signal to deregulate the initializing cofactor for this important developmental pathway due to accumulation of mutations in mouse PGCs.

5.5 Discussion

Characterization of embryonic germinal cells as precursors to male or female gonads in mammals is essential for designing research related to infertility, gametogenesis, and cancer during early development. The numerous possible uses of these cell lines for further basic studies made them an invaluable research tool. Investigations of oxidative stress as a cellular mechanism involved in accumulation of mutations in tumorigenesis, disease development, or cell aging have increased our understanding about different pathways of cell pathogenesis. It is well understood that cells increase the rate of MSI due to accumulation of DNA damage that override DNA repair mechanisms and tumor suppressor pathways, leading to a best-case scenario of apoptosis or a worst-case scenario of tumor transformation. Many mouse models have been developed to study cellular stress response signals (Matzuk MM., 1998). Knockout mice for the *Sod1* gene, an antioxidant molecule responsible for the cellular stress response that defends against damage accumulation from oxidative stress, is a noteable research model used in our study. Associated with the aging process, *Sod1* knockout mice have displayed increases in DNA damage and MSI that are involved in the induction of spontaneous tumors such as in lymphoma, liver, and spleen cancer (Busuttil *et al.*, 2005; Elchuri *et al.*, 2005; Matzuk *et al.*, 1998). Additionally, these knockout *Sod1* mice have developed neurodegenerative disorders such as amyotrophic lateral sclerosis and Parkinson's disease that have been linked to the oxidative damage (Philips and Robberecht, 2011).

This mouse knockout strain (B6; 129S7-*Sod1*$^{tm1Leb/J}$) is an ideal model for our study on the etiology of early ovarian cancer signals. This model has led us to understand and clarify early molecular signals implicated during ovarian development,

ovarian tumor transformation, and ovarian cancer progression due to the accumulation of DNA damage by oxidative stress. Genomic instability in PGCs might be the first step of impairment for cell migration and early differentiation in the genital ridges. Our focus is the study of possible signals of genomic instability that induce germinal mutations during the first germ cell commitment in embryonic development. It is known that these signals have been linked to the origin of different cancers such as breast and endometrial carcinomas.

Our results indicate that PGCs accumulate MSI in particular markers located near important genes involved in cell proliferation, differentiation, and migration. This event could be a signal that modulates gonadal colonization by PGCs and selection of the germ cell pool that will be arrested for future gametogenesis in adult mice. We found that PGCs on *Sod1* knockout mice have increased spontaneous mutations as determined by detection of high frequencies of MSI in five out of ten markers we tested. Female and male *Sod1* knockout mice were significantly unstable in contrast to the complete stability detected for PGCs samples from *Sod1* wild type and *Sod1* $^{+/-}$ heterozygous mice.

The induction of MSI in mouse PGC samples from female and male *Sod1* knockout embryonic mice are directly related to the increased sensitivity of spontaneous mutations due to antioxidant defense disruption. Furthermore, our results were in agreement with the observation that *Sod1* knockout females are reproductively deficient while *Sod1* knockout males are fertile (Matzuk *et al.*, 1998). PGC samples from female *Sod1* knockout mice showed instability in four markers located near genes previously linked to neuroectoderm cell lineage commitment and ovarian cancer development. These genes are responsible for normal migration and colonization abilities of the

embryonic germinal tissue early during development as well in abnormal invasion and metastasis abilities seen during cell transformation and tumorigenesis.

Female and male *Sod1* knockout PGCs were significantly unstable for markers *Dxmit249* and *D13mit16* in contrast with female and male *Sod1* wild type and $Sod1^{+/-}$ heterozygous mice who were stable. Marker *Dxmit249* is near the carbonic anhydrase 5b, mitochondrial (*Car5b*) gene that is involved in the conversion of pyruvate to lactic acid in the presence of oxygen. The *Car5b* gene catalyzes the reversible hydratation of CO_2 to HCO_3 in order to maintain tissue pH homeostasis (Woelber *et al.*, 2010). In cancer cells, high levels of intracellular lactate give rise to over expression of acid-regulating proteins like carbonic anhydrases (Hynninen *et al.*, 2006) (Table 5.4). Our results infer that MSI of marker *Dxmit249* could be a signal that deteriorates pH cell defense mechanisms implicated in ovarian cancer disease. Marker *D13mit16* is located near engulfment and cell motility protein 1(*Elmo1*) gene that is responsible for stimulation of normal cell migration. Although its role in different cell processes has not been clearly defined, it is known that *Elmo1* protein links to *Dock180* protein to form a protein complex (*Dock180-Elmo1*complex) that plays a critical role in cell adhesion, proliferation, dissemination and invasion of ovarian cancer (Wang *et al.*, 2010) (Table 5.4). The *Dock180-Elmo1*complex activates *Rac1,* a member of the Rho GTPase family, which participates in the modulation and regulation of the actin cytoskeleton that is essential in cell migration during cancer cell invasion (Jarzynka *et al.*, 2007). Our results suggest that MSI in marker *D13mit16* could be an early manifestation of the invasive potential that ovarian cancer cells display at the adult stage. However, further studies are needed to conclusively determine the role, if any, that MSI in marker *D13mit16* has.

Significantly high frequencies of MSI in markers *D13mit78* and *4-4-19844* were detected in female *Sod1* knockout PGC samples, but both markers were stables in male *Sod1* knockout PGCs, as well as in male and female wild type *Sod1* and heterozygous *Sod1* $^{+/-}$ PGCs. Marker *D13mit78* is located near the fibroblast growth factor 10 precursor (*Fgf-10*) gene that has been linked to cell development (Tables 5.3 and 5.4). The *Fgf10* gene has been detected in normal human ovarian theca, stroma and endometrial cells that play a role in stimulating the growth of activated follicles (Chaves *et al.*, 2010). Impairment of *Fgf10* gene expression influences paracrine signaling of cell survival, showing its importance for maintenance of follicles and follicular growth (Chaves *et al.*, 2010). The results of this study denote that MSI on marker *D13mit78* could negatively affect early follicular development of female primordial gonads, resulting in increased risk of infertility. Marker *4-4-19844* was unstable and it is located near the adrenergic receptor kinase, beta 1(*Adrbk1* also known as *Grk2*) gene which has a key role in cell signal transduction through the process of receptor desensitization and internalization, avoiding excessive stimulation (King *et al.*, 2007) (Tables 5.3 and 5.4). The follicle stimulating hormone receptor (FSHr) is a clear example of a *Grk2* transmembrane receptor which is expressed in the ovarian granulosa cells. It has been reported that Grk2 protein translation is affected by the presence of oxidative stress, giving rise to uncontrolled receptor signaling (Cobelens *et al.*, 2007). As a consequence of this, decreased expression of the *Grk2* gene has been involved in human granulosa cell tumors probably due to improper receptor desensitization and prolonged activation of FSHr (King DW, 2007). Taken together, our findings suggest that high risk of female infertility and ovarian cancer could be a manifestation from MSI of markers *D13mit78* and *4-4-19844* in PGCs.

Male *Sod1* knockout PGCs were significantly unstable in one marker, *D19mit68*. MSI instability was not detected in male *Sod1* knockout PGCs or in female and male wild type *Sod1* and heterozygous *Sod1* +/- PGC samples. The marker *D19mit68* is located near low density lipoprotein receptor related protein 5 precursor (*Lrp5*) gene that acts as a cofactor of the Wnt pathway. The importance of Wnt pathway lies in many cell processes such as cell development, proliferation, fate, and death. It is known that specific mutations of genes that encode this pathway contribute to different types of cancer such as breast, ovarian, and prostate (Johnson and Rajamannan, 2006). Our results suggest that MSI on marker *D19mit68* could be responsible for malignant cell transformation in male mouse PGCs in the presence of oxidative stress.

In conclusion, our results indicate that accumulation of DNA damage is present in *Sod1* knockout mice. PGC samples from *Sod1* mice at the time of migration and colonization of the gonad acquired spontaneous mutations due to oxidative stress response deficiencies by *Sod1* gene disruption. The presence of MSI during specific times in mouse embryonic development could be a signal for PGC pool selection in the female and male genital ridges and, additionally, to be the on-switch for cell transformation into ovarian tumorigenesis when aging deterioration occurs during adult life. Extrapolation of the instability of these markers and genes in the mouse model has also been described in the human genome. Therefore, identification of target mouse genes involved during cell stress responses might shed some light toward determining mechanisms that control oxidative stress consequences in human PGCs. These novel markers might allow for useful screening methods to detect initiation, determination, and progression of human ovarian carcinomas. Supplementary characterization of these

genes and their expression status needs to be done in the future to determine the specific functions they have in the evolution of human tumorigenesis.

Table 5.1 Complete list of 21 microsatellite mouse markers

n.	MARKER	SIZE (bp)	REPEAT MOTIF	MARKER LOCATION
1	M4-3	164	(GAAAAA)6	Chrom 4
2	M4-4	137	(CTTTT)17	Chrom 4
3	M4-2	129	(GAAAAA)9	Chrom 4
4	mBat37	121	(A)37	Chrom 6
5	D8mit120	130	(GT)28	Chrom 8
6	D8mit47	198	(TG)14	Chrom 8
7	D8mit88	113	(TG)14	Chrom 8
8	D13mit16	209	(TG)24	Chrom 13
9	4-4-13-45870	390	(GAGAA)40	Chrom 13
10	D13mit78	225	(CA)25	Chrom 13
11	D14mit5	178	(GT)9	Chrom 14
12	MT2620	99	(CA)13	Chrom 15
13	D17mit20	176	(CATA)13	Chrom 17
14	4-4-19844	280	(CAGGCT)30	Chrom 19
15	D19mit68	132	(TG)21	Chrom 19
16	DXmit54	192	(CA)15 (GA)16	Chrom X
17	DXmit249	114	(TG)17	Chrom X
18	DXmit116	102	(CA)19	Chrom X
19	DXmit192	123	(CA)24	Chrom X
20	mBat-24	98	A(24)	Chrom X
21	MX-3	115-121	(CA)19	Chrom X

Notes: Fifteen markers were located in various autosomes. Six markers were located in the X chromosome. This table depicts the size in base pairs (bp), repeat motifs, and the chromosome location.

Table 5.2 Microsatellite markers for detection of MSI in primordial germinal cells of mouse

n.	MARKER	CHROMOSOMAL LOCATION (cM)	SIZE (bp)	REPEAT MOTIF	GENBANK NUMBER	PRIMER SEQUENCES	FLUORESCENT LABELS
1	**mBat24**	ChrXq26.1	98	(A)24	14734	CATAGACCCAGTGCTCATCTTCGT CATCGGTGGAAAGCTCTGA	HEX
2	**D13mit78**	Chr13 (75.0)	225	(CA)25	62142	ACAGCACGGGTTTATCATCC TATGCCTGCCAGGCTTCTAT	HEX
3	**DXmit249**	ChrX (60.5)	114	(TG)17	493105	TTATGTGCTTATTAGCCAAGGTG AAAATAGAACTTCAGCAGCATGC	HEX
4	**D19mit68**	Chr19 (6.0)	132	(TG)21	16973	CCAATACAAATCAGACTCAATAGTCG AGGGTCTCCCCATCTTCCTA	HEX
5	**D8mit47**	Chr8 (56.0)	197	(TG)14	109384	AAGATGTGCTTACTCTGACTTCCC GGATCTATCCACATGTGGTGC	HEX
6	**D8mit88**	Chr8 (61.66)	113	(CA)14	94457	GTCCCTTGTAAACACTCTTGCC CTCTTTGCCCACGGTTATGT	HEX
7	**D17mit20**	Chr17 (34.3)	176	(CATA)13	12266	AGAACAGGACACCGGACATC TCATAAGTAGGCACACCAATGC	HEX
8	**D13mit16**	Chr13 I (10.0)	207	(TG)24	109406	CCAGCTGAAGGCTTACTCGT AAAGTTAGAATCAGCCATTCAAGG	FAM
9	**mBat37**	Chr6qC3 (35.94)	121	(A)37	1350935	TCTGCCCAAACGTGCTTAAT CCTGCCTGGGCTAAAATAGA	FAM
10	**4-4-19-844**	Chr19 (42.0)	280	(CAGGCT)30	R96357	CAGTTCACAGGGTAGCCACA AAGGTACTGCACCTGCTTGG	FAM

Notes: This table shows the specific chromosome location, size of marker (bp), repeat motifs, genbank access number, primer sequences amplified and dye labels for each marker

Table 5.3 Frequencies of MSI at five significantly informative microsatellite markers in male and female mouse primordial germinal cells

GENDER	GENOTYPE	EMBRYO AGE (days post-coitum)	LOCI*														
			4-4-19844			*D13mit16*			*D13mit78*			*DXmit249*			*D19mit68*		
			n	*m*	*f*	*n*	*m*	*f*	*n*	*m*	*f*	*n*	*m*	*f*	*n*	*m*	*f*
MALE	Mutated	11 dpc	37	0	0.000	35	2	0.031	28	0	0.000	28	2	0.062	33	2	0.055
		18 dpc	45	0	0.000	34	0	0.000	28	0	0.000	38	0	0.000	44	0	0.000
	Heterozygous	11 dpc	14	0	0.000	44	0	0.000	36	0	0.000	46	0	0.000	47	0	0.000
		18 dpc	27	0	0.000	44	0	0.000	28	0	0.000	40	0	0.000	42	0	0.000
	Wild Type	11 dpc	41	0	0.000	44	0	0.000	41	0	0.000	30	0	0.000	41	0	0.000
		18 dpc	46	0	0.000	91	0	0.000	42	0	0.000	43	0	0.000	44	0	0.000
FEMALE	Mutated	11 dpc	26	3	0.075	26	2	0.051	22	5	0.150	39	7	0.086	41	0	0.000
		18 dpc	36	0	0.000	42	0	0.000	39	1	0.012	48	0	0.000	48	0	0.000
	Heterozygous	11 dpc	45	0	0.000	46	0	0.000	39	0	0.000	47	0	0.000	48	0	0.000
		18 dpc	74	0	0.000	82	0	0.000	45	0	0.000	42	0	0.000	42	0	0.000
	Wild Type	11 dpc	40	0	0.000	42	0	0.000	35	0	0.000	43	0	0.000	41	0	0.000
		18 dpc	30	0	0.000	46	0	0.000	44	0	0.000	40	0	0.000	40	0	0.000

Notes:

*[Number of estimated alleles (n), number of mutant alleles (m), mutation frequency and (f) were calculated using SP-PCR software version 2.0 (M.D. Anderson Cancer Center, Houston, TX)

Table 5.4 Summary list of 5 informative markers and related genes

MARKER	CHROMOSOME LOCATION (cM)	REPEAT MOTIF	MARKER LOCATION	GENE	GENE LOCATION	GENE FUNCTION
4-4-19844	Chr19 (42.0)	(CAGGCT)30	chr19:4288135-4288414	Adrbk1	Intron 18-19	(Adrenergic receptor kinase, beta 1) cell signals involved in inflammation
D13mit16	Chr13 I (10.0)	(TG)24	chr13:20385311-20385519	Elmo1	5'Upstream 0.2Mb	(Engulfment and cell motility protein 1) protein binding, apoptosis
D13mit78	Chr13 (75.0)	(CA)25	chr13:119618032-119618260	Fgf-10	5'Upstream 0.1Mb	(Fibroblast growth factor10 precursor); cell processes during embryogenesis, adult tissue homeostasis, and carcinogenesis
DXmit249	ChrX (60.5)	(TG)17	chrX:160413766-160413877	Car5b	5'Upstream 0.01Mb	(Carbonic anhydrase 5b, mitochondrial gene); catalysing the interconversion of carbon dioxide and bicarbonate
D19mit68	Chr19 (6.0)	(TG)21	chr19:3645155-3645286	Lrp5	5'Upstream 0.1Mb	(Low-density lipoprotein receptor-related protein5 precursor) act as a coreceptor of Wnt-pathway

Notes: This table shows the specific chromosome location, repeat motifs, nucleotide marker location in regards to the chromosome, related genes, marker location of adjacent genes, and gene function information from NCBI, NLM, and NIH databases or from reference papers.

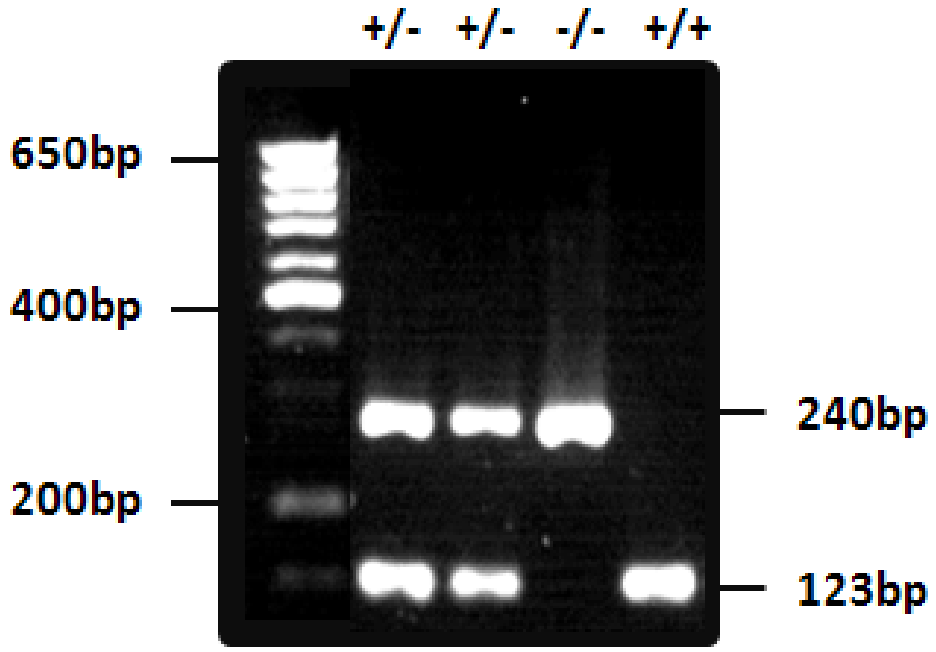

Figure 5.1 Determining genotype of mouse fetuses with STS markers: *MR0781* and *MR0878*

Notes: Amplifications from STS markers: *MR0781* and *MR0878* were analyzed through gel electrophorsis in a 4% NuSieve agarose gel. 1000bp ladder (EZ BioResearch LLC, Saint Louis, MO) (line1). *Sod1* heterozygous (+/-) samples showed both 240 bp and 123 bp bands (lines 2 and 3). *Sod1* homozygous (-/-) samples showed only 240 bp band (line 4). *Sod1* homozygous (-/-) wild type samples showed only 123 bp band (line 5).

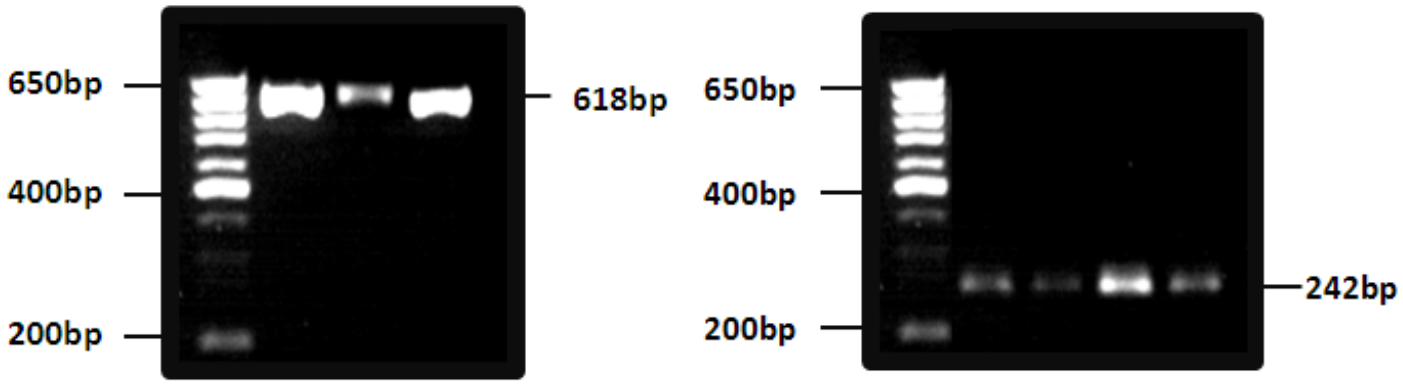

Figure 5.2 Determining sex of mouse embryos with sex specific STS markers: *Zfy* and *DXNd3fR*

Notes: Amplifications from STS markers: *Zfy* and *DXNd3fR* were analyzed through gel electrophorsis in a 4% NuSieve agarose gel. *Zfy* (618 bp) will only amplify for males and *DXNd3fR* (242 bp) will amplify for the presence of X chromosome. A) 1000 bp ladder (EZ BioResearch, LLC, Saint Louis, MO) (line1). *Zfy* amplification (618 bp) band from three male mouse embryo samples (lines 2-4). B) 1000 bp ladder (EZ BioResearch, LLC, Saint Louis, MO) (line1). *DXNd3fR* amplification (242 bp) band in four mouse female embryos.

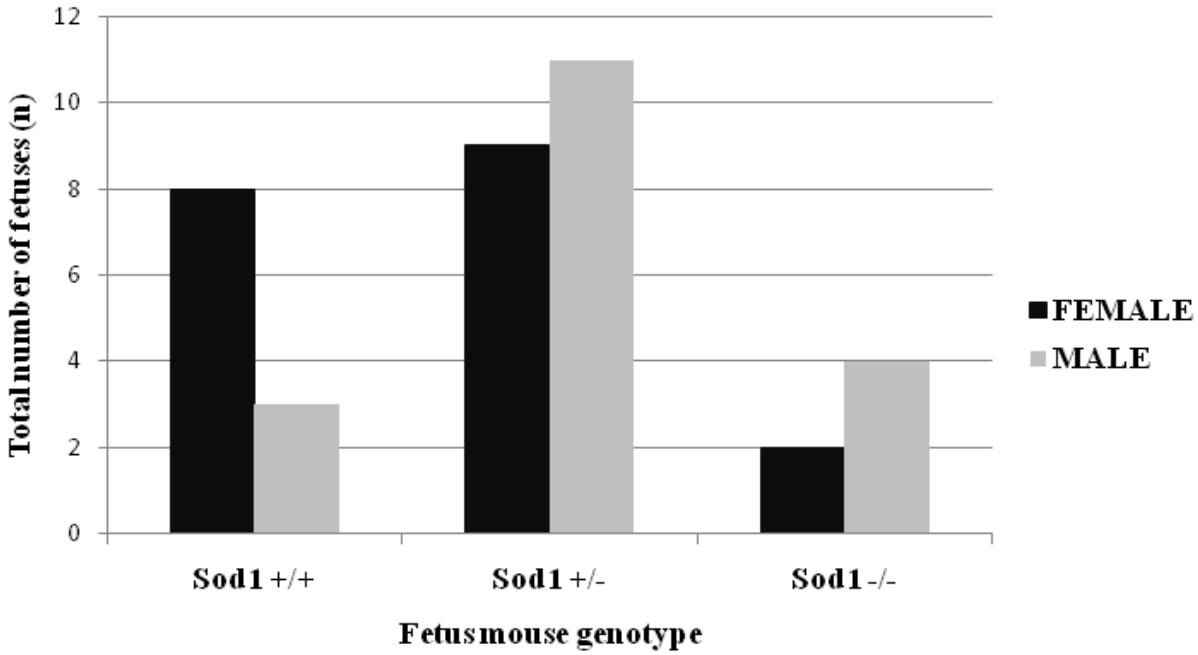

Figure 5.3 Total number of fetuses dissected from mouse uteri according to genotypes

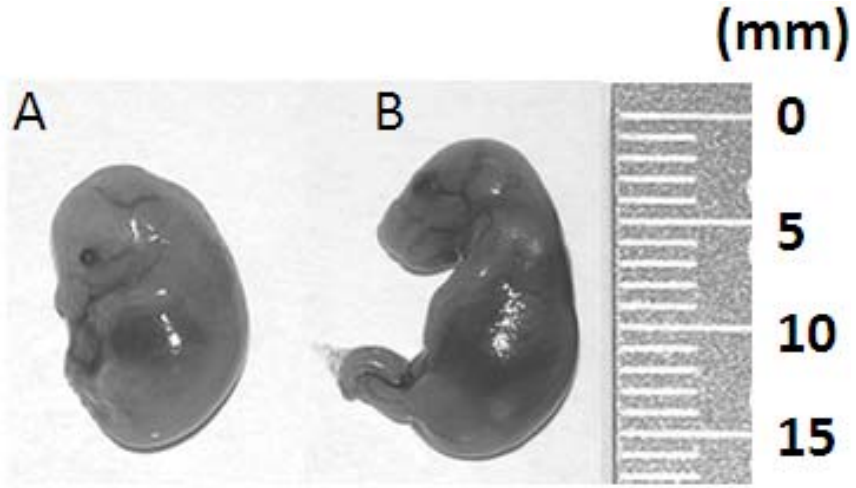

Figure 5.4 Measurement of mouse embryos at 10.5 dpc

Notes: A) Female *Sod1* homozygous -/- mouse embryo at 10.5dpc. B) Male *Sod1* homozygous -/- mouse embryo at 10.5 dpc. Measurements were in millimeters.

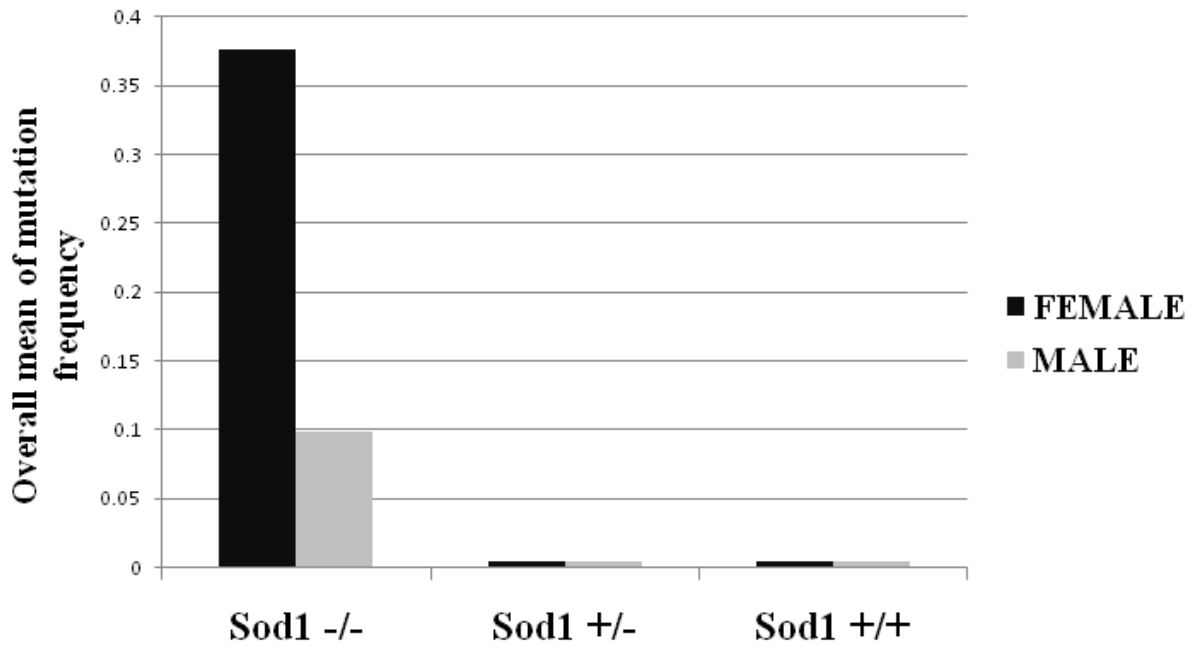

Figure 5.5 Overall mean frequencies of MSI for all three PGC

Notes: mutation frequencies calculated with SP-PCR software version 2.0 (M.D. Anderson Cancer Center, Houston, TX).

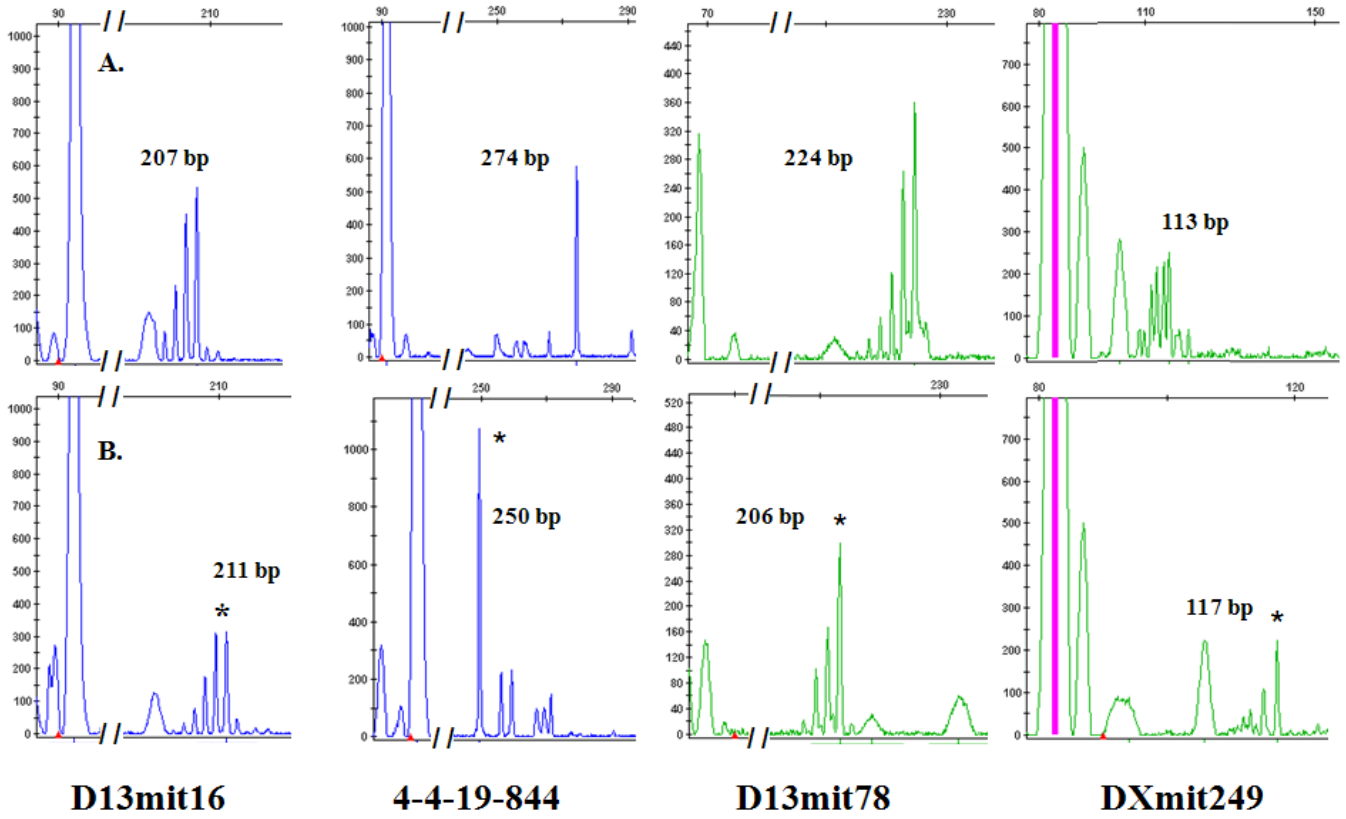

Figure 5.6 Example of microsatellite electropherograms for normal and mutant alleles

Notes: PCR fragment sizes (bp). Panel A.Wild type allele. Panel B. Mutant allele. Markers are indicated along the bottom of figure. In blue are FAM- labeled, and markers in green are HEX -labeled.

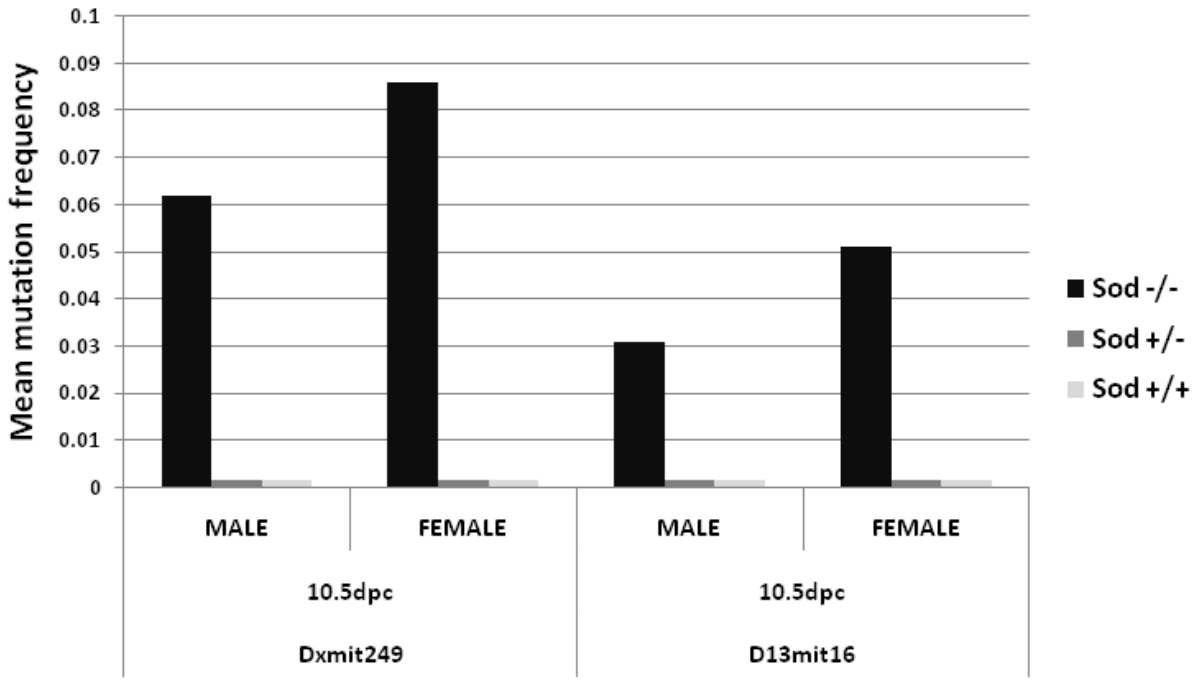

Figure 5.7 Significantly high MSI in *Dxmit249* and *D13mit16*

Notes: MSI for these markers were detected in both male and female *Sod1* -/- knockout PGC samples at 10.5 dpc.

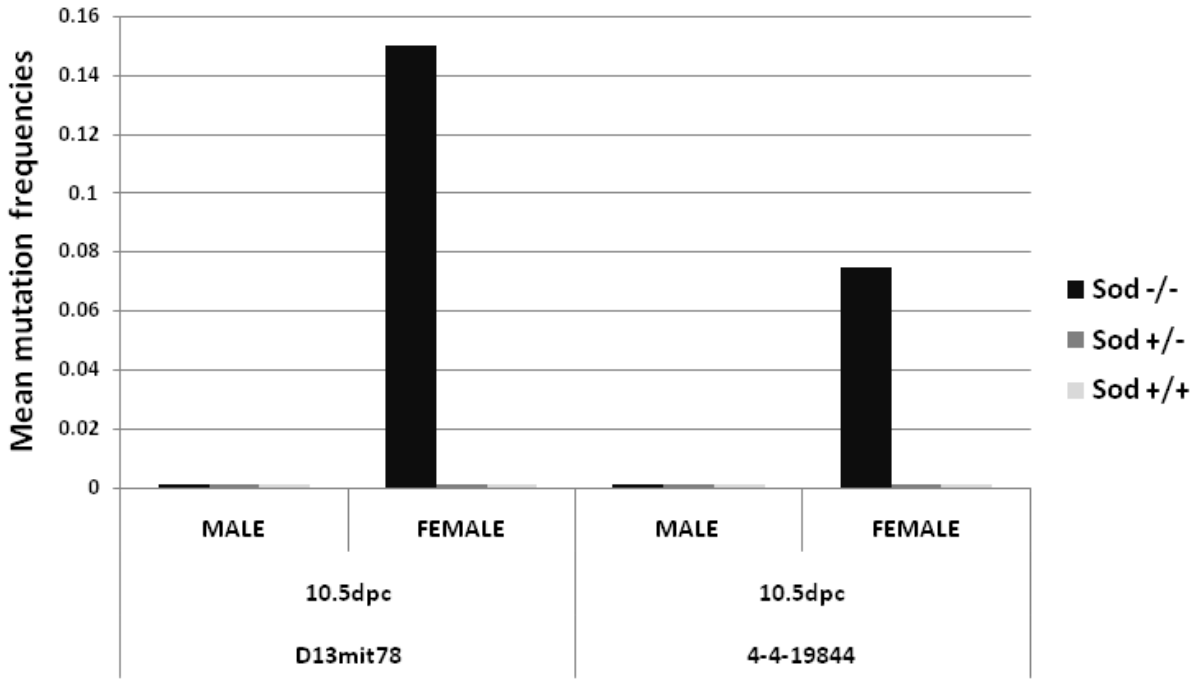

Figure 5.8 Significantly high MSI in *D13mit78* and *4-4-19844* markers

Notes: MSI for these markers were detected in female *Sod1* -/- knockout PGC samples at 10.5 dpc. No MSI was detected at 18 dpc.

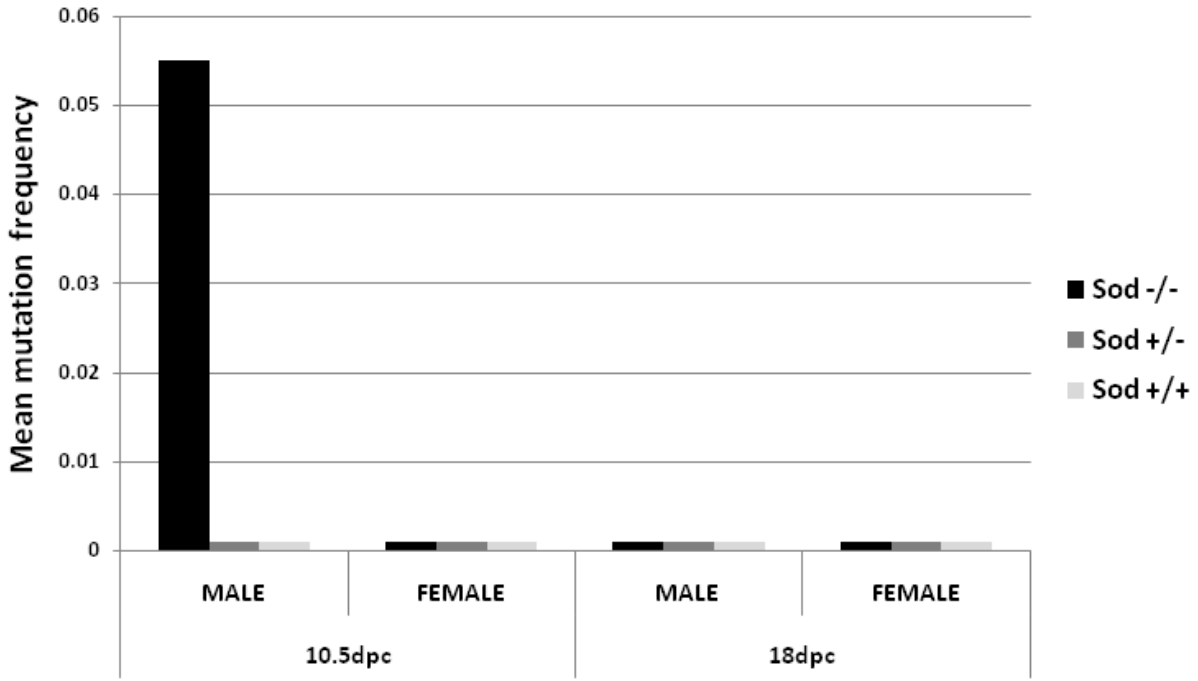

Figure 5.9 Significantly high MSI in D19mit68 marker

Notes: MSI was detected for *D19mit68* marker in male *Sod1* -/- knockout PGC samples at 10.5 dpc. No MSI was detected at 18 dpc.

5.6 References

Agarwal A, Gupta S, and Sharma RK. (2005) Role of oxidative stress in female reproduction. Reprod Biol Endocrinol 3:28-49.

Bendel-Stenzel M, Anderson R, Heasman J, and Wylie C. (1998) The origin and migration of primordial germ cells in the mouse. Semin Cell Dev Biol 9:393-400.

Busuttil RA, Garcia AM, Cabrera C, Rodriguez A, Suh Y, Kim WH, Huang TT, and Vijg J. (2005) Organ-specific increase in mutation accumulation and apoptosis rate in CuZn-superoxide dismutase-deficient mice. Cancer Res 65:11271-11275.

Carlsson LM, Jonsson J, Edlund T, and Marklund SL. (1995) Mice lacking extracellular superoxide dismutase are more sensitive to hyperoxia. Proc Natl Acad Sci USA 92:6264-6268.

Chaves RN, Lima-Verde IB, Celestino JJ, Duarte AB, Alves AM, Matos MH, Campello CC, Name KP, Báo SN, Buratini J Jr, and Figueiredo JR. (2010) Fibroblast growth factor-10 maintains the survival and promotes the growth of cultured goat preantral follicles. Domest Anim Endocrinol 39:249-258.

Cobelens PM, Kavelaars A, Heijnen CJ, Ribas C, Mayor F Jr, and Penela P. (2007) Hydrogen peroxide impairs GRK2 translation via a calpain-dependent and cdk1-mediated pathway. Cell Signal 19:269-277.

Coolbaugh-Murphy M, Maleki A, Ramagli L, Frazier M, Lichtiger B, Monckton DG, Siciliano MJ, and Brown BW (2004) Estimating mutant microsatellite allele frequencies in somatic cells by small-pool PCR. Genomics 84:419-430.

Coolbaugh-Murphy MI, Xu J, Ramagli LS, Brown BW, and Siciliano MJ (2005) Microsatellite instability (MSI) increases with age in normal somatic cells. Mech Ageing Dev 126:1051-1059.

De Felici M, Dolci S, and Pesce M. (1992) Cellular and molecular aspects of mouse primordial germ cells migration and proliferation in culture. Int J Dev Biol 36:205-213.

De Felici M. (2000) Regulation of primordial germ cells develop in the mouse. Int J Dev Biol 44:575-580.

Elchuri S, Oberley TD, Qi W, Eisenstein RS, Jackson Roberts L, Van Remmen H, Epstein CJ, and Huang TT. (2005) CuZnSOD deficiency leads to persistent and

widespread oxidative damage and hepatocarcinogenesis later in life. Oncogene 24:367-380.

Essick EE, and Sam F. (2010) Oxidative stress and autophagy in cardiac disease, neurological disorders, aging and cancer. Oxid Med Cell Longev 3:168-77.

Gatcliffe TA, Monk BJ, Planutis K, and Holcombe RF. (2008) Wnt signaling in ovarian tumorigenesis. Int J Gynecol Cancer 18:954-962.

Ho YZ, Magnenat JL, Gargano M, and Cao J. (1998) The nature of antioxidant defense mechanisms: a lesson from transgenic studies. Environ Health Perspect 106(suppl 5): 1219-1228.

Ho YS, Gargano M, Cao J, Bronson RT, Heimler I, and Hutz RJ. (1998) Reduced fertility in female mice lacking copper-zinc superoxide dismutase. J Biol Chem 273:7765-7769.

Huang TT, Yasunami M, Carlson EJ, Gillespie AM, Reaume AG, Hoffman EK, Chan PH, Scott RW, and Epstein CJ. (1997) Superoxide-mediated cytotoxicity in superoxide dismutase-deficient fetal fibroblasts. Arch Biochem Biophys 344:424-432.

Hynninen P, Vaskivuo L, Saarnio J, Haapasalo H, Kivelä J, Pastoreková S, Pastorek J, Waheed A, Sly WS, Puistola U, and Parkkila S. (2006) Expression of transmembrane carbonic anhydrases IX and XII in ovarian tumours. Histopathology 49:594-602.

Jarzynka MJ, Hu B, Hui KM, Bar-Joseph I, Gu W, Hirose T, Haney LB, Ravichandran KS, Nishikawa R, and Cheng SY. (2007) ELMO1 and Dock180, a bipartite Rac1 guanine nucleotide exchange factor, promote human glioma cell invasion. Cancer Res 67:7203-7211.

Johnson ML, Rajamannan N. (2006) Diseases of Wnt signaling. Rev Endocr Metab Disord 7:41-49.

King DW, Steinmetz R, Wagoner HA, Hannon TS, Chen LY, Eugster EA, Pescovitz OH. (2003) Differential expression of GRK isoforms in nonmalignant and malignant human granulosa cells. Endocrine 22:135-142.

Labosky PA, and Hogan BLM. (1999) Mouse Primordial Germ Cells: isolation and in vitro culture. Methods Mol Biol 97**:**201-212.

Ledda S, Bogliolo L, Bebbere D, Ariu F, and Pirino S. (2010) Characterization, isolation and culture of primordial germ cells in domestic animals: recent progress and insights from the ovine species. Theriogenology 74:534-543.

Lu W, Ogasawara MA, and Huang P. (2007) Models of reactive oxygen species in cancer. Drug Discov Today Dis Models 4:67-73.

Matsui Y. (1998) Developmental fates of the mouse germ cell line. Int J Dev Biol 42:1037-1042.

Matzuk MM, Dionne L, Guo Q, Kumar TR, and Lebovitz RM. (1998) Ovarian function in superoxide dismutase 1 and 2 knockout mice. Endocrinology 139:4008-4011.

McLaren A. (2003) Primordial Germ Cells in the mouse. Dev Biol 262:1-15.

Miana-Mena FJ, González-Mingot C, Larrodé P, Muñoz MJ, Oliván S, Fuentes-Broto L, Martínez-Ballarín E, Reiter RJ, Osta R, García JJ. (2010) Monitoring systemic oxidative stress in an animal model of amyotrophic lateral sclerosis. J Neurol Nov 25. [Epub ahead of print]

Moreno-Ortiz H, Esteban-Perez C, Badran W, and Kent-First M. (2009) Isolation and Derivation of Mouse Embryonic Germinal Cells J Vis Exp 32:1-3.

Nagamine CM, Chan KM, Kozak CA, and Lau YF. (1989) Chromosome mapping and expression of a putative testis-determining gene in mouse. Science 243:80-83.

Noor R, Mittal S, and Iqbal J. (2002) Superoxide dismutase-applications and relevance to human diseases. Med Sci Monit 8: RA210-5.

Peled-Kamar M, Lotem J, Okon E, Sachs L, and Groner Y. (1995) Thymic abnormalities and enhanced apoptosis of thymocites and bone marrow cells in transgenic mice overexpresing Cu-Zn SOD: implication in Down Syndrome. EMBO 14:4985-4993.

Pesce M. (2002) Derivation of primordial germinal cells from cells of the mouse epiblast. Mech Dev 112:15-24.

Philips T, and Robberecht W. (2011) Neuroinflammation in amyotrophic lateral sclerosis: role of glial activation in motor neuron disease. Lancet Neurol 10:253-263.

Rana N, Sonali M, and Jawaid I. (2002) Superoxide dismutase- applications and relevance to human diseases. Med Sci Monit 8:RA210-RA215.

Resnic J, Bixler LS, Cheng L, and Donovan PJ. (1992) Long Term Proliferation of mouse primordial germ cells in culture. Nature 359:550-551.

Tam P, and Snow MH. (1981) Proliferation and migration of primordial germ cells during compensatory growth in mouse embryos. J.Embryol Exp Morph 64:133-147.

Van Remmen H, Qi W, Sabia M, Freeman G, Estlack L, Yang H, Mao-Guo Z, Huang TT, Strong R, Lee S, Epstein CJ, and Richardson A. (2004) Multiple deficiencies in antioxidant enzymes in mice result in a compound increase in sensitivity to oxidative stress. Free Radic Biol Med 36:1625-1634.

Wang H, Linghu H, Wang J, Che YL, Xiang TX, Tang WX, Yao ZW. (2010) The role of Crk/Dock180/Rac1 pathway in the malignant behavior of human ovarian cancer cell SKOV3. Tumour Biol 31:59-67.

Woelber L, Mueller V, Eulenburg C, Schwarz J, Carney W, Jaenicke F, Milde-Langosch K, Mahner S. (2010) Serum carbonic anhydrase IX during first-line therapy of ovarian cancer. Gynecol Oncol 117:183-188.

Zhang Y, Monckton DG, Siciliano MJ, Connor TH, and Meistrich ML (2002) Detection of radiation and cyclophosphamide-induced mutations in individual mouse sperm at a human expanded trinucleotide repeat locus transgene. Mutat Res 516:121-138.

APPENDIX A

ISOLATION AND DERIVATION OF MOUSE EMBRYONIC GERMINAL CELLS

(http://www.jove.com/index/Details.stp?ID=1635)

Video Article

Isolation and Derivation of Mouse Embryonic Germinal Cells

Harold Moreno-Ortiz, Clara Esteban-Perez, Wael Badran, Marijo Kent-First
Reproductive Genetics and Stem Cell Laboratory, Department of Biological Sciences, Mississippi State University

Correspondence to: Harold Moreno-Ortiz at hm200@msstate.edu, Marijo Kent-First at mk247@msstate.edu

URL: http://www.jove.com/index/Details.stp?ID=1635
DOI: 10.3791/1635
Citation: Moreno-Ortiz H., Esteban-Perez C., Badran W., Kent-First M. (2009). Isolation and Derivation of Mouse Embryonic Germinal Cells. JoVE. 32. http://www.jove.com/index/Details.stp?ID=1635, doi: 10.3791/1635

Abstract

The ability of embryonic germinal cells (EG) to differentiate into primordial germinal cells (PGCs) and later into gametes during early developmental stages is a perfect model to address our hypothesis about cancer and infertility. This protocol shows how to isolate primordial germinal cells from developing gonads in 10.5-11.5 days post coitum (dpc) mouse embryos. Developing gonadal ridges from mouse embryos (C57BL6J) were dissociated by mechanical disruption with collagenase, then plated in a mouse embryo fibroblast feeder layer (MEF-CF1) that was previously mitotically inactivated with mitomycin C in the presence of knockout media and supplemented with Leukemia Inhibitor Factor (LIF), basic Fibroblast Growth Factor (bFGF), and Stem Cell Factor (SCF). Using these optimized methods for PCG identification, isolation, and establishment of culture conditions permits long term cultures of EG cells for more than 40 days. The embryonic germinal cell lines showed embryonic phenotype and expression of common used markers of the pluripotent state. Isolation and derivation of germinal cells in culture provide a tool to understand their development in vitro and offer the opportunity to monitor cumulative damage at genetic and epigenetic levels after exposure to oxidative stress.

Protocol

Part 1: Pregnant Mouse Laparotomy

1. Using cervical dislocation, euthanize a pregnant C57BL6J female mouse at 10.5-11.5 dpc.
2. Clean the abdomen with antimicrobial soap, and then, shave it.
3. After shaving, wash the abdomen with a saline solution.
4. Then, dry the abdomen with a sterile gauze.
5. Cover the mouse with a new sterile field.
6. Make a ventral incision using forceps and dissection scissors.
7. Identify and remove the entire uterus from the abdominal cavity. Mouse embryos will be visible inside the uterus.
8. Transfer the uterus into a petri dish filled with D-PBS, and keep it on ice.
9. Using a sterile scalpel and forceps, remove the placenta and extra embryonic tissues of each embryo.
10. Transfer embryos into a fresh petri dish filled with D-PBS.
11. Measure the length of the mouse embryos. We found that the sizes differed according to the embryo's age. For example 8.5 dpc measured at an average of 6mm, 10.5 dpc measured at an average of 11mm, and 12.5 dpc measured at an average of 16 mm.
12. Then, remove their tails for DNA extraction.

Part 2: Gonadal Ridge Dissection

Under stereomicroscope and Light source Schott Fostec

1. Place a filter paper in a Petri dish. Then, place the mouse embryo on top of the filter paper to dry the embryo and immobilize for dissection.
2. Using a sterile scalpel, make a transverse cut of the mouse embryo above the origin of the umbilical cord.
3. Under a stereomicroscope, using sterile fine forceps and a sterile fine teasing needle, remove the intestines and liver so that the urinary system is visible.
   The kidneys are located laterally in the abdominal cavity, and the bladder is located medial and caudal in comparison to the kidneys. The embryo can be identified as male because the gonadal ridges are located on either side of the bladder. In the female, the gonadal ridges are firmly attached to the caudal lateral end of the kidneys.
4. Peel the gonadal ridge out by sliding a needle behind it. The gonadal ridge is removed by cutting away the tissues that support it.
5. Transfer the gonadal ridges to a new petri dish filled with fresh D-PBS.
   Microscopically, the male gonadal ridge should be stripped, large and oval in shape. In contrast, the female gonadal ridge should be spotted, have elongated shape and be smaller in comparison to the male gonadal ridge.

Part 3: Gonadal Ridge Digestion

Under stereomicroscope:

1. Mesonephros Dissection: Separate the gonad from the mesonephros and ridge using a fine and sharp needle.
   - It is important to remove the mesonephros from the gonadal ridge because it is a somatic tissue that will overgrow in the PGC derivation process.

2. Gonadal Ridge Digestion: Collect clean gonadal ridges in a 0.5ul drop of fresh D-PBS. Add 20 ml of Collagenase/Dispase Solution (Final concentration at 1mg/ml).
   - Embryos should be processed individually. Each embryo should have its own separate and labeled petri dish.

3. Gonadal Ridge Mincing: Cut the gonadal ridge into small pieces using a sterile needle and sterile fine forceps No. 4.
4. Incubation: Petri dishes are transferred to an incubator at 37°C for 15 minutes.
    - The incubation time could vary between tissues.
5. Pipetting: After 15 minutes, the tissue can be dissociated by pipetting. Using pulled glass capillary pipettes with diameters between 40 -100 mm Break up the pieces by pipetting up and down. This will form small clumps. Transfer the clumps to 0.5ml of a pre warmed D-PBS drop for a final wash.
6. After washing, transfer the clumps to eppendorf tubes.
    - Do not over expose the tissue to collagenase.
    - Do not make a single cell suspension. This is important for colony formation. If it is a single cell suspension, PGCs tend to differentiate and migrate.
    - This process should not be longer than 20 minutes, or your cells will lose viability.
7. Centrifuge at 2000 rpm for 5 minutes at room temperature.
8. After centrifuging, remove the supernatant, and resuspend the pellet in 0.5 ml of supplemented knock out media (Pre-warmed at 37°C).

Part 4: Primordial Germinal Cells Culture

"You should perform the next steps quickly to preserve the viability of PGCs for isolation and derivation.

1. 24 hours before this process you should prepare a mitotically inactivated MEF-CF1 feeder layer following the protocol from Zhang J. et al 2008.
    - Prepare 20 dishes for one pregnant female mouse (6-8 embryos).
    - MEFs lose the ability to be a feeder layer (promote growth and prevent differentiation) after 5-6 passages.
    - Do not use MEFs older than 48 hours.
2. Immediately before plating PGCs, the MEF medium must be slowly removed from the MEF feeder layer.
3. Then, add 0.5 ml/well of pre-warmed supplemented knockout medium onto the MEF feeder layer.
    - MEF media contains fetal bovine serum that induces differentiation of PGCs.
    - Knockout medium must be supplemented with specie specific growth factors immediately before use to ensure the activity of the grow factor.
4. Using symmetrical distribution, plate PGCs over the MEF feeder layer.
    - If these pieces are too close, they tend to aggregate and make dense colonies that attach poorly or begin differentiating.
    - Culture dishes must be labeled with Embryonic Germinal cell line name, passage number, and date.
5. Carefully, transfer the culture dishes into an incubator at 37°C and 5% CO_2.
6. Monitor the cells every 24 hours.
7. After 48 hours, remove 250 ml of media from the very top of the culture to avoid disturbing the colony's attachment. Then, add 250 ml of fresh supplemented knock-out media (pre-warmed at 37°C).
8. After step 7, wait another 48 hours, and then, completely remove all media and replace it with fresh supplemented knock-out media (pre-warmed at 37°C). Do this every 2 days for 8-10 days until PGC colonies form.

Part 5: Embryonic Germinal Cells

1. After 10 days of PGC isolation, embryonic germinal cell colonies are formed.
2. Embryonic germinal cell lines are kept alive by manual passages every 8-10 days. They continue to present an undifferentiated morphology and express pluripotency markers such as alkalyne phosphatase, Oct-4, SSEA-1, and SOX-2

Notes

- Sterile/aseptic conditions are essential in the culture room.
- For derivation and culture, PGCs are processed in a Purifier Class II Bio safety Cabinet.
- Incubations are in a humidified 37°C and 5% CO_2 incubator.
- All media and reagents are filtered prior to use in a 0.2 um filter, stored at 4°C, and pre-warmed at 37°C before use.
- During the dissection steps, all embryos and tissues must be kept on ice.
- All reagent flasks are decontaminated with ethanol before placing in a cabinet.
- Use of gloves, lab coat, and nurse caps are mandatory.

Conclusion

We have provided a video that shows you how to isolate, derive, and culture embryonic germinal cells from gonadal ridges of 10.5-11.5 dpc mouse embryos. The reproducible isolation and long term culture of Embryonic germinal cell lines provides a critical foundation for study of early embryonic development, genetic and epigenetic germinal patterns, gonad formation, environmental effects of surrounding organs during the developmental process of gametogenesis in the male and female embryos, and determination of pathways that leads to cancer and infertility.

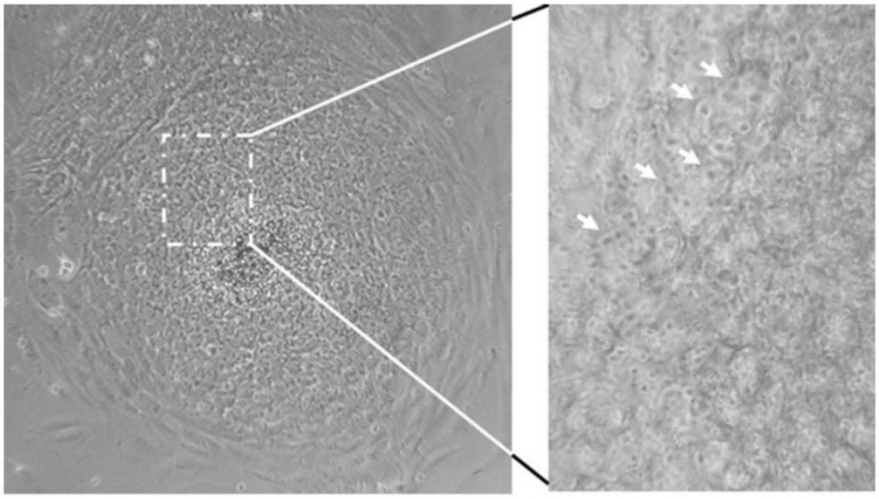

Figure 1. Morphology of Mouse Embryonic Germinal Cells. Characteristic growth and morphology of undifferentiated embryonic germinal cell colony, which grow condensed in a multilayer pattern (Left). Boxed region shows higher magnification image (right) in a three dimensional view of the multilayer colony and displays the morphology typical of germinal cells, high nucleus/cytoplasm ratio (arrows), on the top layer of the colony. (Phase contrast photomicrographs with magnification 20X-left and 60X-right).

Acknowledgements

The authors would like to acknowledge the invaluable help of: Dr Neal First and Kourtney Wilkinson for manuscript editing; Dr Lucy Senter, Dr. Brigit Willeford and Mike Basett for assistance with training and animal care at the MSU ALAC accredited mouse facility; Dr Dwayne Wise for his assistance with microscopy and image capture; Cesar Monroy, Hannah Swoope, and Bobbie Huddleston for their assistance with video production at MSU. This research was funded by Office of Institutional Research and the Department of Biological Sciences at Mississippi State University.

References

1. DeFelici, M. Cell Biology: A laboratory Handbook, Second Edition. Vol. **1**: 73-85 (1998).
2. Donovan P.J., De Miguel M.P. Turning Germ Cells into Stem Cells. Current Opinion in Genetics and Development, **13**:463-471 (2003).
3. Labosky P.A., Hogan B.L.M. Mouse Primordial Germ Cells: isolation and in vitro culture. Methods in molecular Biology **97**:201-212. Totowa, NJ (1999).
4. Mc Laren A., Southee D. Entry of Mouse Embryonic Germ Cells into Meiosis. Developmental Biology **187**, 107-113 (1997).
5. Yoshimizu T., Obinata M., Matsui Y. Stage-specific tissue and cell interactions play key roles in mouse germ cell specification. Development **128**, 481-490 (2001).
6. Zhang J., Hhvorostov I., Teitell M. From MEFs to Matrigel I: Passaging hESCs in the Presence of MEFs. JoVe. 16. http://www.jove.com/index/Details.stp?ID-722, doi:10.3791/722 (2008).

